

MICHIGAN STATE UNIVERSITY LIBRARY
3 0282 03220 0012

T. ZHANG

PH.D.



142
889
THS

2010

2
2011

This is to certify that the
dissertation entitled

MOLECULAR AND FUNCTIONAL ANALYSIS OF A NOVEL
CATION CHANNEL IN *DROSOPHILA MELANOGASTER*

presented by

TIANXIANG ZHANG

has been accepted towards fulfillment
of the requirements for the

Ph.D.

degree in

Department of Microbiology
and Molecular Genetics



Major Professor's Signature

8/25/2010

Date

MSU is an Affirmative Action/Equal Opportunity Employer

LIBRARY
Michigan State
University

PLACE IN RETURN BOX to remove this checkout from your record.
TO AVOID FINES return on or before date due.
MAY BE RECALLED with earlier due date if requested.

DATE DUE	DATE DUE	DATE DUE

**MOLECULAR AND FUNCTIONAL ANALYSIS OF A NOVEL CATION CHANNEL
IN *DROSOPHILA MELANOGASTER***

By

Tianxiang Zhang

A DISSERTATION

**Submitted to
Michigan State University
in partial fulfillment of the requirements
for the degree of**

DOCTOR OF PHILOSOPHY

Microbiology and Molecular Genetics

2010

ABSTRACT

MOLECULAR AND FUNCTIONAL ANALYSIS OF A NOVEL CATION CHANNEL IN *DROSOPHILA MELANOGASTER*

By

Tianxiang Zhang

Voltage-gated ion channels (VGICs) play essential roles in regulating neuronal activities, such as initiation and propagation of action potentials and synaptic transmission. Different families of VGICs play different roles in modulating these activities and in turn differentially contribute to the neuronal excitability and function. The *Drosophila Sodium Channel 1 (DSC1)* gene was identified almost two decades ago. Based on the deduced amino acid sequence, *DSC1* was predicted to encode the first voltage-gated sodium channel in insects. An *in situ* RNA hybridization study of *DSC1* transcripts showed that *DSC1* is expressed mainly in the nervous system of pupae and adult flies. An immunohistochemical study indicated that the *DSC1* protein is present in both central and peripheral nervous systems of adult flies. Contrary to the prediction of a sodium channel, electrophysiological characterization in *Xenopus* oocytes revealed that a *DSC1* orthologue in cockroach, *BSC1*, encodes a novel voltage-gated cation channel that is more permeable to Ca^{2+} ions than to Na^{+} . It is not known whether the *DSC1* channel shares the novel ion selectivity of the *BSC1* channel, nor is the specific role of the *DSC1* channel in the insect nervous system clear.

My dissertation research focuses on the molecular and functional characterization of the *DSC1* gene. I found that the *DSC1* transcript undergoes alternative splicing and potential RNA editing. Several alternative exons contain a premature stop codon that results in truncated proteins. Similar to the BSC1 channel, the DSC1 channel is also a voltage-gated cation channel which is permeable to Na^+ , Ca^{2+} , and Ba^{2+} ions. Analyses of two *DSC1* mutant lines, generated by precise gene knockout via homologous recombination, showed an important role of the DSC1 channel in modulating insect behavior in response to environmental stresses. Specifically, the locomotor activities of the *DSC1* knockout flies exhibit hypersensitivity to heat shock and starvation. These phenotypes are associated with altered electrophysiological properties of the giant fiber system (GFS). Pharmacologically, *DSC1* knockout flies also show enhanced susceptibility to a class of sodium channel activating insecticides, pyrethroids, but not to a sodium channel blocker insecticide N-decarbomethoxyllated JW062 (DCJW), or a γ -aminobutyric acid (GABA)-gated chloride channel inhibitor (fipronil). The enhanced susceptibility of *DSC1* knockout flies is also associated with altered electrophysiological properties of the GFS. Taken together, these results provide evidence for an important role of the DSC1 channel in modulating insect neuronal excitability under environmental stresses.

ACKNOWLEDGMENTS

In my five years of study at Michigan State University, I was supported and assisted by a lot of warm-hearted people. Without their kind help and guidance, I might have ended in “nowhere” along my scientific journey. There are no words sufficient to express my gratitude to them.

First of all, I would like to thank my mentor, Dr. Ke Dong, who supported me most during my research. I was attracted to Ke’s research when I attended a seminar during the first month after I came to MSU. Then I talked with Ke and set up my first rotation in her lab. As I worked and communicated with Ke, I was deeply impressed by Ke’s profound knowledge and optimistic, dauntless spirit. I was encouraged by others in her lab as well. So, after I finished my rotations, I decided to join Ke’s team. Ke has given me tremendous guidance and training and helped me overcome one obstacle after another in my project. She also polished the English of my manuscripts and taught me plenty of skills in scientific writing and presentation, which will benefit my whole career. With this experience, I am now more open-minded and self-confident, which are critical to be a scientist.

Besides Ke, I have four other committee members who have provided indispensable encouragement and support for my study. Dr. Suzanne Thiem gave a lot of suggestions on my molecular biology work. In addition, she also kindly helped me understand American culture. Dr. David Arnosti and Dr. Donna Koslowsky provide many suggestions on the molecular biology and genetics portions of my research. The classes they instructed opened up broad and deep

views of molecular biology, biochemistry and genetics to me. Dr. William Atchison helped me a lot on my understanding of basic neurobiology. Here, I would like to thank them and I believe the passion and perseverance of all my committee members in scientific research will keep influencing me for the rest of my life.

It is my fortune to work with so many talented and warm-hearted people in our lab. Lingxin Wang, Mike Chumbley, and Becky Aslakson are the ones I have been working closely with in obtaining exciting experimental results and maintaining all the *D. melanogaster* stocks. Dr. Zhiqi Liu cloned the *DSC1* cDNA and made the donor construct for the *DSC1* knockout experiments. Dr. Ningguan Luo generated the *DSC1* knockout founder lines. Their work laid the foundation for my project. Dr. Weizhong Song, Dr. Yuzhe Du, and Dr. Zhaonong Hu taught me how to do electrophysiological recording and provided heart-warming assistance during my setting up the recording apparatus. Yoshiko Nomura helped me with my molecular cloning and Rachel Olson helped me with my English. Dr. Sebastien Hayoz, Dr. Rong Gao, and Dr. Eugenio Oliveira gave me many suggestions during my writing manuscripts and thesis. I also would like to thank our collaborators, Dr. Chun-Fang Wu and his lab members, especially Zhe Wang, at the University of Iowa. They taught me basic techniques of recording and analyses of the GF system.

Besides these people, I also thank the Department of Microbiology and Molecular Genetics and especially Dr. Richard Schwartz and Dr. Robert

Hausinger for providing me with the opportunity to study abroad and assisting me along the way.

The last but not the least, I would like to say thanks to my parents, my sister and brother, and my wife, Fengrui Zhang. They care about me even more than they care about themselves. They are the source of my energy, my heart and soul. Without them, I would not have gone this far.

TABLE OF CONTENTS

LIST OF TABLES.....	x
LIST OF FIGURES.....	xii
LIST OF ABBREVIATIONS.....	xiv
 CHAPTER 1	
GENERAL INTRODUCTION	1
1.1 Voltage-gated sodium channels	3
1.1.1 Structure and gating properties of voltage-gated sodium channels	3
1.1.2 The family of mammalian sodium channel α subunit encoding genes	8
1.1.3 The sodium channel β subunit.	10
1.1.4 The <i>Drosophila</i> voltage-gated sodium channel, Para.	11
1.2 The <i>Drosophila</i> Sodium Channel 1 (<i>DSC1</i>)	13
1.2.1 Molecular biology of the <i>DSC1</i>	13
1.2.2 Tissue distribution studies of <i>DSC1</i> transcripts and protein	14
1.2.3 Functional studies of <i>DSC1</i> channels	16
1.3 Pyrethroid insecticides act on the voltage-gated sodium channel.....	19
1.3.1 Pyrethrum and pyrethroids.....	19
1.3.2 Classification based on chemical structure and symptoms.....	20
1.3.3 Mode of action	20
1.4 The giant fiber (GF) system	24
1.4.1 The cellular composition and function of the GF system.....	24
1.4.2 The synaptic connectivity among identified neurons of the GF system...	25
1.4.3 The giant fiber system recording.....	25
 CHAPTER 2	
MOLECULAR AND FUNCTIONAL CHARACTERIZATION OF TWENTY <i>DSC1</i>	
cDNA CLONES.....	37
2.1 Abstract.....	38
2.2 Introduction	38
2.3 Materials and methods.....	41
2.3.1 Amplification and cloning of the coding region of the <i>DSC1</i> gene by	
RT-PCR	41
2.3.2 Sequencing of Twenty <i>DSC1</i> cDNA clones.....	43
2.3.3 Expression of <i>DSC1</i> channels in <i>Xenopus</i> Oocytes	43
2.3.4 Electrophysiological recording and data analysis	44
2.3.5 TTX sensitivity assay	45
2.4 Results	45
2.4.1 Sequence comparison of 20 <i>DSC1</i> full length cDNA clones	45
2.4.2 Functional analysis of <i>DSC1</i> channels in <i>Xenopus</i> oocytes	48
2.4.3 <i>DSC1</i> channels are insensitive to TTX	49
2.5 Discussion.....	50

CHAPTER 3	
BEHAVIORAL AND ELECTROPHYSIOLOGICAL CHARACTERIZATION OF	
<i>DSC1</i> KNOCKOUT MUTANTS	66
3.1 Abstract.....	67
3.2 Introduction	68
3.3 Materials and Methods.....	69
3.3.1 Generation of <i>DSC1</i> knockout lines	69
3.3.2 Climbing assay	71
3.3.3 Heat shock assay	72
3.3.4 Recovery assay	72
3.3.5 Starvation assay	73
3.3.6 Giant fiber system (GFS) recording	73
3.3.7 Statistics.....	75
3.4 Results.....	76
3.4.1 <i>DSC1</i> knockout flies exhibit an abnormal jumping response during heat shock	76
3.4.2 <i>DSC1</i> knockout flies showed a defect on recovery from heat shock	76
3.4.3 Abnormal jump response and shortened life span of <i>DSC1</i> knockout flies during starvation	77
3.4.4 Reduced long latency refractory period (LLRP) in response to heat shock in <i>DSC1</i> knockout flies.....	77
3.4.5 The heat-induced reduction of LLRP was rapidly reversed for <i>w¹¹¹⁸</i> flies, but not for <i>DSC1^a</i> flies	79
3.4.6 The long latency refractory period (LLRP) of <i>DSC1</i> knockout flies was reduced by starvation	80
3.5 Discussion.....	81

CHAPTER 4	
<i>DSC1</i> KNOCKOUT MUTANTS ARE MORE SUSCEPTIBLE TO PYRETHROID	
INSECTICIDES	106
4.1 Abstract.....	107
4.2 Introduction	108
4.3 Materials and Methods.....	110
4.3.1 Fly stocks.....	110
4.3.2 Contact bioassay	110
4.3.3 Topical bioassay.....	111
4.3.4 Giant fiber recording	112
4.3.5 Statistics.....	112
4.4 Results.....	113
4.4.1 <i>DSC1</i> knockout flies are more sensitive to pyrethroids, but not to DCJW and fipronil	113
4.4.2 <i>DSC1</i> knockout flies are more sensitive to knockdown by deltamethrin	113
4.4.3 Pyrethroids destabilized the GFS of <i>DSC1</i> knockout flies to a greater extent.....	115
4.5 Discussion.....	117

CHAPTER 5	
SUMMARY AND CONCLUSIONS	139
5.1 Summary and conclusions.....	140
5.2 Future studies	141
BIBLIOGRAPHY	145

LIST OF TABLES

Table 1-1 Tissue distribution and gating properties of nine mammalian voltage-gated sodium channel α subunits	27
Table 1-2 Size and tissue distribution of four β subunits	29
Table 2-1 <i>DSC1</i> cDNA sequencing primers	54
Table 3-1 Response latencies (ms) of the short latency pathway of w^{1118} and <i>DSC1^a</i> flies measured at different time points of heat shock process	86
Table 3-2 Refractory periods (ms) of the short latency pathway of w^{1118} and <i>DSC1^a</i> flies measured at different time points of heat shock process	86
Table 3-3 Response latencies (ms) of the long latency pathway of w^{1118} and <i>DSC1^a</i> flies measured at different time points of heat shock process.....	87
Table 3-4 Refractory periods (ms) of the long latency pathway of w^{1118} and <i>DSC1^a</i> flies measured at different time points of heat shock process.....	87
Table 3-5 Response latencies (ms) of the short latency pathway of w^{1118} and <i>DSC1^a</i> flies measured at different time points of recovery process.....	88
Table 3-6 Refractory periods (ms) of the short latency pathway of w^{1118} and <i>DSC1^a</i> flies measured at different time points of recovery process	88
Table 3-7 Response latencies (ms) of the long latency pathway of w^{1118} and <i>DSC1^a</i> flies measured at different time points of recovery process	89
Table 3-8 Refractory periods (ms) of the long latency pathway of w^{1118} and <i>DSC1^a</i> flies measured at different time points of recovery process	89
Table 3-9 Response latencies and refractory periods of w^{1118} and <i>DSC1^a</i> flies after 72 hours starvation	90
Table 4-1 Susceptibility of w^{1118} and <i>DSC1</i> knockout flies to permethrin (contact bioassay)	121

Table 4-2 Susceptibility of w^{1118} and <i>DSC1</i> knockout flies to bioresmethrin (contact bioassay)	121
Table 4-3 Susceptibility of w^{1118} and <i>DSC1</i> knockout flies to deltamethrin (contact bioassay)	122
Table 4-4 Susceptibility of w^{1118} and <i>DSC1</i> knockout flies to fenvalerate (contact bioassay)	122
Table 4-5 Susceptibility of w^{1118} and <i>DSC1^a</i> flies to DCJW (contact bioassay)	123
Table 4-6 Susceptibility of w^{1118} and <i>DSC1^a</i> flies to fipronil (contact bioassay)	123
Table 4-7 ED ₅₀ of w^{1118} and <i>DSC1^a</i> flies to knockdown phenotype	124
Table 4-8 ED ₅₀ of w^{1118} and <i>DSC1^a</i> flies to abdomen elongation phenotype	124
Table 4-9 Response latencies and refractory periods of male w^{1118} and <i>DSC1^a</i> flies recorded before and after exposure to 4ng/fly bioresmethrin for 15 minutes	125
Table 4-10 Response latencies and refractory periods of male w^{1118} and <i>DSC1^a</i> flies recorded before and after exposure to 0.4ng/fly deltamethrin for 15 minutes	126

LIST OF FIGURES

IMAGES IN THIS DISSERTATION ARE PRESENTED IN COLOR

Figure 1-1 Two-dimensional molecular map of the α -subunit and β -subunit of the voltage-gated sodium channel	30
Figure 1-2 Distribution of alternative exons on <i>para</i> transcripts	32
Figure 1-3 Structure of commercial type I and type II pyrethroids.....	33
Figure 1-4 The <i>Drosophila</i> giant fiber system	35
Figure 2-1 Molecular characterization of 20 <i>DSC1</i> full-length cDNA clones	55
Figure 2-2 Alignment of amino acid sequences of DSC1-1.1, BSC1 and Para proteins	57
Figure 2-3 DSC1 currents recorded from <i>Xenopus</i> oocytes expressing DSC1-1.1 channels	64
Figure 3-1 Generation of <i>DSC1</i> knockout <i>D. melanogaster</i> lines	91
Figure 3-2 Schematic illustration of the giant fiber pathway.....	92
Figure 3-3 <i>DSC1</i> knockout flies have normal locomotor activity but are more jumpy than <i>w¹¹¹⁸</i> flies.	93
Figure 3-4 <i>DSC1</i> knockout flies recover more slowly from heat shock than <i>w¹¹¹⁸</i> flies.	95
Figure 3-5 <i>DSC1</i> knockout flies jump more and die earlier during starvation	96
Figure 3-6 Giant fiber recording carried out on <i>w¹¹¹⁸</i> and <i>DSC1^a</i> flies at different time points during heat shock	98
Figure 3-7 Giant fiber recording carried out on <i>w¹¹¹⁸</i> and <i>DSC1^a</i> flies at different time points during a recovery process after heat shock	101
Figure 3-8 Giant fiber recording in <i>w¹¹¹⁸</i> and <i>DSC1^a</i> flies after 72 hours of starvation	104
Figure 4-1 Deltamethrin dose-response relation to knockdown phenotype of <i>w¹¹¹⁸</i> and <i>DSC1^a</i> flies	127

Figure 4-2 Abdomen elongation phenotype of w^{1118} and $DSC1^a$ flies	128
Figure 4-3 Time-response curves of knockdown phenotype of w^{1118} and $DSC1^a$ flies	130
Figure 4-4 The GFSs of w^{1118} and $DSC1^a$ flies respond differently to bioresmethrin	131
Figure 4-5 The GFSs of w^{1118} and $DSC1^a$ flies respond differently to deltamethrin	134
Figure 4-6 Pyrethroids destabilize the GFS of $DSC1$ knockout flies to a greater extent.....	137

LIST OF ABBREVIATIONS

ANOVA- analysis of variance

AP - action potential

CNS - central nervous system

DCJW - N-decarbomethoxyllated JW062

DLM - dorsal longitudinal muscles

DSC1- *Drosophila* Sodium Channel 1

GABA - γ -aminobutyric acid

GF - giant fiber

GFS – giant fiber system

HRP - horseradish peroxidase

LL - long latency

LLRP - long latency refractory period

PNS - peripheral nervous system

PSI - peripherally synapsing interneuron

SCBIs - sodium channel blocker insecticides

SL - short latency

SLRP - short latency refractory period

TTM - tergotrochanteral muscle

TTX - tetrodotoxin

UAS - upstream activation sequences

VGIC - voltage-gated ion channels

HEPES - 4-(2-hydroxyethyl)-1-piperazineethanesulfonic acid

LC₅₀ - median lethal concentration

ED₅₀ - median effective dose

CHAPTER 1
GENERAL INTRODUCTION

To communicate with the outer world and to maintain the homeostasis of the inner environment, higher metazoans develop a neural system to receive stimulations and make corresponding reactions. Although neurons from different parts of the neural system may have different conformations and functions, they do have a common basic character – they use action potentials to propagate signals.

An axon action potential is a brief, spike-like depolarization that propagates as an electrical wave along dendrites or axons of a neuron. During 1940s and 1950s, Alan Hodgkin and Andrew Huxley performed a series of experiments and demonstrated that action potentials are the result of different ions moving through the cell membrane. They also proposed that the movement of ions is mediated by a channel-like structure on the cell membrane by means of activating (open) and inactivating (close) in response to changes of the membrane potential (Hodgkin and Huxley, 1952). The channel like structures were later found to be transmembrane proteins, termed voltage-gated ion channels (VGIC). These channel proteins are located not only on neurons, but also on muscle and endocrine cells. In response to changes in membrane potential, these channels mediate rapid ion flux through a highly selective pore. Based on the ion selectivity, voltage-gated ion channels can be grouped as sodium channels, potassium channels, calcium channels, chloride channels. Or they can be just named as voltage-gated cation or anion channels if the channel is permeable to more than one type of cation or anion (Catterall, 1992; Catterall et al., 2005).

In this dissertation, research was conducted to study the molecular biology,

electrophysiology, and neurobiology of a novel cation channel, *Drosophila* Sodium Channel 1 (DSC1), in *Drosophila melanogaster*. Because of the sequence similarity between the sodium channel and the DSC1 channel, this chapter will start with the literature on voltage-gated sodium channels.

1.1 Voltage-gated sodium channels

1.1.1 Structure and gating properties of voltage-gated sodium channels

In Hodgkin and Huxley's studies, they demonstrated that the movement of sodium ions through the cell membrane is essential for the generation and propagation of action potentials. They also characterized three key features of the structure mediating sodium currents: 1) voltage-dependent activation; 2) quick inactivation; 3) selective conductance of sodium ions (Hodgkin and Huxley, 1952). Subsequently, many labs tried to isolate the voltage-gated sodium channel. But, for a long time, the sodium channel protein could not be isolated and the topology of the channel protein remained unclear until 1980. By using photo labeling technique, Beneski et al. first isolated a large polypeptide (260 kDa) and a smaller polypeptide (36 kDa) from synaptosomal membranes of the rat brain with a photoactivable derivative of scorpion toxin, a sodium channel specific neurotoxin (Beneski and Catterall, 1980). At the same time, another group also isolated a polypeptide of the channel protein with similar size as the larger one mentioned above from the electric organ of the eel, *Electrophorus electricus*, by using radioactive-labeled tetrodotoxin (TTX), a high affinity blocker of sodium channels (Agnew et al., 1980). The larger peptide was denoted as α subunit while the small

one was denoted as β subunit.

The understanding of voltage-gated sodium channel advanced a big step in 1984 when Noda et al. (Noda et al., 1984) screened the expression library of the eel, *Electrophorus electricus*, with rabbit antiserum to purified *El. electricus* sodium channel peptides and isolated the full-length cDNA encoding the sodium channel α subunit. The deduced amino acid sequence indicated that the α subunit is a transmembrane protein that consists of 1820 amino acids folded into four domains (DI – DIV) with six transmembrane segments (S1 – S6) in each domain (Fig. 1-1) (Catterall, 2000). In segment four of every domain, there are five to eight positively charged amino acids which are considered to sense the change of the membrane potential and guide the opening and closing of the whole channel. These results also support the hypothesis that the α subunit is the pore forming subunit. Later studies on the α subunit of the rat brain sodium channel showed that the α subunit was sufficient to mediate sodium current when expressed in *Xenopus* oocytes indicating that the α subunit is the pore-forming subunit while the β subunit works as a auxiliary subunit (Noda et al., 1986).

Depending upon the membrane potential, voltage gated sodium channels have three functional states: closed (ready to open), activated (opened), and inactivated. At resting membrane potential, sodium channels are closed. When the membrane potential is depolarized to certain level, sodium channels open through a series of conformational changes which is defined as activation. As soon as sodium channel opens, sodium ions flow from the outside of cell membrane to the inside due to the concentration gradient of sodium ions. The

kinetics of the sodium current passing through open channels is very rapid, reaching its peak in less than one millisecond and declining to baseline within a few milliseconds due to a second conformational change defined as fast inactivation.

In the past several decades, an extensive effort has been made to understand the molecular structure and the mechanism of gating of the pore-forming α subunit. Several substructures such as the selectivity filter, voltage sensor, and inactivation gate that were identified are essential for the channel function (Fig. 1-1).

Facilitated by site-directed point mutagenesis and crystal structure studies of a voltage-gated potassium channel, it is a consensus now that all the four domains contribute to form the pore structure of the channel. The S5, S6, and the P-region connecting them from each domain form the inner surface of the channel, while the S1-3 of each domain form the supportive structure and outer surface of the channel. Currently, the inner surface is divided into two structures, outer pore and inner pore, which are facing the extracellular and intracellular sides, respectively. It is well established that the ion selectivity of voltage-gated sodium channels is determined by the amino acids D, E, K, and A in the pore positions of domains I, II, III, and IV, respectively (i.e., the DEKA motif) (Catterall, 2000) (Fig. 1-1). Four other amino acids E, E, M, and D, which are also located in the pore position of domain I-IV, determine the ion selectivity of voltage-gate sodium channel as well (the EEMD motif, Fig. 1-1) (Terlau et al., 1991). These eight amino residues are highly conserved in sodium channels of different species (Catterall, 2000).

Substitution of DEKA with EEEE in a rat brain sodium channel changes the selectivity of a sodium channel to a calcium channel (Heinemann et al., 1992). The amino acids composing the selectivity filter are also the primary binding sites of TTX (Fig. 1-1) (Noda et al., 1989; Du et al., 2009a).

S4 segments of each domain are critical for voltage sensing. The positively charged arginine or lysine residues in S4 of each domain work as voltage sensors responding to the change of the membrane potential (Catterall, 1986; Guy and Seetharamulu, 1986). Mutation of the voltage sensor can profoundly change the activation of sodium channels (Stühmer et al., 1989; Kontis et al., 1997). S1-S4 are coupled with S6 via the S4–S5 linker helix. This coupling enables channel opening and closing upon changes in the membrane potential. It is the nature of the coupling between the S6 and the voltage-sensor domains that decides if the channel will open or not at a certain voltage level (Männikkö et al., 2002). Three comparable models have been proposed to explain the coupling of voltage sensor with surrounding residues and the movement of S4 during activation; the helical screw model, the transporter model, and the paddle model (Börjesson and Elinder, 2008). However, none of the models explain all the experimental results. Currently, the helical screw model has received the most proponents. This model assumes that the positive residues of S4 pair with negatively charged residues in the neighboring segments. When the membrane is depolarized, this pairing is disrupted and the S4 segments move outward causing a conformational change, which results in opening of the channel pore (Catterall, 1992).

Inactivation is a very important gating property of all voltage gated ion

channels; it closes the channel and prevents it from reopening until there has been sufficient time for recovery. During this time, which is also termed as refractory period, the channel will not open no matter how membrane potential alters. This has two functions. The first one is to determine the frequency of action potential firing. The other one is to prevent a breakdown of ionic gradients and cell death during a long depolarization. Many toxins, such as insecticides, and clinically used drugs function by affecting sodium channel inactivation.

For voltage gated sodium channels, normally, inactivation kinetics can be divided into two categories, which are named as fast inactivation and slow inactivation respectively, and each of these can be modulated by cellular factors or accessory subunits. The mechanism of slow inactivation is still controversial, but there is a widely accepted 'ball-and-chain' or 'hinged lid' model for fast inactivation model, in which a cytoplasmic region (the inactivating particle) occludes the pore by binding to a region nearby (the docking site) at certain membrane potential level. The short intracellular linker connecting DIII and DIV is where the 'ball' and the 'chain' locate. Three contiguous hydrophobic amino acid residues, isoleucine, phenylalanine, and methionine (IFM) positioned in the middle of the linker are the central structure of the 'ball' (West et al., 1992). Recently, a fourth amino acid, threonine, was suggested to be important for fast inactivation and redefined the inactivation particle as IFMT motif (Rohl et al., 1999). The docking sites for the inactivating particle include the S4-S5 linkers of DIII and DIV along with the cytoplasmic portion of DIVS6 (Goldin, 2003). The docking sites are buried in the channel protein when channels are closed. It is

hypothesized that the conformational change brought up by the movement of S4 exposes the hydrophobic residues of docking site to the IFMT motif to lock it in and occlude the channel. The conformational change underlining the folding the 'chain' was elucidated by studying the bacteria sodium channel (Zhao et al., 2004). Based on this study, a glycine residue flanking the inactivation particle is suggested to serve as a 'hinge' that facilitates the folding of the 'chain' and binding of to the docking sites with IFMT motif.

1.1.2 The family of mammalian sodium channel α subunit encoding genes

In mammals, the sodium channel is composed of one α subunit and one or two β subunit(s) (Fig. 1-1). A variety of different isoforms of the mammalian voltage-gated sodium channel α subunit have been identified. Based on their amino acid sequences, these isoforms are grouped into three families, Na_v1 - Na_v3 . Na_v1 family has 10 members while Na_v2 and Na_v3 have 3 and 1 members respectively. To date, sodium currents have not been recorded from members of Na_v2 and Na_v3 . However, nine of ten members of the Na_v1 family have been functionally expressed and named as $\text{Na}_v1.1$ - $\text{Na}_v1.9$. These nine mammalian sodium channel isoforms share more than 50% amino acid sequence similarity. They vary in the tissue and developmental distribution, biophysical properties and sensitivity to neurotoxins (Goldin, 2001). $\text{Na}_v1.1$, $\text{Na}_v1.2$, and $\text{Na}_v1.3$ are expressed in the central nervous system (CNS) and are inhibited by nanomolar concentrations of TTX. Recently, $\text{Na}_v1.1$ was also identified in the rat peripheral

nervous system (PNS). Na_v1.4 is expressed in skeletal muscles while Na_v1.5 is expressed in all striated muscles. Na_v1.6 can be detected on both CNS and PNS while Na_v1.7, Na_v1.8, and Na_v1.9 are detected only in PNS.

In addition to variable tissue distribution, Na_v1 isoforms have been verified to have unique developmental profiles. Na_v1.1, Na_v1.2, and Na_v1.6 are present at high levels in the adult CNS, but their presence in embryonic stages and neonatal stages are different. Na_v1.1 becomes detectable shortly after birth, whereas Na_v1.2 becomes detectable during embryonic stages. Both of them reach maximal levels during the adult stage. Na_v1.6 is the most abundant isoform in the adult CNS, but the highest level is in late embryonic and early postnatal periods. Na_v1.3 can only be detected during embryonic and neonatal stages. Transcripts of Na_v1.5 are detectable in neonatal skeletal muscles but are replaced by Na_v1.4 in adult skeletal muscles (Goldin, 2001).

The nine isoforms in Na_v1.1 family exhibit significant differences in functional properties. The voltage required for activation and inactivation of these isoforms is listed in Table 1-1. The combination of channel subtypes in individual cells is a key determinant of the membrane excitability, conduction velocity, and in some tissues the resting membrane potential. Alterations in expression or activity of sodium channel subtypes are associated with several disease states such as epilepsy, stroke, and pain (Wood et al., 2004; Stafstrom, 2007).

1.1.3 The sodium channel β subunit.

Compared with the pore-forming α subunit, the β subunit works as an auxiliary subunit and is not required for the *in vitro* expression of sodium channels. Currently, four β subunit ($\beta 1$ - $\beta 4$) encoding genes have been identified (Goldin, 2001; Yu et al., 2003). The size and tissue distribution of the four β subunits are listed in Table 1-2.

The function of β subunits has two aspects. First, β subunits modulate the channel gating and in turn modulate the excitability of neurons. The sodium current mediated by α subunit alone does not exhibit the “fast-gating” kinetic parameters observed in neurons. Coexpression with $\beta 1$ and $\beta 2$ subunits increases the rate of both activation and inactivation (Isom et al., 1992; Isom et al., 1995). Interaction between the α subunit and β subunits also regulates the persistent sodium current (Aman et al., 2009). Second, β subunits are likely responsible for targeting the sodium channel complex to the node of Ranvier by interacting with other cell adhesion molecules (Ratcliffe et al., 2001). The β subunit is composed of an extracellular immunoglobulin-like fold, a transmembrane α -helix, and a short intracellular tail. The effect of the β subunit is mediated entirely by the extracellular immunoglobulin-like fold. In neurons, the interaction between the α subunit and the β subunits is either covalent or noncovalent. The noncovalently linked β subunits include $\beta 1$ and $\beta 3$ (Isom et al., 1992; Morgan et al., 2000). The loop on the extracellular side of transmembrane segment DIVS6 was suggested as an interaction point of $\beta 1$ subunit. On the other hand, the $\beta 2$ and $\beta 4$ subunits covalently link to the α subunits via disulfide bonds

(Isom et al., 1995; Yu et al., 2003).

1.1.4 The *Drosophila* voltage-gated sodium channel, *Para*.

In contrast to the multiple sodium channel genes in mammals, there is only one functional sodium channel α subunit encoding gene identified in insects (Dong, 2007), such as *para* from *Drosophila* (Loughney et al., 1989). Similar to mammalian counterparts, the insect sodium channel α subunit has four homologous domains, each containing 6 transmembrane segments.

In *Drosophila*, *para* is the only gene that encodes a functional sodium channel. In 1971, Suzuki et al. (Suzuki et al., 1971) isolated a temperature- sensitive paralysis mutant, *para*^{ts}. The phenotype of this mutation is immediate paralysis when exposed to restrictive temperatures (37°C). This phenotype is due to a temperature-dependent blockage in the propagation of nerve action potentials (Siddiqi and Benzer, 1976). In 1989, Loughney *et al.* (Loughney et al., 1989) mapped the *para*^{ts} locus to 14C6-D1 of the X chromosome and cloned the *para* cDNA and genomic DNA as well. The full-length genomic sequence of the *para* gene is about 65 kb whereas the *para* cDNA is 6.8 kb after splicing. In 1997, Warmke *et al.* confirmed that *para* encodes a voltage gated sodium channel and has all of the expected channel functions and electrophysiological properties when expressed in *Xenopus* oocytes (Warmke et al., 1997).

The ortholog of β subunit encoding gene has not been identified in *Drosophila*. However, a structurally different subunit, TipE, has been identified to have a function similar to that of the β subunit (Feng et al., 1995). TipE increases the

Para sodium current in *Xenopus* oocytes when coexpressed with the Para protein. Recently, four *tipE* like genes, termed as *TEH1-4*, were identified (Derst et al., 2006). *TEH1* is CNS-specific while *TEH2*, *TEH3* and *TEH4* are more widely expressed. *TEH1* substantially increases the sodium current amplitude, while *TEH2* and *TEH3* increase the sodium current amplitude to a medium extent. *TEH4* has no effect on the sodium current amplitude. The fast inactivation and recovery from fast inactivation can be altered by coexpression of *TEH1*, indicating that *TEH1* works as an auxiliary subunit.

Although *para* is the only gene that encodes functional sodium channels in *Drosophila*, electrophysiological studies showed that the properties of sodium currents detected in various isolated insect neurons are not exactly the same (O'Dowd et al., 1995; Wicher et al., 2001; Defaix and Lapied, 2005). How do insects achieve the diversity of sodium channels? Recent research from both our lab and others demonstrate that the *para* and other insect sodium channel transcripts undergo extensive alternative splicing and RNA editing.

To date, seven alternative exons, a, b, e, f, h, i, j plus four mutually exclusive exons, c/d, k/l, have been identified in *para* transcripts (Loughney et al., 1989; Thackeray and Ganetzky, 1994; O'Dowd et al., 1995; Thackeray and Ganetzky, 1995; Olson et al., 2008). Detailed study of the *para* transcripts in embryonic and adult stages indicated that alternative splicing of *para* transcripts is developmentally regulated and varies extensively, resulting in a variety of sodium channel isoforms with different gating properties (Thackeray and Ganetzky, 1994; Lin et al., 2009).

RNA editing is another post-transcriptional mechanism to increase the diversity of sodium channels in insects (Liu et al., 2004; Song et al., 2004; Olson et al., 2008). For example, a U-to-C editing event resulting in an F/S1950 amino acid substitution on the Para channel generates a sodium channel variant with a unique persistent current. This RNA editing event and its functional consequence are conserved in the German cockroach sodium channel transcript (Liu et al., 2004).

1.2 The *Drosophila* Sodium Channel 1 (*DSC1*)

1.2.1 Molecular biology of the *DSC1*

The *DSC1* gene was first discovered in the 1980s by probing a *Drosophila* genomic DNA phage library with an eel sodium channel cDNA (Salkoff et al., 1987; Ramaswami and Tanouye, 1989). Sequence analysis predicted that *DSC1* encodes an ion channel that has more than 50% similarity to the vertebrate sodium channel protein. The *DSC1* channel protein has four homologous domains each containing six membrane-spanning segments connected by extracellular or intracellular linkers of various sizes. Sequences that are presumed to be critical for channel function, such as the voltage sensor, S5 and S6, which form the inner surface of channels, and the intracellular linker connecting D3 and D4, show high evolutionary conservation compared to the channels identified in rat and eel. Because of its overall similarity in deduced amino acid sequence with mammalian sodium channel, *DSC1* was proposed to encode a putative sodium channel protein. *In situ* hybridization showed that *DSC1* locates within a single

site at region 60E on chromosome 2R.

1.2.2 Tissue distribution studies of DSC1 transcripts and protein

In 1994, Chang-Sook Hong and Barry Ganetzky (Hong and Ganetzky, 1994) examined the spatial and temporal expression patterns of both *para* and *DSC1* transcripts in 12th-, 13th-, 15th- and 17th-stage embryos, 3rd instar larvae, 25 and 72 hr old pupae, and the adult. In embryos, the 5' un-translated region of *para* gene was detected during late stage 12, suggesting the initiation of *para* transcription. The transcripts were detected in neurons but not in neuroblasts of both CNS and PNS during early stage 13 and the following stages. *DSC1* transcripts were detected in cells clustered along the ventral nerve cord at early stage 12 prior to germ band retraction. In PNS, several cells appearing in the dorsal wall of the foregut are *DSC1* transcripts positive. The position of these cells indicates that they may belong to the stomatogastric nervous system. By stage 15, *DSC1* is expressed in a regular pattern in some cells located along the longitudinal commissures of the CNS. In the PNS of the same stage, *DSC1* transcripts are expressed prominently in the frontal ganglionic region. Also at this stage, there are several cells in the CNS labeled by *DSC1* probe, but they may not be neurons since they could not be labeled by a neuron-specific anti-HRP antibody. In third instar larvae, *para* transcripts were detected in the CNS including larval brain, ventral ganglia, and the PNS, such as eye discs and leg discs. In the CNS, *para* expression was limited to mature neurons that regulated the behavior of the larva. The *para* expression pattern in ventral ganglia reflects

the continued expression of *para* in embryonically derived neurons. In the PNS, *para* transcripts detected in photoreceptor cells in eye discs and some sensory neurons in leg discs. However, in this stage, *DSC1* transcripts were identified only in the laminar region of the optic lobes. Interestingly, the expression pattern of both *para* and *DSC1* in the CNS were completely overlapped in the pupal and adult stages. Transcripts of these two genes were present in brain, thoracic ganglion, visual system, and antennal neurons. However, the expression of *para* and *DSC1* was distinctive in the developing pupal wing. At 25 hours after pupariation, only transcripts of *para*, but not *DSC1*, were detected in some sensory neurons along the anterior margin of the wing and in campaniform sensilla along the third wing vein.

Castella et al. (Castella et al., 2001) used a *DSC1* polyclonal antibody and a neuronal specific monoclonal antibody, 22C10, to study the tissue distribution of *DSC1* channels in the nervous systems of adult *D. melanogaster*. *DSC1* expression was detected exclusively in neurons, but not in other excitable cells such as muscle cells. In the CNS, *DSC1* is mainly distributed in synaptic regions and axonal tracts in the brain and in thoracic ganglions. However, *DSC1* was not detected in the cell body of neurons, which is a main difference from *Para*. This is not consistent with the in situ hybridization study by Hong and Ganetzky (Hong and Ganetzky, 1994), which showed that the *DSC1* transcripts were localized in the cortical cell bodies. In the PNS, the distribution of the *DSC1* protein is strikingly wide. *DSC1* signal was very weak in compound eyes but strong in the antennal sensilla and nerves. *DSC1* was also detected on sensory neurons and

motor neurons of the proboscis, thoracic muscles, legs, anal plate, and the penis apparatus.

1.2.3 Functional studies of DSC1 channels

To study the function of the DSC1 channel Germeraad et al. (Germeraad et al., 1992) examined sodium currents from primary cultured embryonic neurons of a *DSC1* homozygous deficiency line using the voltage-clamp technique. Their results suggested that these DSC1 absent neurons expressed sodium currents similar to those from the wild type neurons, indicating that *para* is the major sodium channel encoding gene in embryonic neurons.

One study suggested a functional role of the DSC1 channel in olfaction (Kulkarni et al., 2002). A *P*-element insertion line, *smi60E*, exhibits a three-fold shift in the dose response for avoidance of benzaldehyde, a repellent odorant to *Drosophila*, toward higher odorant concentrations. The *P*-element insertion was mapped to the second intron of the *DSC1* gene. To verify the olfactory defect phenotype is due to the *P*-element insertion, *smi60E* was crossed with 6 EP insertion lines, which are mapped 58 bp downstream of the *P*-element insertion site at the same intron of the *DSC1* gene. The heterozygous offspring failed to complement the olfactory defect, indicating the association of the *P*-element insertion and the olfactory defect. There is another gene, *L41*, at the insertion site. Southern blot analysis showed a 66% reduction in the *DSC1* transcripts and 41% reduction in the *L41* transcripts. When the *P*-element was excised, the olfactory

impairment could be rescued even though the transcription level of *L41* was not restored, suggesting that the olfactory defect is not associated with *L41*.

Although *DSC1* was isolated two decades ago, the function of the *DSC1* channel remains undetermined. Liu et al. (Liu et al., 2001) cloned a *DSC1* ortholog, *BSC1*, from *Blattella germanica*. The amino acid sequences between the predicted *DSC1* and *BSC1* proteins share 81%, 78%, 80%, and 88% identities in the transmembrane domains I-IV, respectively. Furthermore, *BSC1* transcripts are found to be alternatively spliced in a tissue-specific and developmental stage-specific manner.

The *BSC1* channel was successfully expressed in *Xenopus* oocytes and was found to function as a cation channel that is permeable to Na^+ , K^+ , Ca^{2+} , and Ba^{2+} (Zhou et al., 2004). Interestingly, both Co^{2+} and Cd^{2+} block the *BSC1* channel, similar to their effects on voltage-gated calcium channels (Hille, 1992). The *BSC1* channel is permeable to monovalent cations (i.e., Na^+ , K^+) in the absence of external Ca^{2+} . The permeability ratios were $P_{\text{Ba}}/P_{\text{K}} \approx 30$ and $P_{\text{Ba}}/P_{\text{Na}} \approx 22$ for the *BSC1* channel, indicating that the *BSC1* channel is more permeable to $\text{Ca}^{2+}/\text{Ba}^{2+}$ than to either Na^+ or K^+ . That is much lower than the permeability ratio for L-type Ca^{2+} channels ($P_{\text{Ba}}/P_{\text{Na}} \approx 470$ and $P_{\text{Ca}}/P_{\text{Na}} \approx 1170$) and much higher than the ratio for sodium channels ($P_{\text{Ca}}/P_{\text{Na}} \approx 0.1$) (Hille, 1992).

In addition to the unique ion selectivity, the *BSC1* channel is also different from voltage-gated sodium channels with respect to the kinetics of activation, deactivation, and inactivation. The *BSC1* channel is a high-voltage-activated

channel with a half-maximal activation voltage of 50 ± 8 mV. Both activation and inactivation of the BSC1 channel are slower than those of sodium channels, resulting in a large tail current upon repolarization. It took a 40-ms depolarization to fully activate the channel, and there was no significant inactivation observed when BSC1 currents were recorded with 40-ms depolarization pulses from -50 to 80 mV from the holding potential of -100 mV. However, complete inactivation was evident when a long depolarization pulse (500 ms) was applied.

As described in Chapter 1.1.1, single amino acids located in the P-regions of four domains determine the ion selectivity of sodium channels and calcium channels. These amino acids are D, E, K, and A in sodium channels and E, E, E, and E in calcium channels, respectively. Comparison of the sequence of BSC1 with voltage-gated sodium and calcium channels shows that the BSC1 channel has D, E, E, and A at the same positions, respectively. The permeability to Ba^{2+} of the BSC1 channel is reduced when the second E was substituted with K. Moreover, the permeability to Na^{+} was enhanced with the same amino acid substitution, indicating that the E residue in domain III is important for the selectivity of the BSC1 channel toward Ba^{2+} or Ca^{2+} . Phylogenetic analysis of the relationship between the BSC1 channel and other voltage-gated sodium and calcium channels suggests that BSC1 and DSC1 channels belong to a novel family of ion channels that are closely related to calcium channels as they are to sodium channels (Zhou et al., 2004).

1.3 Pyrethroid insecticides act on the voltage-gated sodium channel

1.3.1 Pyrethrum and pyrethroids

Pyrethrins are a series of natural compounds found in pyrethrum extract from chrysanthemum flowers. The insecticidal properties of pyrethrins were discovered two centuries ago (McLaughlin, 1973; Casida, 1980). They are esters of chrysanthemic acid (Fig. 1-3). However, because of its instability under the sun, the pyrethrum extract and pyrethrins are mainly used in control of household insect pests, such as mosquitoes and houseflies, not used as an agricultural insecticide. With an increasing demand for organically grown products, use of pyrethrum extract has also increased.

The synthetic analogs of the pyrethrins, termed as pyrethroids, are a group of environmentally friendly, highly effective and selective insecticides which are used globally for pest control. The first several pyrethroids were discovered from 1940 to 1970 (Elliott and Janes, 1978; Elliott, 1980). A few of these compounds, such as allethrin, tetramethrin, and resmethrin, exhibited excellent insecticidal activity. However, similar to pyrethrins, they are not very stable in the environment. The successful synthesis of permethrin in 1973 by Elliott and coworkers (Elliott et al., 1973) announced the first potent and photostable pyrethroid, opening a new era of synthetic pyrethroid research and development. Following permethrin, several pyrethroids, such as cypermethrin and deltamethrin, were synthesized and proven to be highly potent and effective for pest control (Hall, 1978). Nowadays, numerous photostable pyrethroids have emerged that exhibit an extreme efficiency as agricultural insecticides (Elliott and Janes, 1978; Elliott, 1980) (Fig.

1-3).

1.3.2 Classification based on chemical structure and symptoms

Based on whether there is an α -cyano-3-phenoxybenzyl alcohol structure in the molecule, pyrethroids are grouped into two groups, named as type I and type II pyrethroids. (Fig. 1-3). Type I pyrethroids do not contain the α -cyano-3-phenoxybenzyl alcohol structure while type II pyrethroids do. Interestingly, type I and type II pyrethroids can cause different poisoning symptoms (Gray and Soderlund, 1985; Soderlund and Bloomquist, 1989; Bloomquist, 1993). At doses toxic to mammals, type I pyrethroids cause a whole-body tremor, or T syndrome (Verschoyle and Aldridge, 1980) while type II pyrethroids produce choreoathetosis (sinuous writhing) and profuse salivation, indicating an intoxication to the CNS (Verschoyle and Aldridge, 1980). Differential poisoning syndromes caused by type I and type II pyrethroids also occur in insects, but they are less distinct than those observed in mammals (Soderlund and Bloomquist, 1989; Bloomquist, 1993). Actually, the type I and type II classifications are not absolute in either insects or mammals, and certain compounds show effects intermediate between the two classes (Soderlund and Bloomquist, 1989).

1.3.3 Mode of action

The symptoms of pyrethroids intoxication suggest a disruption of the nervous system. The earliest electrophysiological study on the mechanisms of pyrethrum

insecticides was carried out using extracellular electrodes to record compound nerve action potentials in insect and crayfish ventral nerve cord preparations (Lowenstein, 1942; Welsh and Gordon, 1947). Isolated nerve fibers exposed to pyrethrins generate repetitive discharges in response to a single stimulus. These findings were confirmed in the first intracellular recording studies (Narahashi, 1962b, a), in which low concentrations of allethrin prolonged the falling phase of the nerve action potential in cockroach giant fiber preparations and induced repetitive discharges, whereas high concentrations of the same compound reduced the amplitude of the action potential, eventually blocking nerve conduction. These results were also the first to indicate that the voltage-gated sodium channel is one of the primary targets of allethrin in modulating the nerve action potential. Following studies on invertebrate giant axons (Clements and May, 1977; Lund and Narahashi, 1983) and frog sciatic nerve (Vijverberg et al., 1982) have shown that type I compounds produce repetitive discharges similar to those described for pyrethrins and allethrin, whereas type II compounds do not produce repetitive discharges, but lead to stimulus-dependent nerve depolarization and blockage of the action potential.

Voltage clamp technique brought the research on the mode of action of pyrethroids to a new level. With this technique, studies using various nerve preparations have shown that the repetitive firing and depolarization caused by pyrethroids resulted from prolonged opening of sodium channels (Soderlund and Bloomquist, 1989; Vijverberg and van der Bercken, 1990; Narahashi, 1992; Bloomquist, 1993). Pyrethroids slowed or delayed the inactivation of sodium

channels resulting in a prolonged open state. Pyrethroids also produced a slowly decaying sodium current, known as tail current, that continues to flow after the membrane is repolarized. At the cellular level, the delayed shutting of pyrethroid-modified sodium channels leads to a persistent inward current to flow after an action potential, resulting in repetitive firing (type I pyrethroids) and depolarization the nerve membrane (type II pyrethroids) (Soderlund and Bloomquist, 1989; Vijverberg and van der Bercken, 1990; Narahashi, 1992; Bloomquist, 1993). Voltage-clamp experiments also showed different decay kinetics of the tail current induced by type I and type II pyrethroids. The decay of tail currents induced by type II pyrethroids is at least one order of magnitude slower than those induced by type I pyrethroids. These quantitative differences in tail-current decay kinetics between type I and type II pyrethroids may account for their different actions on the nervous system (Dong, 2007).

The patch-clamp technique is another powerful tool for studies of the mode of action of pyrethroids. This method allows more detailed analysis of pyrethroid modification of sodium currents at the single-channel level. Analysis of single sodium channel currents in the presence of pyrethroids revealed a population of channels with slowed kinetic transitions between different channel states (Narahashi, 1992; Bloomquist, 1993). Channels modified by pyrethroids display normal single-channel conductance but exhibit a prolonged open state with altered activation kinetics (Narahashi, 1992; Bloomquist, 1993). Single-channel and tail-current analysis indicate that the open state of the sodium channel is more apt to be modified by pyrethroids than the closed state due to lower affinity

for this state (Narahashi, 1992). The higher affinity for open channel could, at least in part, explain the stimulus-dependent effects of the pyrethroids (Narahashi, 1992).

Wide use of pyrethroids in pest control stems not only from their high efficiency, but also their relatively lower toxicity to mammals. Pyrethroids exhibit a highly selective toxicity to insects over mammals. Potency evaluation *in vitro* showed that allethrin was 1000-fold more potent on cockroach sodium channels than rat TTX- sensitive sodium channels (Narahashi et al., 2007). Another important factor affecting pyrethroid activity is temperature. Pyrethroids are much more potent at low temperatures than at high temperatures. The enhanced sensitivity of sodium channel to pyrethroids is due to increase in the time constant and the amount of charge during the tail current (Song and Narahashi, 1996; Motomura and Narahashi, 2000). This temperature dependence becomes an important factor for pyrethroids safety because there is a 10°C difference in body temperature between mammals and insects.

Voltage-gated sodium channels are the primary target of pyrethroids. Nevertheless, there are several lines of evidences suggesting that pyrethroids also affect other ion channels (Ray and Fry, 2006), such as voltage-gated calcium channels (Shafer and Meyer, 2004), and chloride channels (Burr and Ray, 2004). However, it is still premature to draw a solid conclusion that these channels are also important to the acute neurotoxicity of pyrethroids.

1.4 The giant fiber (GF) system

1.4.1 The cellular composition and function of the GF system

Giant nerve fibers are a group of neurons, which are associated with animal escape response in many invertebrates and some lower vertebrates, including *D. melanogaster* (Trimarchi and Schneiderman, 1995c; Trimarchi and Schneiderman, 1995b; Trimarchi and Schneiderman, 1995a). The classic case is when there is a predator approaching; the shadow of the predator stimulates the visual system of the insect and initiates a powerful jump with the middle legs. Once the fly is airborne, flight usually follows (Trimarchi and Schneiderman, 1995c). The entire circuit, including giant fiber neurons, interneurons, motor neurons, and muscle cells, is termed as the GF system and is schematized in Fig. 1-4.

In *Drosophila*, the somas of giant fiber neurons are located in the brain with their large axons extending to the thorax, where the terminals of the giant fiber axon form synaptic connections with two different neurons: a large motoneuron that innervates the tergotrochanteral muscle (TTM) and a peripherally synapsing interneuron (PSI). The PSI axon crosses the midline and synapses with motor neurons, which innervate the dorsal longitudinal muscle (DLM). The GF neurons on each side are connected by the giant commissural interneurons (GCIs) that ensure the right and left sides respond simultaneously. Three groups of thoracic muscles, the TTM, DLMs, and dorsoventral muscles (DVMs) (not shown in Fig. 1-4), provide the major forces for jump and flight. Visually evoked jump-flight behavior is mediated by the GF system (Trimarchi and Schneiderman, 1995b; Trimarchi and Schneiderman, 1995a) and is assumed to be an escape reflex.

1.4.2 The synaptic connectivity among identified neurons of the GF system

As illustrated in Fig. 1-4 B, the GF-TTMn and GF-PSI synapses are mixed electrochemical synapses. However, the neurotransmitter of these mixed-synapses is not very clear. The neurotransmitter of the synapse between the PSI and DLM motor neurons is acetylcholine (Gorczyca and Hall, 1984), while glutamate is the transmitter at neuromuscular junctions in the GFS (Kosaka and Ikeda, 1983; Koenig and Ikeda, 2005).

1.4.3 The giant fiber system recording

In the laboratory, the GF pathway can be triggered from different neurons by giving electronic stimuli through electrodes poking into either compound eyes or thorax (Fig. 1-4 C). The activity of the GFS can be reflected by recording muscle potentials from either the TTM or DLM (Tanouye and Wyman, 1980). The time interval between the stimulus and the first muscle potential is termed the response latency. It reflects the time required for the stimulation signal to conduct from activated neurons to the innervated muscle where the recording electrode is located. Based on the length of latency, the responses can be grouped into two classes, long latency (LL) and short latency (SL) responses. When a relatively low-strength stimulus (i.e., low voltage) is applied, a muscle potential with longer response latency is usually elicited. As the strength of the stimulus becomes higher, the muscle response with shorter response latency is triggered. The difference between these distinct response latencies is due to the involvement of afferent neurons presynaptic to the giant fiber neuron (Fig. 1-4 C). The afferent

neurons are involved in the long latency response, but will be bypassed when higher strength stimuli are applied. Therefore, the giant fiber neurons are activated directly resulting in a shorter response latency. Based on the difference, the GFS can be referred as long latency and short latency pathways. The lowest voltage by which the long latency response is elicited is termed the long latency threshold and the lowest voltage to elicit the short latency response is called the short latency threshold. When a pair of identical pulses separated by a variable interval is delivered, the longest interval at which a muscle potential is elicited by the first pulse but not by the second one is termed the refractory period, which is an indication of the stability of the GF circuit. Both long and short latency pathways exhibit distinct refractory period. Usually, the long latency refractory period (LLRP) is around 40 ms and has big variations (around 10 ms or more), while the short latency refractory period (SLRP) is less than 10 ms and varies much less than the LLRP.

Table 1-1. Tissue distribution and gating properties of nine mammalian voltage-gated sodium channel α subunits (Goldin, 2001; Catterall et al., 2005).

Isoform	Species	Primary Tissue Distribution	Activation (mV)	Inactivation (mV)
Na _v 1.1	Rat Guinea pig	CNS, PNS	-33	-72
Na _v 1.2	Rat Human	CNS	-24	-53
Na _v 1.3	Rat	CNS	-23 to -26	-65 to -69
Na _v 1.4	Rat Human	Skeletal muscle	-30 ^a or -26 ^b	-50.1 ^c or -56 ^d
Na _v 1.5	Rat Human	Denervated skeletal muscle, heart muscle	-47 -56 ^e -27 ^f	-84 -100 ^e -61 ^f
Na _v 1.6	Rat Human Mouse Guinea pig	CNS, PNS	-8.8 ^g -17 ^h -26 ⁱ -37.7 ^j	-55 ^k -51 ^l -97.6 ^m
Na _v 1.7	Rat Human Rabbit	PNS	-31 ⁿ -45 ^o	-65 ^p -78 ^q -60.5 ^r -39.6 ^s
Na _v 1.8	Rat Mouse Dog	PNS	-16 to -21 ^t	~-30 ^t
Na _v 1.9	Rat Mouse Human	PNS	-47 to -54 ^t	-44 to -54 ^t

a rat α subunit in *Xenopus* oocytes

b human α subunit in CHO cells

c human α subunit in *Xenopus* oocytes with 200-ms depolarizations using macropatch voltage-clamp

d human α subunit in CHO cells with 500-ms depolarizations

e with phenylalanine as the major anion in the intracellular solution

f with aspartate as the major anion in the intracellular solution

g mouse α subunit in *xenopus* oocytes with cut-open oocyte voltage-clamp

Table 1-1 (continued)

- h mouse α subunit with $\beta 1$ and $\beta 2$ in xenopus oocytes with cut-open oocyte voltage-clamp
- i mouse α subunit with inactivation removed and b1 and b2 in xenopus oocytes with cut-open oocyte voltage-clamp
- j rat α subunit in *Xenopus* oocytes with macropatch voltage-clamp
- k mouse α subunit in *Xenopus* oocytes with 500-ms depolarizations using two-electrode voltage-clamp
- l mouse α subunit with $\beta 1$ and $\beta 2$ in *Xenopus* oocytes with 500-ms depolarizations using two-electrode voltage-clamp
- m rat α subunit in *Xenopus* oocytes with 5-s depolarizations using macropatch voltage-clamp
- n rat α subunit in *Xenopus* oocytes with macropatch
- o TTX-sensitive current in DRG neurons
- p TTX-sensitive current in DRG neurons with 50-ms to 1-s depolarizations using whole-cell patch clamp
- q rat α subunit in *Xenopus* oocytes with 10-s depolarizations using two-electrode voltage-clamp
- r human α subunit in HEK cells with 2-s depolarizations using whole-cell patch clamp
- s human α subunit with $\beta 1$ subunit in HEK cells with 2-s depolarizations using whole-cell patch clamp
- t rat DRG neurons

Table 1-2. Size and tissue distribution of four β subunits (Goldin, 2001; Yu et al., 2003).

Name	Species	Tissue	Size (aa)	Genbank access number
Nav β 1.1	Rat	CNS	218	M91808
	Human			L10338
	Rabbit			U35382
Nav β 1.2	Rat	CNS	215	U37026
				U37147
Nav β 1.3	Human	CNS	215	AF007783
	Rat			AJ243395
Nav β 1.4	Human	CNS, PNS	228	AJ243396
	Human, mouse, rat			BK001031.1
				BK001030.1
				AY149967.1

Figure 1-1. Two-dimensional molecular map of the α -subunit and β -subunit of the voltage-gated sodium channel showing how they fold and cross the plasma membrane. The α -subunit is composed of four homologous domains (I to IV), each of which contains six transmembrane segments (1 to 6). Cylinders represent α -helical transmembrane segments. Linkers and connections are illustrated as solid lines, roughly in proportion to their length in the amino-acid sequence of the sodium channel. Positive charged amino acid residues are indicated (+) on the S4 transmembrane segments, which serve as voltage sensors. The S5 and S6 segments and the P-region between them together form the walls of the sodium-ion-conducting pore. Circles indicate the positions of amino acids DEKA and EEDD which are important for ion conductance and selectivity ('+' positively charged, '-' negatively charged) that are important for ion conductance and selectivity. Solid gray circle indicates the inactivation particle, IFMT (isoleucine, phenylalanine, methionine, threonine), which is thought to fold into and block the ion-conducting pore. The β subunit is composed of an extracellular immunoglobulin-like fold, a transmembrane α -helix, and a short intracellular tail. One α subunit can combine with one to three different β subunits to form the sodium channel complex. (Modified from Catterall, 2000)

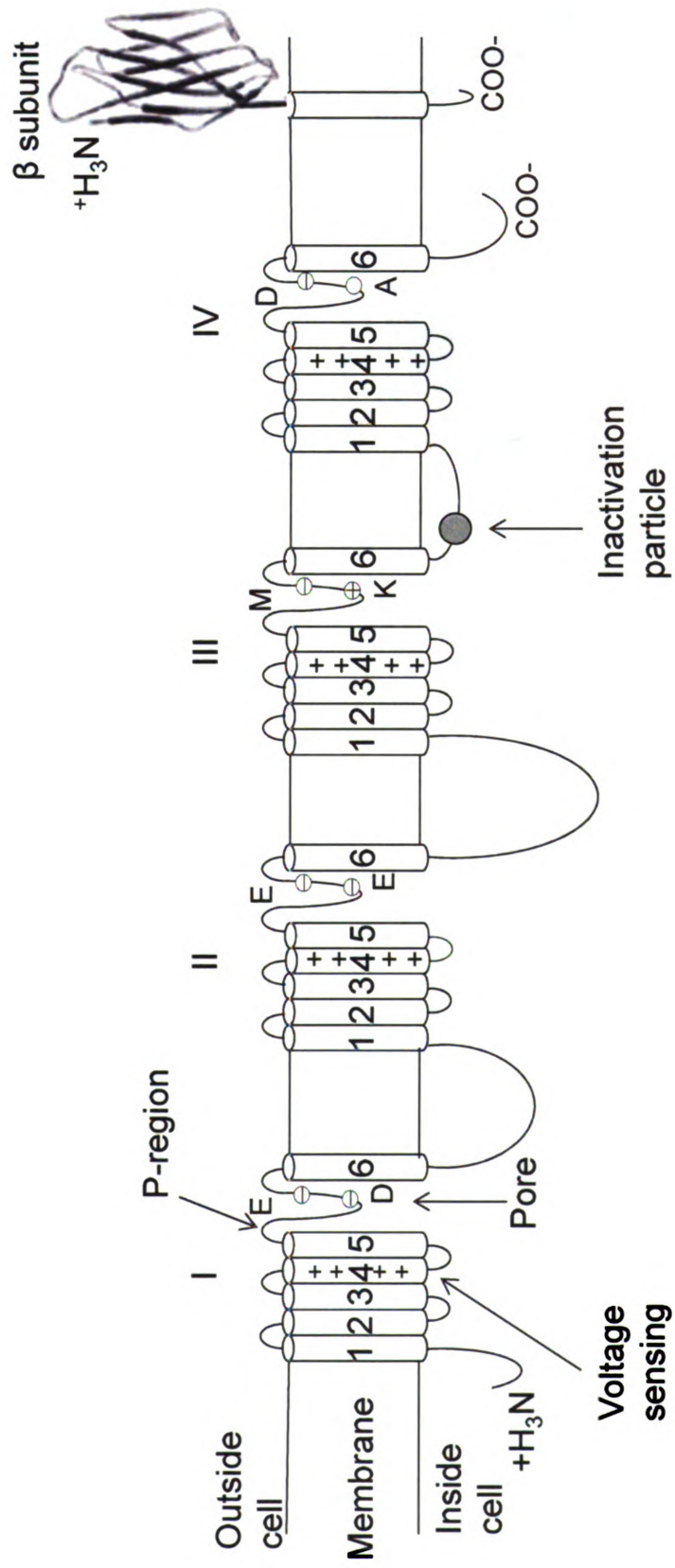


Figure 1-2. Distribution of alternative exons on *para* transcripts. A schematic diagram of the Para protein topology labeled with names and locations of 11 alternative exons identified in *para* transcripts. Exons a, b, e, f, h, i, and j are optional exons. Exons b/c and l/k are two pairs of mutually exclusive exons. (Adapted from Olson et al., 2008)

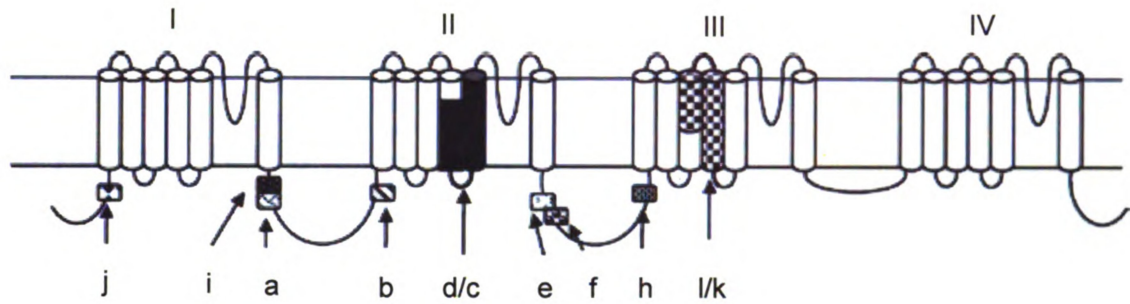
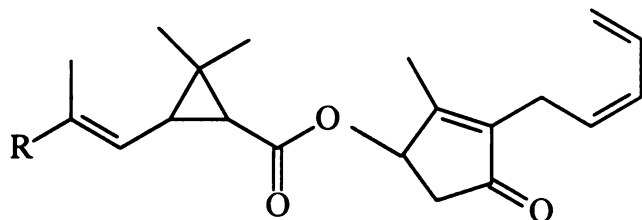


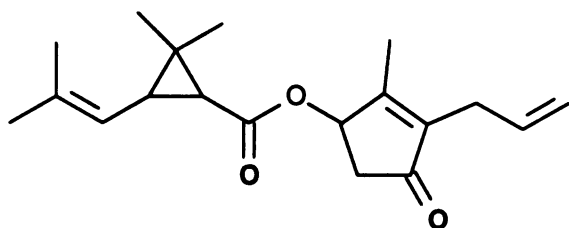
Figure 1-3. Structure of commercial type I (A) and type II (B) pyrethroids. The cyano group in the structure of type II pyrethroids is marked.

A

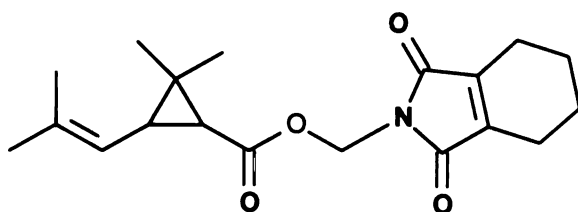


Pyrethrin I $R=CH_3$

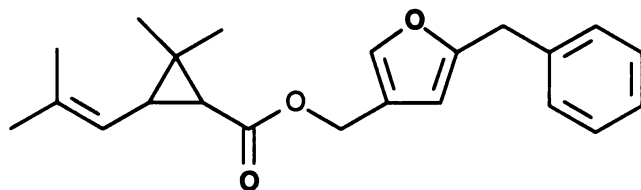
Pyrethrin II $R=COOCH_3$



Allethrin

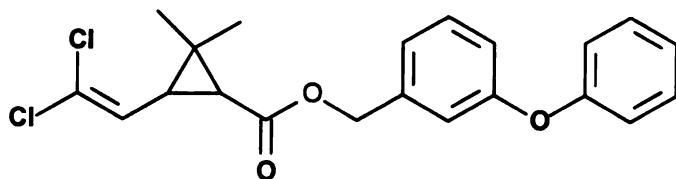


Tetramethrin



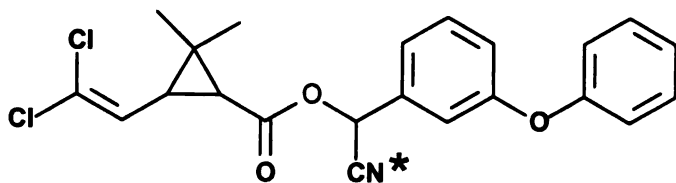
Bioresmethrin

Figure 1-3 (continued)

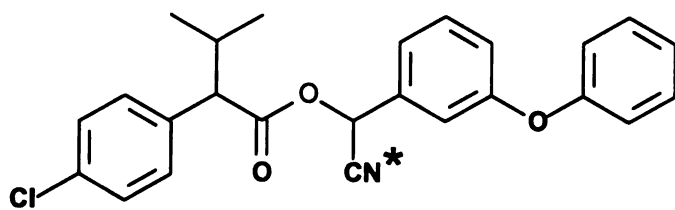


Permethrin

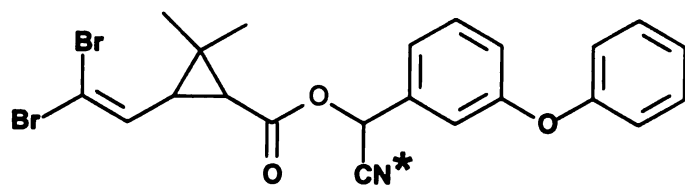
B



Cypermethrin



Fenvalerate



Deltamethrin

Figure 1-4. The *Drosophila* giant fiber system. **A.** Schematic display of the position of the *Drosophila* CNS and the neurons and muscles of the giant fiber (GF) system. **B.** The nature of the synaptic connections in the GF system. In the brain, the giant fibers (GF) form electrical synapses with the giant commissural interneurons (GCIs). In the mesothoracic neuromere, the GFs form mixed electrochemical synapses with the motoneurons (TTMn) of the tergotrochanteral muscle (TTM; left) and with the peripherally synapsing interneuron (PSI). The PSI forms chemical synapses with the motoneurons (DLMns) of the dorsal longitudinal muscles (DLMs; right). The neuromuscular junctions are chemical synapses. Note that in **A** only one of the TTMn axons is shown exiting the CNS and contacting the muscle on the left side and one set of DLMns and the corresponding neuromuscular junctions are shown on the right side; in **B** only one side of the bilateral pathway and two of the DLMns and DLMs are shown (modified from Allen, 2006). **C.** Schematic illustration of the giant fiber pathway (one side shown). High-voltage stimulation (high) activates the cervical giant fiber (CGF) to induce a short-latency response, whereas low voltage stimulation (low) excites brain afferent neurons to trigger a long-latency response. (TTM) Tergotrochanteral muscle; (TTMn) TTM motoneuron; (DLM) dorsal longitudinal muscle; (DLMn) DLM motoneuron; (PSI) peripherally synapsing interneuron. (Adapted from Engel et al. 2000)

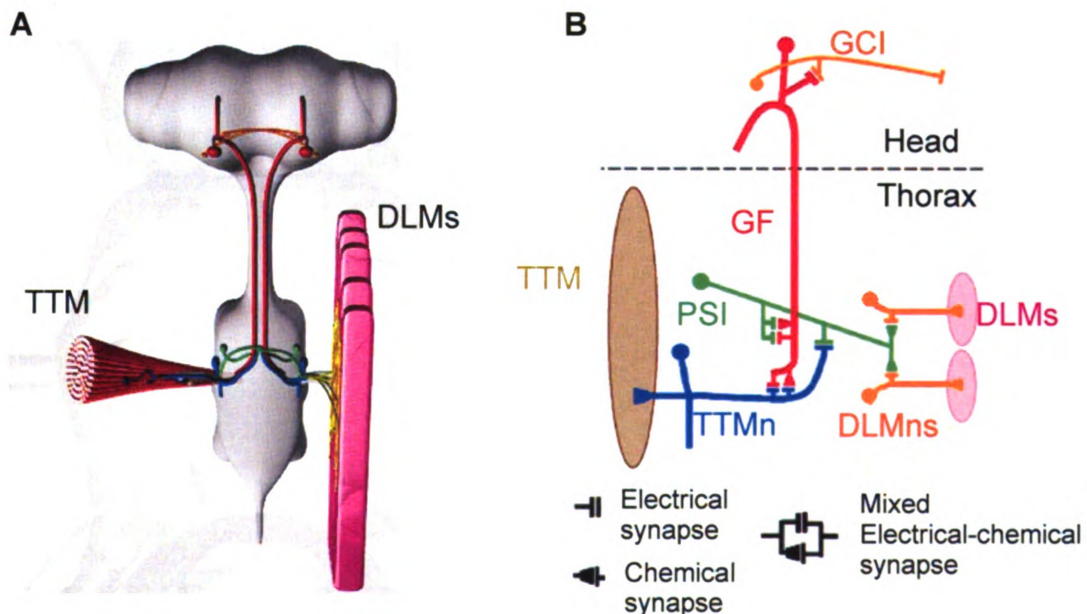
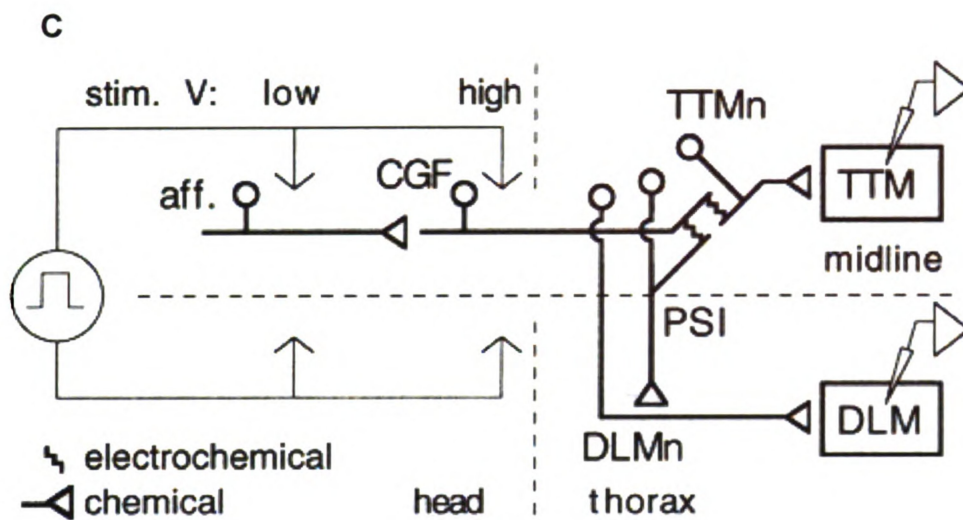


Figure 1-4 (continued)



CHAPTER 2

MOLECULAR AND FUNCTIONAL CHARACTERIZATION OF TWENTY

***DSC1* cDNA CLONES**

2.1 Abstract

Drosophila Sodium Channel 1 (DSC1) was predicted to encode a sodium channel due to a high sequence similarity with vertebrate and invertebrate sodium channel genes. However, *BSC1*, a *DSC1* ortholog in *Blattella germanica*, was recently shown to encode a cation channel with ion selectivity towards Ca^{2+} in *Xenopus* oocytes. To functionally characterize the DSC1 channel, we isolated 20 cDNA clones that covered the entire coding region of the *DSC1* gene from adults of *D. melanogaster*. The 20 clones can be grouped into nine splice types. Sequence analysis revealed ten optional exons, four of which contain in-frame stop codons. Optional exons containing premature stop codons were found in seven clones. Only three variants generated DSC1 currents when expressed in *Xenopus* oocytes. Like the BSC1 channel, all three functional DSC1 channels are permeable to Ca^{2+} and Ba^{2+} , and also to Na^+ in the absence of external Ca^{2+} . Furthermore, the DSC1 channel is insensitive to tetrodotoxin (TTX), a potent and specific sodium channel blocker. Our study shows that *DSC1* undergoes extensive alternative splicing and encodes a voltage-gated cation channel similar to the BSC1 channel in *B. germanica*.

2.2 Introduction

Voltage-gated ion channels are a diverse group of integral transmembrane proteins that are essential for electrical signaling in neurons, muscle and

endocrine cells. In response to changes in membrane potential, these channels mediate rapid ion flux through a highly selective pore. Voltage-gated sodium and calcium channels are responsible for inward movement of sodium and calcium ions, respectively, during electrical signaling in cell membranes. Both sodium and calcium channels consist of a large α -subunit and a variable number of smaller subunits (Yu et al., 2005). The α -subunit forms the ion conducting pore while the associated subunits modulate channel expression and gating. Although the amino acid sequences of the pore-forming α -subunits of sodium and calcium channels are quite different, the overall topology is similar, which consists of four repeated homologous domains (I-IV), each having six membrane spanning segments (S1-S6). The S1-S4 segments serve as the voltage sensing module and the S5 and S6 segments and their connecting P loop serve as a pore-forming module (Catterall, 2000).

Analysis of the genome of *Drosophila melanogaster* revealed only two sodium channel-like sequences, *para*, and *DSC1* (Littleton and Ganetzky, 2000). It is well-established that *para* and *para*-orthologs in other insect species encode functional sodium channels (Warmke et al., 1997). Extensive alternative splicing and RNA editing of the transcripts of *para* and *para*-orthologs generate molecular and functional diversity of sodium channels in insects (Dong, 2007; Olson et al., 2008; Lin et al., 2009). *DSC1* (*Drosophila Sodium Channel 1*) was first discovered two decades ago by probing a *Drosophila* genomic DNA library with an eel sodium channel cDNA (Salkoff et al., 1987). It was predicted to encode a sodium channel based on its overall similarity in deduced amino acid sequence

and domain organization with eel and mammalian sodium channels. However, the function of the DSC1 channel remains largely unknown. A *P*-element insertion in the second intron of *DSC1* in a *smell-impaired (smi)* mutant, *smi60E*, reduced *DSC1* transcript level by two-fold and results in a three-fold decrease in olfactory response to benzaldehyde (Kulkarni et al., 2002), suggesting that the DSC1 channel plays an important role in olfaction. Sodium currents in embryonic neurons from homozygotes for a chromosome deficiency at 60E5/6, where the DSC1 gene is located, were similar to those from wild-type neurons, indicating that *para*, not *DSC1*, is the primary sodium channel gene in embryonic neurons (Germeraad et al., 1992). Comparative studies revealed different spatial and temporal expression patterns of *DSC1* and *para* transcripts and proteins, particularly in the adult peripheral nervous system, suggesting different functions of DSC1 and Para channels in the nervous system. For example, in adults, expression patterns of *DSC1* and *para* transcripts overlap in the CNS based on the RNA in situ hybridization study (Hong and Ganetzky, 1994). However, an immunohistochemical study indicated that DSC1 channels were only distributed in synaptic regions and axonal tracts while Para channels were also localized on cell bodies in the PNS. Only weak DSC1 signal could be detected from compound eyes where the expression level of Para channels is high. The dense localization of the DSC1 protein was detected in the nerve endings of motor neurons in the thorax, leg muscles and also in the proboscis, tibia and tarsi, where the mechanoreceptors or chemosensory organs are located (Castella et al., 2001).

DSC1 orthologs have been identified in other insect species including *Blattella germanica*, and *Heliothis virescens* (Park et al., 1999; Liu et al., 2001). Tissue-specific alternative splicing of *BSC1* has been reported (Liu et al., 2001). More significantly, *BSC1* was confirmed to encode a cation channel with ion selectivity toward Ca^{2+} more than Na^{+} (Zhou et al., 2004). Although the complete mRNA sequence of *DSC1* (NM_166696.2) has been deduced from the corresponding genomic sequence (NT_033778.3) and also from the RT-PCR analysis of partial cDNAs (Kulkarni et al., 2002), no alternative splicing and functional analysis has been reported for *DSC1*. In this study, we isolated 20 cDNA clones covering the entire coding region of the *DSC1* gene from adults of *D. melanogaster*. Sequence analysis revealed that *DSC1* transcripts undergo extensive alternative splicing. Functional analysis in *Xenopus* oocytes confirmed that, like *BSC1*, *DSC1* encoded a cation channel. Furthermore, the *DSC1* channel was insensitive to tetrodotoxin (TTX), a potent and specific sodium channel blocker.

2.3 Materials and methods

2.3.1 Amplification and cloning of the coding region of the *DSC1* gene by RT-PCR

Five to seven day-old *w*¹¹¹⁸ adults were used to isolate total RNA. First-strand cDNA was synthesized using Oligo dT primers (Invitrogen, Carlsbad, CA), and the SuperScript[®] II reverse transcription kit (Invitrogen, Carlsbad, CA).

Conditions for the first-strand cDNA synthesis reaction were: 42°C for 2 min followed by a 60 min incubation at 48°C. RNA was removed by a 20 min incubation with RNaseH at 37°C. The PCR primers for amplification of the cDNA were, 5'- CCGCTCGAGGCCACCATGGGTGATGATCAAGCGACG -3', and 5'- TACCCCTAGGAAATATCAGATAGAAAGTTC -3'. To improve the expression efficiency, a Kozak sequence (GCCACCATGGGT) was added to the forward primer and the first nucleotide of the second codon was substituted from A to G to meet the sequence requirement. The *Xho* I and *Avr* II restriction enzyme sites (underlined) were added to the forward and reverse primer, respectively, to facilitate the cloning of the PCR product into a modified pGH19 vector in which an *Xho* I restriction site was removed by site-directed mutagenesis. The original pGH19 (a *Xenopus* expression vector containing the 3' and 5' untranslated regions of the *Xenopus* β -globin gene at the 3' end of T7 promoter and 5' end of SP6 promoter, respectively) was kindly provided by Barry Ganetzky, University of Wisconsin, Madison, WI. The PCR reaction conditions were the same as described previously (Zhou et al., 2004). The reaction mixture (50 μ l) contained 0.5 μ l cDNA, 50 pmol each primer, 200 μ M each dNTP, 1 U eLONGase (Invitrogen), 1.5mM MgCl₂, and 1xPCR reaction buffer. PCR was carried out as follows: one cycle of 94°C for 1 min; 33 cycles of 94°C for 30 s, 58°C for 30 s, 68°C for 8 min; and one cycle of 68°C for 15 min. The PCR products were purified using the QIAEX II Gel Extraction Kit[®] (QIAGEN Sciences, MD) and cloned into the modified pGH19. MAX Efficiency Stbl2-competent cells (Invitrogen) were used as host cells.

2.3.2 Sequencing of Twenty DSC1 cDNA clones

The inserts of *DSC1* cDNA clones were sequenced by moderate throughput sequencing (ABI 3730xl, Research Technology Support Facility, Michigan State University). The sequences of the sequencing primers are listed in Table 2-1. Sequence data were analyzed using software Lasergene 6[®] (DNASTAR, Inc., Madison, WI).

2.3.3 Expression of DSC1 channels in *Xenopus* Oocytes

Oocytes were obtained surgically from healthy female *Xenopus laevis* (*Xenopus* I, Ann Arbor, MI) and incubated with 1 mg/ml type IA collagenase (Sigma Inc. St. Louis, MO) in a Ca²⁺-free ND-96 medium, which contains 96 mM NaCl, 2 mM KCl, 1 mM MgCl₂, and 5 mM 4-(2-hydroxyethyl)-1-piperazineethanesulfonic acid (HEPES), pH 7.5. Follicle cells remaining on the surface of oocytes were removed manually with forceps. Isolated oocytes were incubated in ND96 culture medium containing 1.8 mM CaCl₂ supplemented with 50 µg/ml gentamicin, 5 mM pyruvate, and 0.5 mM theophylline (Goldin, 1992). Healthy stage V–VI oocytes were picked and used for cRNA injection. To prepare DSC1 cRNA, plasmid DNA containing full-length DSC1 cDNA was linearized with NotI (New England Biolab, Inc., Ipswich, MA), which does not cut the insert, followed by *in vitro* transcription with T7 polymerase using the mMESSAGE mMACHINE Kit (Ambion, Inc., Austin, TX). Procedures for oocyte preparation and cRNA injection were identical to those described by

Tan et al. (Tan et al., 2002). Each oocyte was injected with 3 ng *DSC1* cRNA. After injection, oocytes were incubated in ND-96 culture solution containing 96 mM NaCl, 2 mM KCl, 1.8 mM CaCl_2 , 1 mM MgCl_2 , 5 mM HEPES, 2.5 mM Na-pyruvate, 0.5 mM Theophylline for 24-72 hours before recording.

2.3.4 Electrophysiological recording and data analysis

Methods for electrophysiological recording and data analysis are similar to those described previously (Zhou et al., 2004). Currents were recorded using standard two-electrode voltage clamp technique. The borosilicate glass electrodes were filled with filtered 3 M KCl in 0.5% agarose and had resistance at 4-6 M Ω . Currents were measured using the oocyte clamp instrument OC725C (Warner Instrument Corp., Hamden, CT), Digidata 1200A interface (Axon Instrument, Inc., Foster City, CA), and pCLAMP 8.2 software (Axon Instrument, Inc., Foster City, CA). Three recording solutions, sodium, calcium and barium solution were used to check the current mediated by the *DSC1* channel. The sodium recording solution consisted of 50 mM NaOH, 45 mM TEAOH, 10 mM HEDTA, and 10 mM HEPES. The calcium solution consisted of 50 mM $\text{Ca}(\text{OH})_2$, 55 mM TEAOH, and 10 mM HEPES. The barium solution consisted of 50 mM $\text{Ba}(\text{OH})_2$, 55 mM TEAOH, and 5 mM HEPES. All recording solutions were adjusted to pH 7.0 with methanesulfonic acid. The recording protocol consisted of a 15-ms depolarization from -100 mV to 80 mV followed by repolarization to -100 mV. All experiments were performed at room temperature (22°C-25 °C).

2.3.5 TTX sensitivity assay

For the application of TTX, the disposable perfusion system developed by Tatebayashi and Narahashi (Tatebayashi and Narahashi, 1994) was used. The test solution was transferred into a Petri dish placed on a support stand. Two glass capillary tubes (10 cm in length) connected together with a short length of Tygon tubing were used to aid solution flow from the Petri dish to the recording chamber. The solution flow was controlled by hydrostatic force created by adjusting the level of the Petri dish relative to the recording chamber. Disposable recording chambers (1-1.5 ml volume) were made with glue dams in the Petri dish. To avoid cross contamination, recording chambers, perfusion system, and the glass agarose bridges connecting the oocyte chamber with the ground electrode chamber were all discarded after a single use. The TTX working solutions were diluted from a stock solution (2 mM) using the external recording solution immediately before use. Effects of TTX on peak currents reached a steady-state level within 5 min after perfusion.

2.4 Results

2.4.1 Sequence comparison of 20 DSC1 full length cDNA clones

For functional characterization of the DSC1 channel in *Xenopus* oocytes and detection of possible alternative splicing variants, we isolated cDNA clones that covered the entire coding region of the *DSC1* gene by RT-PCR from total RNA isolated from adults of *D. melanogaster*. A total of 20 *DSC1* cDNA clones were isolated and sequenced. Sequence comparison of the 20 cDNA clones with the *DSC1* genomic sequence (NT_033778.3) revealed 20 exons, named 1 to 20 (Fig.

2-1A). In addition, 10 optional exons, named exon 4A, 6A, 11A, 11B, 11C, 16A, 17A, 17B, 17C, and 19A respectively, were also found (Fig. 2-1 A, B). Exon 6A encodes a sequence in the N-terminal region, but is found in the middle of exon 6 which encodes the linker connecting domain I and II, suggesting a trans-splicing event. Exon 4A encodes part of the loop sequence connecting S5 and S6 in domain I. Exons 11A, 11B, and 11C are three tandem exons that encode part of the linker connecting domains II and III. Exons 17A, 17B, and 17C are another group of tandem exons encoding part of the linker connecting domains III and IV as well as part of IVS1. Exon 16A encodes part of the loop connecting S5 and S6 in domain III. Finally, exon 19A encodes a sequence in the C-terminal region. Exons 4A, 11C, 16A, 17A, 17B, 17C, and 19A have the consensus GT and AG sequences at the 5' donor and 3' acceptor sites, respectively, whereas exon 6A lacks the consensus GT and AG sequences. The donor sites of exons 11A and 11B do not have the GT sequence.

Based on optional exon usage, the 20 cDNA clones can be grouped into nine unique splice types, named DSC1-1 to DSC1-9 (Fig. 2-1 C). These cDNA clones belonging to the same splice type contain additional scattered amino acid differences (see below) and are named according to the splice type. For example, the six cDNA clones in splice type 1 are named DSC1-1.1 to DSC1-1.6. The nucleotide sequence of DSC1-1.1 has been deposited in GenBank (DQ466888.1) and its deduced amino acid sequence is presented in Figure 2-2. The most common optional exons (17B and 19A) are present in splice type 1 variants (Fig. 2-1 C). Exons 6A and 11B are 19 bp

(5'-CTCAACGTAAAAAACTAA-3') and 15 bp (5'-ATTTTCAAGAAGAAG-3') long, respectively. The nucleotide sequences of other longer optional exons are deposited in GenBank (HM 348600-348607). Intriguingly, exons 4A, 11A, 16A, and 17A contain in-frame stop codons. Inclusion of these exons in *DSC1* transcripts create truncated proteins. Type 1 and 2 splice variants, the two most abundant types, do not include these exons and are predicted to produce full-size *DSC1* proteins. However, seven other splice types are predicted to encode truncated proteins containing only domain I, domains I and II or the first three domains, because of inclusion of one or two of stop-codon-containing exons (Fig. 2-1 C). In addition, although exon 6A contains 19 nucleotides without a stop codon, inclusion of this exon, as in *DSC1*-7.1 causes a frame shift in the downstream sequence, resulting in a premature stop codon.

The deduced amino acid sequence of *DSC1*-1.1 was compared with those of *BSC1* and *para* (Fig. 2-2). The *DSC1*-1.1 protein shares 52% identity in the overall sequence with *BSC1*, and 29% with *Para*. The highest sequence identities are found in the transmembrane domains with 83%-90% between *DSC1*-1.1 and *BSC1* proteins, and 48% -54% between *DSC1*-1.1 and *Para* proteins. The sequence identities of the first intracellular linker connecting domains I and II and the second linker connecting domains II and III are less than 30% between *DSC1*-1.1 and *BSC1* proteins. It is worth mentioning that the second linker of the *DSC1*-1.1 channel is much longer (838 amino acids) than those of *BSC1* and *Para*, which have 330 and 257 amino acids, respectively. Interestingly, the linker connecting domains III and IV is highly conserved

between DSC1-1.1 and BSC1 (90% identity) or Para (52% identity). It is well established that this linker, particularly the IFM (mammals) or MFM (insects) motif in the middle of the linker, is critical for fast inactivation of sodium channels (Catterall, 2000). Corresponding to the MFM motif in Para, the DSC1-1.1 and BSC1 channels have “VFL” and “MFL,” respectively.

In comparing the deduced amino acid sequence of our 20 cDNA clones with the deduced amino acid sequence of *DSC1* in GenBank (NM_166696.2), we found 9 to 27 scattered amino acid changes in each cDNA clone. An A-to-I editing site in the linker connecting domains III and IV was previously reported in *DSC1* transcripts (Hoopengardner et al., 2003). This editing event occurred in 13 clones, including DSC1-1.1 resulting in a M2027V change in the VFL motif (Fig. 2-1). The other seven clones contain the conventional MFL motif. Further molecular analysis is required to determine whether other nucleotide differences in these clones are the result of RNA editing or errors introduced during RT-PCR. In addition, nucleotide substitutions introduced premature stop codons in four clones, two of which also contain stop-codon-containing exons. A six nucleotide sequence, CCGTCT, was found in all 20 cDNA clones, but not in the genomic DNA sequence (NT_033778.3). This difference might be caused by sequence polymorphisms between fly lines used in the genome sequence project (*y; cn bw sp; +; +*) and our study (*w*¹¹¹⁸).

2.4.2 Functional analysis of DSC1 channels in *Xenopus* oocytes

To determine whether the DSC1 channel is also a cation channel with gating

properties reported for the BSC1 channel (Zhou et al., 2004), I examined the 20 DSC1 variants in *Xenopus* oocytes using two-electrode voltage clamp technique. To elicit DSC1 currents, membrane potential was depolarized to 80 mV for 15 ms from a holding potential of -100 mV and then repolarized back to -100 mV (Fig. 2-3 A). Only three variants, DSC1-1.1, DSC1-1.2 and DSC1-5.1 produced detectable currents (Fig. 2-3 B). None of the 10 variants that encode truncated proteins produced currents using this recording protocol. I also did not observe detectable currents from seven *DSC1* clones that do not contain a premature stop codon. Using Ba^{2+} -containing recording solution, I detected a small outward current during depolarization followed by a large tail current associated with repolarization (Fig. 2-3 B). When Ca^{2+} - or Na^{+} -containing recording solution was used, the amplitude of tail current was smaller.

2.4.3 DSC1 channels are insensitive to TTX

The sodium channel blocker TTX inhibits insect sodium channels at nanomolar concentrations (Catterall, 2000). To determine whether TTX also inhibits DSC1 channels, we recorded DSC1 currents in Ba^{2+} -containing recording solution in the absence or presence of TTX using the recording protocol described above. Even at 10 μM , TTX did not reduce the amplitude of either the outward current or the tail current, indicating that DSC1-1.1 channel is TTX-insensitive (Fig. 2-3 C).

2.5 Discussion

In this study, my sequencing analysis of 20 cDNA clones reveals extensive alternative splicing of *DSC1* transcripts. A total of 10 optional exons were identified, four of which contain in-frame stop codons. Surprisingly, none of these optional exons is homologous to those identified in the *BSC1* gene (Liu et al., 2001). The only alternative splicing site conserved between the two genes results in optional exons 11A-C in *DSC1* and optional exons at splicing site B in *BSC1* (Liu et al., 2001). Like alternative exon 11A in *DSC1*, the two optional exons at the splicing site B in *BSC1* also contain in-frame stop codons, generating truncated proteins containing the first two domains. Furthermore, transcripts containing these *BSC1* optional exons were detected only in leg muscle, suggesting a possibly tissue-specific role of these truncated proteins (Liu et al., 2001). The conservation of this splicing site in two phylogenetically distant species raises the possibility that two-domain truncated proteins might play a role in insect neurophysiology.

Interestingly, premature stop codon-containing alternative exons are also detected in voltage-gated sodium and calcium channel genes. For example, transcripts containing two mutually exclusive exons, 18A and 18N, encoding IIS3-S4, are found in mouse $\text{Na}_v1.6$ (Plummer et al., 1997). Exon 18N contains a stop codon and transcripts containing it are detected in fetal brain and non-neuronal cells (Plummer et al., 1997). Moreover, this stop-codon containing exon is conserved in sodium channel genes of human, pufferfish, and the German cockroach (Tan et al., 2002). Other sodium channel genes also

produce premature stop-codon-containing alternative exons, such as exon 17A in $\text{Na}_v1.2$ and $\text{Na}_v1.3$, exon 17B in $\text{Na}_v1.3$, and exon 16A in $\text{Na}_v1.7$ in mouse and human (Kerr et al., 2008). Like exon 18N, the inclusion of exon 17A is tissue- or developmental stage-specific (Kerr et al., 2008).

In my experiments, only three of the 20 clones produced detectable currents. While it is not surprising that the 10 truncated DSC1 proteins did not produce any current, it is not clear why 7 clones that contain no premature stop codon did not produce currents. We previously encountered a similar problem with functional expression of BSC1 variants in *Xenopus* oocytes. While one BSC1 variant gave robust currents (Zhou et al., 2004), no currents were detected from other two BSC1 clones that do not contain premature stop codon (Chung, Liu and Dong, unpublished data). It is likely that unidentified accessory subunits or other chaperone proteins are required for the expression of these variants in *Xenopus* oocytes. It is also possible that the lack of channel expression from these clones is caused by sequence differences that are independent of alternative exons.

I found that the DSC1 channel is permeable to Na^+ , Ca^{2+} , and Ba^{2+} . These results are similar to those recorded from BSC1 channels (Zhou et al., 2004), suggesting that, like BSC1, DSC1 encodes a voltage-gated cation channel that is more permeable to bivalent cations. Other gating properties, such as voltage dependence of activation and inactivation, of the DSC1 channel remain to be investigated.

It is well established that the ion selectivity of voltage-gated sodium channels is determined by the amino acids D, E, K, and A in the pore positions of domains I,

II, III, and IV, respectively (i.e., the selectivity-filter motif “DEKA”) (Catterall, 2000). In contrast, four glutamic acids (EEEE) at the corresponding positions determine the ion selectivity for voltage-gated calcium channels (Catterall, 2000). It has been shown that a K to E substitution in the DEKA motif in a mammalian sodium channel altered the sodium selectivity to more toward calcium (Heinemann et al., 1992). Both the DSC1 and BSC1 channels contain the DEEA motif instead of DEKA or EEEE motifs. Substitution of the second E with K in the DEEA motif reduced the ion selectivity of the BSC1 channel for Ba^{2+} , demonstrating its critical role in modulating ion selectivity of the BSC1 channel (Zhou et al., 2004). It is likely that such a substitution will have a similar effect on the ion selectivity of the DSC1 channel.

In sodium channels, the selectivity-filter motif “DEKA” and the outer-ring motif “EEMD” (mammals) or “EEID” (insects) in the pore region of domain I-IV are critical for TTX binding (Catterall, 2000). In DSC1/BSC1 channels the amino acid sequences “DEEA” and “EEIN,” respectively, are found in the corresponding positions. Because the DSC1 channel is insensitive to TTX (Fig. 2-3 C), I speculate that the K to E substitution in the DEEA motif of the DSC1/BSC1 channels might be involved in TTX resistance since a charge-reversal substitution of the K residue in the DEKA motif renders rNa_v1.2 channels extremely resistant to TTX (Catterall, 2000). On the other hand, the N residue in the EEIN motif may not be involved in TTX resistance because an S to N substitution made varroa mite sodium channels more sensitive to TTX (Du et al., 2009a). Besides these two motifs, a non-aromatic residue, cysteine or serine, immediately after the first

E of the EEMD motif has been shown to be responsible for TTX resistance of rNav1.5, rNav1.8 and rNav1.9 channels (Satin et al., 1992; Sivilotti et al., 1997). Interestingly, both DSC1 and BSC1 channels have a non-aromatic residue (N359 in DSC1, N366 in BSC1) in this position. Therefore, N359/N366 may also contribute to TTX-insensitivity of DSC1/BSC1 channels.

In conclusion, *DSC1* gene encodes a voltage-gated cation channel that is permeable to Ba^{2+} , Ca^{2+} , and Na^{+} . *DSC1* transcripts undergo alternative splicing just like transcripts of the sodium channel gene *para*. Different exon usage might be a mechanism in regulating *DSC1* expression level or in yielding channels with distinct gating properties to regulate neuronal excitability.

Table 2-1 *DSC1* cDNA sequencing primers

Primer Name	Primer Sequence
T7	5'- TAATACGACTCACTATAGGG -3'
DSF0	5'- GGCGGAGTACATCTTTCTGGCC -3'
DSF1	5'- CCATGCTGACGACATTCCAGC -3'
DSF2	5'- GCCATAGCGCAACTGAACGCC -3'
DSF3	5'- GGTGGTGATCGATGACCTACCCG -3'
DSF3A	5'- CTCGACGATCCGCGCTCTTGG -3'
DSF4	5'- CAAGAGCGCAAGGATCGCAAGG -3'
DSF5	5'- CTCTTCGGGAGTGAGTACCC -3'
DSF6	5'- CTTGCAGGAGGAAGAGGAACTGC -3'
DSF7	5'- GCAAGATCGATGAGGACTTTAGC -3'
DSF8	5'- GCTGGCTGCTCTTACCGAGC -3'
DSF9	5'- CCTCAGAAGTGCTACGACC -3'
DSF10	5'- GGCAAGGAATGCGGATTGTAG -3'
DSF11	5'- GAAGAAGTATGAAGGAGGAG -3'
DSF12	5'- CGTTACTTCGGGTGGTCCGC -3'
DSF13	5'- CTTCAATCAGGCGCACCAGG -3'
Zhang77a	5'-TTATCGATTGTTTGGTCGAA -3'
Zhang77b	5'-CGGATCGTTCTTCACACTGA -3'
Zhang77c	5'-AATGGTGCTCCTCAAATGC -3'
Zhang77d	5'-GGCCTCTATCTTCGGGATTC -3'

Figure 2-1. Molecular characterization of 20 *DSC1* cDNA clones. **A.** The genomic organization of the coding region of the *DSC1* gene deduced from the sequence of DSC1-1.1 (Genbank No. DQ466888.1). Solid boxes represent exons. Positions of the alternative exons are labeled with arrows. **B.** Schematic drawing of the topology of the DSC1 protein indicating locations of alternative exons. All alternative exons are optional. **C.** Exon usage of 20 *DSC1* cDNA clones. Splice variants are named according to the splice types. Variants of each splice type contain sequence differences due to scattered amino acid differences. For example, the two variants in splice type 3 are designated as DSC1-3.1 and DSC1-3.2.

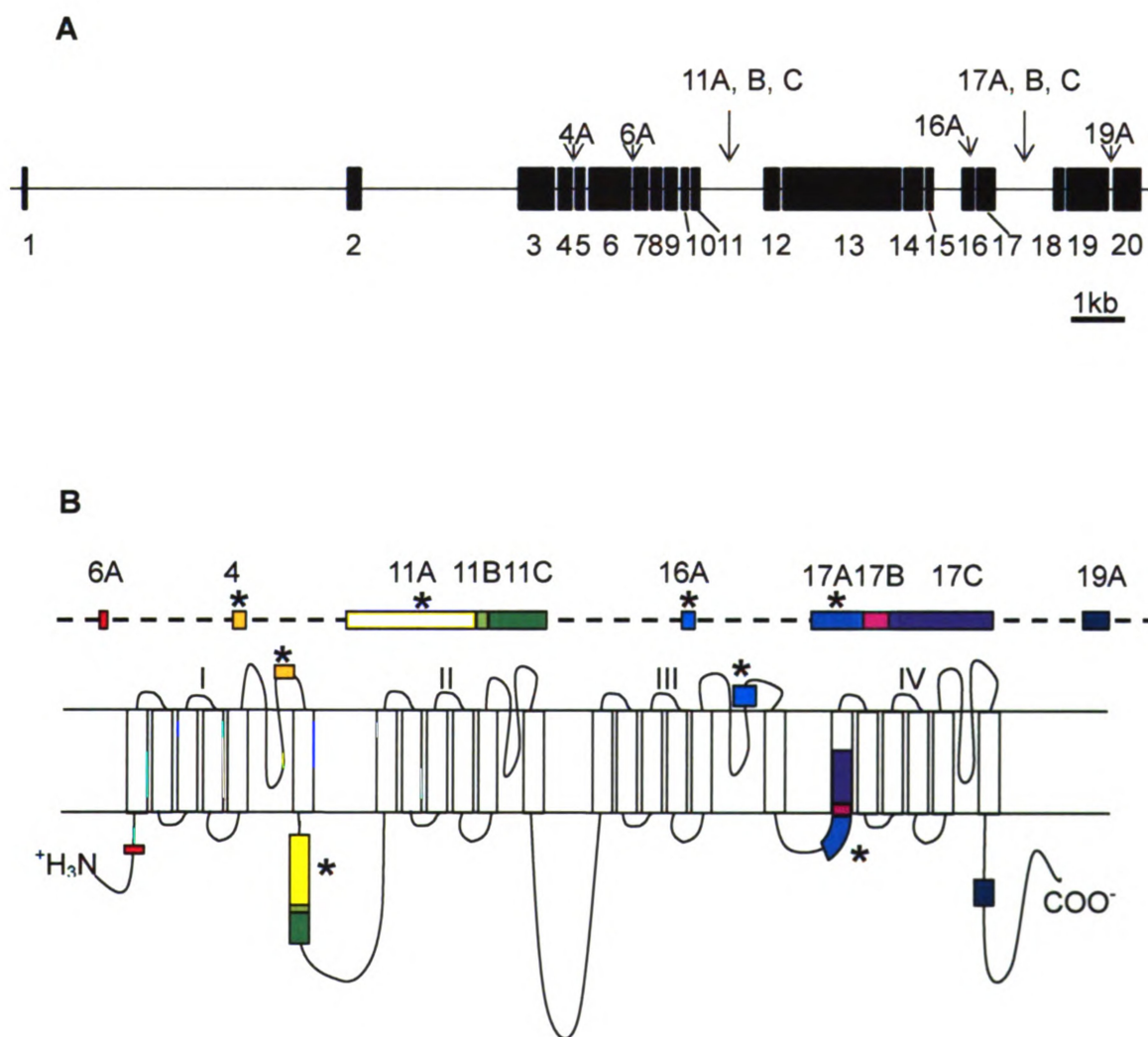


Figure 2-1 (continued)

C




















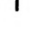
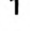



Splicing type	Alternative Exons										# of clones
	6A	4A	11 A	11 B	11 C	16 A	17 A	17 B	17 C	19A	
1											6
2						*					5
3											2
4											2
5			*								1
6		*				*	*				1
7											1
8											1
9			*								1

Figure 2-2. Alignment of amino acid sequences of DSC1-1.1, BSC1 and Para proteins. Dots represent amino acid residues in BSC1 and Para that are identical to those in DSC1-1.1. Dashes indicate gaps introduced to maximize sequence alignment. The four homologous domains (I to IV) and six transmembrane segments (S1 to S6) in each domain are marked above the sequences. Exons 17B and 19A are highlighted. Locations of other optional exons (which are not included in DSC1-1.1) are marked with arrowheads. The optional region C in BSC1 is highlighted. Locations of optional regions A and B (which are not present in BSC1) are marked with arrows. Amino acid residues in DSC1-1.1 and BSC1 corresponding to the MFM motif in Para (i.e., IFM motif in mammalian sodium channels) that is critical for fast inactivation are boxed. The amino acid residues which are important for ion selectivity and TTX binding are indicated with asterisks. The GenBank accession numbers are DQ466888.1, AF312365.1 and M32078.1 for DSC1-1.1, BSC1 and Para, respectively.

Figure 2-2 (continued)

```

DSC1-1.1 455 SKKKTRRKKTKGGKEGGTNGNGNSNGDDNKS DATSPGPSPRHSATE-
BSC1 464 .R. . . . .R. RPRAGGS. SG. EN. NN. NNGQSEHGGS R. AT. . . . .GSGP
para 493 .PTYSCISYELFVGGEKG. DDN. KEKMSIRSVEVESE. VSVIQ. QP. PTT

504 -----RPSALTM-----QAQKQYQQMEQQHKLAKSGSGG
514 CPPSAPSPES. .HS. .LS-PPSVVKGLSNPEQEEEEEQ. .EP. QQEEQPP
543 AHQATKVRKVSTTS. SLPGSPFNIRGRSRSSHK. TIRNGRGRFGIP. .DR

533 -----SNTF-----MAPTPKGRISFQDSGMGVKNP--NML--YPSDY
563 -----QQP. QLQRFLQ. PIAAPAPAEHASDTLHPV--. T. GKLGP PH
593 KPLVLSTYQDAQQHLPYADDSNAVTPMSEEN. AIIVPVYYGN. GSRH. S.

566 -----KGQLIANSG-----QPSSNSSGVNRESSQDDSGVVD---
603 -----R. . .L. SRH-----PS. N. .DSN. . . . .L. . . . .---
643 TSHQSRISYTSH. D. LGGMVVMGVSTMTKE. KLR. .NTRNQSV. ATNGGT

597 -----DHEERDTTND-----MGHVSTVELALSPREV-----
634 ----- . . . .G. V. SEDVAQIPNVVQR. EP. TV. . .SK. I-----
693 TCLDTNHL. .RDYEIGLECTDEAGKIKH. DNPFI EPVQTQT. VDMKDV M

623 ---RLIKCNG-NIARIKHN--NVYALHQE-----FSSEV--VVIDDL
668 ---. V. . . . .VSPGHGTQK--HL. T. PSD-----YL. HI--. LN. .
743 VLNDI. EQAAGRHS. ASDRGVS. .YFPT. DDEDEGPT. KDKALE. ILKGI

IIS1
657 PDRNCDCRVHWCTDYESWLQFQNC LYKVVRDPLFELAITLCIVLNTAFLA
703 . . . . .K. TQC. V. .DG. .R. .SG. . . . . .D. L. . . .I. .M. .
793 -. VF. VW--DC. W--V. .K. .EWVSLI. F. .FV. .F. . . . .V. .M. M.

IIS2
707 MEHHGMSESFRNALDVGNKVFTSI FTFCIVKLMA LS-KDFFLCGWNIFD
753 . . . . .V. Q. . .I. . . . .L. .FL. IL. . .-EY. A. . . . .
837 .D. .D. NKEMERV. KS. .YF. .AT. AI. ATM. . . .M. P. YY. QE. . . .

IIS3 IIS4
756 LLIVTASLLDIIFELVDGLSVLRGLRLRLRVLKL AQSWTTMKVLLSIIIST
802 .I. .S. . . .LS. .M. S. V. .C. . . . .R. . . . .
887 FI. .AL. .ELGL. G. Q. . . . .SF. . . .F. .K. .P. LNL. I. .MGR.

IIS5
806 IRALGNLTLLIVIVIYIFAVIGMQLFSKD YTP--EKFD PDPVPRWNFNDF
852 .G. . . . .FV. . . . .A--D. Y. .I. . . . .
937 MG. . . . .FV. C. I. F. . . .M. . . .G. N. HDHKDR. PDGDL. . . .T.

```

Figure 2-2 (continued)

```

                                     IIS6
DSC1-1.1 854 FHSFMMIFRILCGEWIE* * PLWDCMRAEEEQGASTCFAIFLPTLVMGNFMVL
BSC1 900 .....V.....T.....KLT..E.....A.....
para 987 M....IV..V.....SM.....-YV.DVS.IPF..A.V.I..LV..
      exon 11A, 11B, 11C ▽ region B
      904 NLFLALLLNSFNSEELKSKKEEVGEESKLARSIERVRDLIRKKRQERKDR
      950 D.....F..L.SIV....HA-.EK
      1033 .....SN.G.SS.SAPTAD-NDTN.I.EAFN.IGR-----

      954 KERKFAEKFQQIVLDAQQAHAQTLSHQAAVGLERGDKPGVLAETKFHRLS
      999 T.NEQNMRLEEM.-----
      1070 -----

      1004 YQESMNRPVSGSDFGFQIPLHDGLHTIVDGLYDDTGDLP EQIQLQAHAL
      1012 -H.V.S.HAAEKCYT-----AS.V.ET.I.RTI.H-----
      1070 FKS WK.NIAD-C.KL---IRNK.TNQISD---QPS.ERTN.-----

      1054 PPTS DSMPPTYESAMMAT TGGSFSSVNGNGTCQNLT P FVQAERRLQH QIS
      1041 -----KRHAAL..ETMS..RA--
      1106 -----WIWSE.K.V.R-----

      1104 SGVSTQQYDSCEEATYTESIELRLLGQYNSTDTDPYANDQ RSGCGSFNRG
      1057 -----Q.Q
      1118 -----IS.EHGDN-..E.-----

      1154 DSLQDNSSRRYGSEEHDEAFLKYQKSLLTRSPSYRKSLDRLSQSSGQSQR
      1060 QQE.Q.DGS..NPDAENN-----
      1131 -----

      1204 SLLKSEEAEMRRHSSGQSLNSMSIEQDELLSQQGNLREELLNCDQKELFQ
      1078 -----DED RNG.HS-----
      1131 -----GHDEI.ADG.IKKGI.---

      1254 FLQEEEEELQKGTKLRRISNVMRSRRPSSQMGQPENETMVEHSEFDNIIQS
      1088 -----PT.PRNVN.
      1148 -----

      1304 FEKELEEEIKRSTTSLEKLSNLSEPSPAADEATKAIMEHIAIITGASERS
      1097 -----V..EL.--
      1148 -QTQ.-----V..GD.M----

```

Figure 2-2 (continued)

```

DSC1-1.1 1354 AADEVVLPLNPYDSYDLSSVPRRSQSVSAAAQRQSVKLRRSLEKQRKID
BSC1 1104 -----
para 1160 -----

1404 EDFSISNEIRKICDQIHAPFVAMEAMAVAATSASQAQPNQSPFLRRKVDP
1105 RKY.V.-----H.N-----NKHMED
1160 -E.T.HGDMKN-----NK.KK.KY.NNAT.D

1454 FTVQFDRFKRLSLIERVEEVPEEEKPISTLRIESEKMPRKFLHGPDQLRL
1122 -----Y.V-----
1185 D.ASINSY-----GSHKN.P.-----

1504 DSLSLKSTNSYENLLIQKQKLGMATPPAVPATPPTSLKSSIEPPTLAQIS
1128 -----L.KSAQSA.-----
1201 -----

1554 SLKTTPLAALTEHQQHFHATSIQAAPTPAHTHAHSQAHAHSMAGQRRRM
1137 -----DEDNK.SEDSVL-----
1201 -----KDESHKGS.ET.E.EEK.-

1604 EHPQSTLDKAASFQSARTESHSSGAADASSALALAMAQKTEQSQSTAPDA
1150 --HPLV..RT.LTTQQ...KDESNPEE.--IE.EVLD.APGETE.MLPP
1219 -----DA.KED.GLDEELDEEGEC----

                                region C
1654 TQKPSAFTRLTEKPWHCLVSCVDDLTVGGRNSQGAYNDPM-TFPSYGAT
1195 AET.KKTRSI.K...NA.APY..E.....D...H.V.G.GS..GFARN
1238 -----EEGPLD.DIIHAHDE.ILDEY.A----

1703 KAAKVPDDCFPQKCYDHFYFRCPWFMS- --MDTQSAKHWRVTRTAVLTV
1245 .TV...Q....H..Q-----LC.DKYLE.PCGQR..HI..Q..S.
1262 -----C.DSY.KK.-----ILAGDD--SPFWQG.GNL.LKTFRL

                                IIIS1                                IIIS2
1750 VDTPAFEWFVLVLIFASSITLCFEDINLDKNKALKRVLYWINFSFCLIFV
1288 ....V....I.....Y..Q.LV..N....T.LG..AL.S
1298 IEDKY..TA.ITM.LM..LA.AL..VH.PQRPI.QDI..YMDRI.TV..F

                                IIIS3
1800 VEMILKWLALGFSKYFTSFWTILDFIIVFVSFSL- --IEENENLKVLR
1338 I..M.....WR.....I....-M.....
1348 L..LI.....KV.L.NA.CW...V..M..LINFVASLVGAGGIQAFKT

```

Figure 2-2 (continued)

	IIIS4	IIIS5
DSC1-1.1 1848	LRTLRLRPLRAISRWQGMRIVVNALMYAIPSI	FNVLVCLVFWLIFSIM
BSC1 1386
para 1398	M.....M..M....V.....VQ.....	I.....A..
	exon 16A▼	
1898	GVQFFGGKFFKCVNEMGELLPI	TEVNDKWDCIEQNYTWINSKITFDHVGM
1436DDE.N....SV.DGMLE.EDK..S.V.....N..N	
1448	...L.A..Y...EDMN.TK.SHEIIPNRNA.ESE....V..AMN.....N	
	IIIS6	
1948	GYLALLQVATFEGWMEVMADA	VDARGVDLQPQREANLYAYIYFVIFIVCG
1486	A....F.....E..NM.....L...V.....	
1498	A..C.F.....K..IQI.N..I.S.E..K..I..T.I.M.L...F..IF.	
	exon 17A▼	
1998	SFFTLNLFIVGVIIDNFNMLKKKY	BGGVLEFVFLTESQKHYYTAMKKLGRKK
1536	M.....
1548EQ...-A..S..M.M..D..K..S...M.S..	
	exon 17C▼	
2048	PQKVIKRPINHF	LAMPFYDLSNSRRFEIAIFVLIFLNMLTMGIEHYDQPHA
1586M.QV..T.....	Q....
1597	.L.A.P..RWRPQ.IVFEIVTDKK.D.I.MLF.G...F..TLDR..ASDT	
	IVS1	
	IVS2	
2098	VFFILEVSNAFFT	TVFGLEAIVKIVGLRHYFTVPWNVDFLLVLASIFG
1636	I.....L.....V...L.
1647	YNAV.DYL..I.VVI.SS.CLL..FA.....IE...L..VVV.IL..L.	
	IVS3	
	IVS4	
2148	ILMEDIMIDLPI	SPTLLRVVRVFRIGRILRLIKAAGIRKLLFALVVSLP
1686F.V.....	
1697	LVLS..IEKYFV.....AKV..V...V.G.....T.....AM...	
	IVS5	
2198	ALFNIGALLGLITFIYAILGMSLFGNVKLQ	GALDDMVNFQTFGRSMQLLF
1736A.....I...V..H..Q.....E.....	
1747CL..F.VM..F..F...F.MH..EKSGIN.VY..K...Q..I...	
	IVS6	
2248	RLMTSAGWNDVLES	LMIQPPDCDPFIHGHT-NGNCGHPLLAITYFTSFII
1786VG.....N.N.TYNNQP-..D..S.....	
1797	QMS....DG..DAI-.NEEA...PDNDKGYP....SATVG..FLL.YLV	
	exon 19A	
2297	ISYMIVINMYIAI	ILENFNAHQEEEEIGIVEDDLEMFIYIRWSKY-----
1835	DPHATQ
1846	..FL.....V....YS..TEDVQE.LTD..YD.Y.EI.QQFDPEGTQ	

Figure 2-2 (continued)

```

DSC1-1.1 2341 -----
BSC1 1885 FIRFSQLSDFIASLDPPLGIPKPNTVALVSFNLPIARGNKIHCLDILHSL
para 1896 YIRYDQLSEFLDVLEPPLQIHKPNKYKIISMDIPICRGDLMYCVDILDAL

2341 -----VFSS
1935 VKYVLGH----VEETDDFKKLQDQMDIKFKKQFPTRKELEIVSSTRIWKR
1946 TKDFFARKGNPIEETGEIGEIAAR-----PDTEGYEPVSSTLWRQR

2345 DSRPNRRI-----SPKAARQTIQRTL
1981 QDKAA.T.QGAFREYIRLKREREREPLDLEDEMTQTS..GGGW.SRLSAF
1987 EEYCA.L.QHAWRK--HKARGE GGSFEPDTHGDGGD.D.G-----

2366 LTIP-----SDLLADTIHMP-----
2031 .HVHRGSRASSRKSSRASDASEL.E.GGAWLNL.LLFLSGAHQGQTEDLL
2027 ---DPAPDEATDGDAPAGGDSVNGTAE-----GAADADESNVN

2381 -----PNLY--TSRNCPIILLPLSIHH----
2081 DPGHGSNGNSNVCITVSEPS PDT-G.P.NEE.KPSTSMV..V.VKDELRE
2063 SPGEDAAAAAAAAAAAAAGTTTAGSPGAGSAG.QTAV.V-----ESDG

2400 -----
2130 PLTVGDVSI LVTQPSPEGAGVPVDRGTEDRRPSNSSGESFHQIDSSERT
2107 FVTKNHGKVVIIHSRSPSITSRTADV-.ARPRPPLQDARE-Y.H-----

2400 -----WAP
2180 MPGVETTLSSSGTTTAALDRHPLGLLRPVGTVLSLFFPMQLGNGGDLGST.
2148 EYVLDVACCISDAAAT-VS.QQ-----QQQGE-QQA.--FSA-----

2403 RSP-----
2230 .K.ASEAVTG PVD MHPLRV RPGTAFSLPPSEIVKPLAKSSPERRRARSRR
2181 -----

2406 -----IM-----SL.
2280 RPSDGT LVRVLVHRESEESNDDKG.-.W
2181 -----...KNTIQTSKQQHKNNKQTRIN

```

Figure 2-3. DSC1 currents recorded from *Xenopus* oocytes expressing DSC1-1.1 channels. **A.** Recording protocol consisted of a 15 ms depolarization from -100 mV to 80 mV followed by repolarization back to -100 mV. **B.** Superimposed Na^+ , Ca^{2+} and Ba^{2+} currents recorded from an oocyte four days after injection with 3 ng *DSC1-1.1* cRNA using the protocol illustrated in A. **C.** Superimposed DSC1-1.1 currents recorded using a Ba^{2+} containing recording solution from an oocyte two days after injection with 3 ng *DSC1-1.1* cRNA before and after exposure to 10 nM TTX using the protocol illustrated in A.

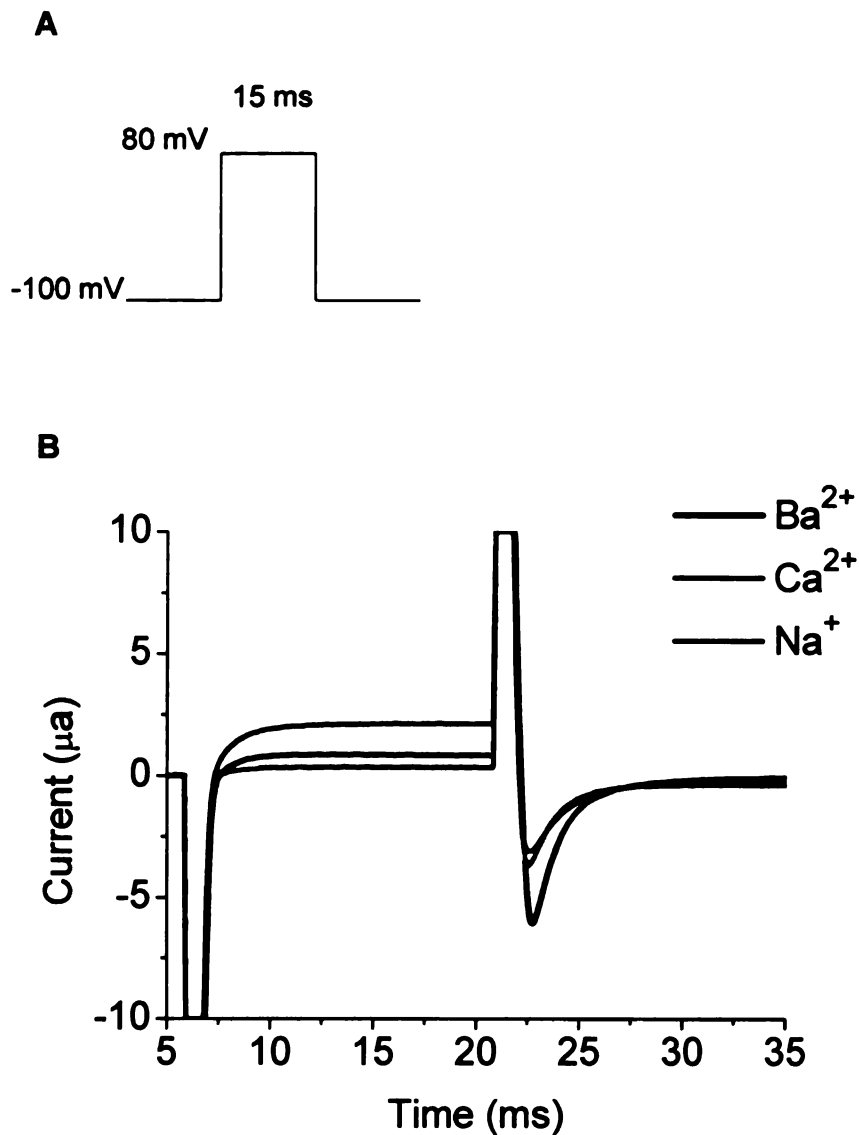
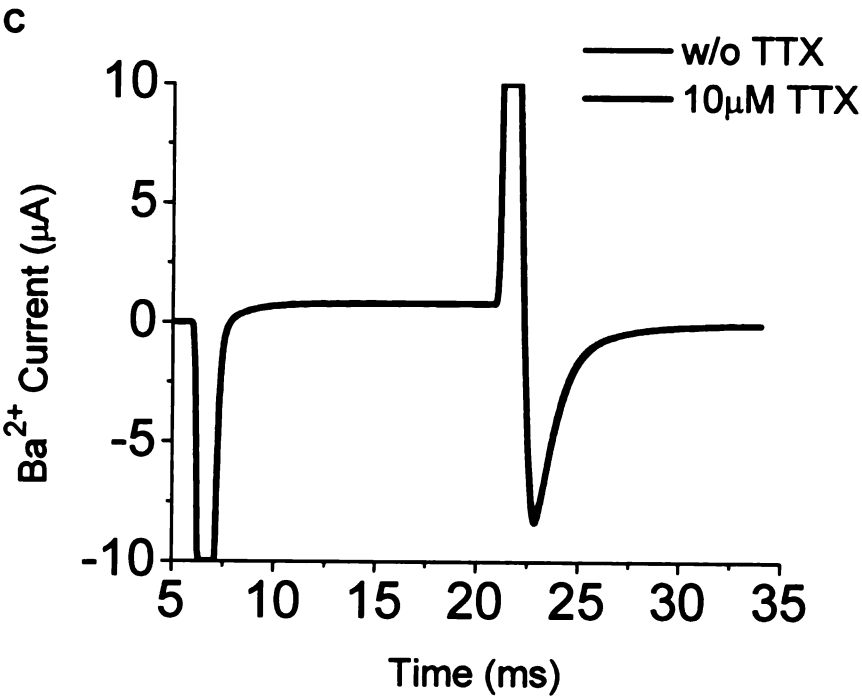


Figure 2-3 (continued)



CHAPTER 3

**BEHAVIORAL AND ELECTROPHYSIOLOGICAL CHARACTERIZATION
OF *DSC1* KNOCKOUT MUTANTS**

3.1 Abstract

The *Drosophila Sodium Channel 1* (*DSC1*) gene encodes an ion channel protein that is homologous to voltage-gated sodium channel α subunits. However, functional study in *Xenopus* oocytes shows that *DSC1* is a voltage-gated cation channel that is permeable to both sodium and calcium ions. The physiological role played by the *DSC1* channel in insects is not clear. In this study, *DSC1* mutant *D. melanogaster* lines were generated and tested for phenotypic changes at both behavioral and electrophysiological levels. Behaviorally, *DSC1* knockout flies jumped more frequently during heat shock compared with wild-type flies although they have comparable kinetics of temperature-induced paralysis. Moreover, the locomotor activity of *DSC1* knockout flies recovered significantly more slowly than wild-type flies and failed to recover completely following a 40-min recovery period after heat shock. *DSC1* knockout flies also jumped more frequently and had a shorter life span than wild-type flies when they were subjected to starvation. Electrophysiological study of the giant fiber (GF) pathway showed that the long latency refractory period of *DSC1* knockout flies was similar to that of wild-type flies at room temperature but was shortened more dramatically in response to heat shock and starvation. These results provide strong evidence for a critical role of the *DSC1* channel in regulating neuronal activities and associated behavior in response to environmental stresses.

3.2 Introduction

Voltage-gated ion channels are a class of transmembrane proteins located on the surface of every excitable cell. Modulation of the membrane potential causes voltage-gated ion channels to open, permitting current, in the form of ions, to pass across the membrane. The ion component is determined by the ion selectivity of the channel. The current mediated by a channel protein in turn depolarizes or hyperpolarizes the membrane potential and facilitates cellular functions, such as action potential (AP) initiation and propagation and neurotransmitter release.

Voltage-gated ion channels can be classified into several groups based on their ion selectivity and play important roles in modulating specific cellular functions. For example, voltage-gated sodium channels are responsible for the rising, or depolarizing, phase of an AP, whereas voltage-gated potassium channels mediate the falling phase of an AP (Hodgkin and Huxley, 1952). There are nine voltage-gated sodium channel genes in mammals (Yu and Catterall, 2003). In contrast, only one confirmed sodium channel encoding gene, *para*, has been reported in *D. melanogaster* (Loughney et al., 1989).

The *Drosophila Sodium Channel 1 (DSC1)* gene was identified over two decades ago (Salkoff et al., 1987). The deduced amino acid sequence of *DSC1* was highly similar to those of sodium channels, including the Para sodium channel. RNA *in situ* hybridization studies indicated that *para* is expressed in the central nervous system (CNS) and peripheral nervous system (PNS) at all developmental stages, whereas *DSC1* is expressed only in a few neurons in embryonic and larval stages. The expression of *DSC1* almost overlaps with that

of *para* in the CNS in pupae and adult stages (Hong and Ganetzky, 1994). An immunohistochemical study showed that the DSC1 protein is found only in synapse regions and axonal processes, but not in the cell bodies of the cortex, where Para is found. DSC1 is also widely distributed in the PNS, such as motor neurons in thorax muscles, neuromuscular junctions, and sensory neurons in compound eyes, antenna, proboscis, and tibia (Castella et al., 2001).

Electrophysiological analysis of BSC1, a DSC1 orthologue from cockroaches, revealed that BSC1 is not a sodium channel, but the founding member of a novel family of voltage-gated cation channel with ion selectivity toward Ca^{2+} (Zhou et al., 2004). My work described in Chapter 2 showed that the DSC1 channel mediates currents characteristic of those conducted by the BSC1 channel. Despite these advances, the physiological role of BSC1/DSC1 channels in insects remains elusive.

In this study, I performed behavioral and in vivo electrophysiological characterization of two *DSC1* null mutants. My data reveals a critical role of the DSC1 channel in regulating neuronal activities and associated behavior in response to environmental stresses.

3.3 Materials and Methods

3.3.1 Generation of *DSC1* knockout lines

As illustrated in Fig. 3-1, total DNA was isolated from *Drosophila* and ~4.5 kb genomic DNA fragments (from primers (5'-AGCAGCGGCCGCAACAGA

ATATCTCCGGTTGCC-3') and (5'-TACCGGTACCAGATTTGACGGACTCAC CTC-3') and primers (5'- AGCAGGCGCGCCTAATGGCTCTGCAGGAACG-3') and (5'- TACCCGTACGTACCTCTCTCCAGACCAAC-3') containing *DSC1* gene were PCR-amplified using platinum *Taq* DNA polymerase High Fidelity (Invitrogen, Inc., Carlsbad, California). The DNA fragments were cloned into PCR2.1 vector (Invitrogen, Inc., Carlsbad, California), respectively. One stop codon was introduced into both the upstream and downstream fragments by PCR from primers (5'-CGTCATGGCCACCATTCTGTTC-3') and (5'-CGTTAGTCGAAG AACTGGTTGG-3') and primers (5'- TTCTGTAAACACAGCCTTTTTGGCC-3') and (5'- TTCAAAGTGTGATGGCCAGCTC-3') with *Pfu* DNA polymerase (Agilent Technologies, Inc., Santa Clara, CA), and a *Mlu* I or an *EcoR* I cleavage site was introduced together with each nonsense mutation, respectively. The upstream stop codon terminates translation after the first 129 amino acids that only cover the N-terminal of the *DSC1* protein. The downstream stop codon results in a *DSC1* protein truncated after the 687th amino acid that only contains the first two domains and part of the second intracellular linker. The upstream fragment and the downstream fragment were then cloned into the *pW25* vector (generously provided by Kent Golic) through *Not*I and *Acc*65I sites, and *Bsi*WI and *Asc*I sites, respectively.

Two *DSC1* knockout lines, *DSC1-3* and *DSC1-6*, were generated using an ends-out targeting technique (Gong and Golic, 2003). The mini-white (*w*⁺) marker gene in the donor plasmid provides additional enzyme sites for identifying correct gene targeting events. *DSC1* knockout was confirmed by Southern blot analysis

and sequencing of the region spanning the downstream premature stop codon (Fig. 3-1).

The two initial *DSC1* knockout founder lines, DSC1-3 and DSC1-6, were back-crossed to *w*¹¹¹⁸ for five generations to generate *DSC1*^a and *DSC1*^b, respectively. *w*¹¹¹⁸ was used as the wild-type control in all experiments. Flies were fed on regular cornmeal-molasses-agar medium and raised at room temperature with 70% humidity and under a 12-hr light/dark cycle.

3.3.2 Climbing assay

An adult fly climbing assay was adopted from a previous study (Godenschwege et al., 2009). Briefly, five- to seven-day-old flies were collected and slightly immobilized by CO₂. Ten flies (five males and five females) were transferred into a 95×25 mm plastic vial (Genesee Scientific, Inc., San Diego, CA). After the flies had acclimated for 30 minutes at room temperature, another empty vial was placed upside-down on top of the first vial. The rims of the two vials were aligned and sealed so that the flies could climb into the top vial freely. The bottom vials were tapped gently and flies were given 30 seconds to climb. The number of flies that climbed into the top vial was recorded, and a climbing score was given. For example, if there were eight flies that climbed into the top vial, the climbing score would be eight. This procedure was repeated five times for each group of flies and mean values were calculated for statistical analysis.

3.3.3 Heat shock assay

Flies were collected and transferred as described above (3.3.2). To avoid using damaged flies, a climbing assay was performed and only flies that could climb into the top vial were collected for the heat shock assay. Flies (10 flies in each vial) were incubated in a 40°C humidified hybridization oven (Hybaid, Thermo Scientific, Inc. Waltham, MA) with a glass front door which allowed direct observation of fly behavior during heat shock. The number of paralyzed flies was counted every minute during the heat shock period (15 minutes). Paralysis is defined as loss of the ability to walk. Percentage of paralysis was calculated. Additionally, the number of jumps in each vial (10 flies) was recorded from the 5th to 10th minutes during the heat shock period. A jump was defined as taking off from the wall followed by landing on the bottom of the vial.

3.3.4 Recovery assay

Flies were returned back to room temperature after heat shock. A modified climbing assay was performed at various time points to determine the recovery of flies. The flies were tapped down to the bottom and given 30 seconds to stand up and climb. The number of flies that could climb on the wall of the vial was recorded. The assay was performed every 2 minutes during the first 20 minutes and every 5 minutes during the second 20 minutes of the recovery period. At the end of the recovery period, the locomotor activity was recorded after a brief vortex (Vortex- Genie 2, VWR Scientific Products, West Chester, PA) at the highest speed for 1 minute.

3.3.5 Starvation assay

The method for this assay is similar to that described in the study done by Walker et al. (Walker et al., 2006). Thirty, two- to three-day-old, male flies were evenly divided into six groups and raised on regular fly food for another two days before being transferred to vials containing 0.5% agar (five ml) instead of food. Flies were kept in the agar-containing vials to determine lifespan. The number of live flies was counted every 3-8 hours for six days. Percentage survival was calculated.

A jumpy phenotype similar to that induced during the heat shock was elicited by a single bang of the vial on the bench and videotaped. The number of jumps per vial (five flies) was counted during the second to tenth seconds after tapping. The jump phenotype was examined every day for three days.

3.3.6 Giant fiber system (GFS) recording

Giant fibers (GF) are a group of neurons which are associated with the animal escape response in many invertebrates and some lower vertebrates (Trimarchi and Schneiderman, 1995b; Trimarchi and Schneiderman, 1995a). The large axons of the giant fibers extend from the brain to the thoracic ganglion. In the thoracic ganglion, the terminal of giant fiber axons forms synaptic connections with two different neurons: a large motoneuron that innervates the tergotrochanteral muscle (TTM) and a peripherally synapsing interneuron (PSI). The PSI axon cross the midline and synapses with another motor neuron which innervates a group of muscles called dorsal longitudinal muscles (DLM). Thus, the

entire circuit, including the giant fiber neurons, interneurons, motor neurons, and muscle cells, is termed as the GF system and is illustrated in Fig. 3-2 (Engel et al., 2000).

Methods for recording GF-driven muscle potentials with electrical stimulation were adopted from the study of Engel and Wu (Engel et al., 2000). Briefly, adult flies were exposed to ether for 10 to 20 seconds before being affixed on the top of a wire mount that was glued behind the neck of the fly. The fly was placed in a position that does not interfere with wing or limb mobility. All stimulating and recording electrodes were uninsulated tungsten wires sharpened by electric etching. Stimulating voltage pulses (0.1-ms duration) generated by a Grass S88 stimulator (Grass Technologies, Inc., West Warwick, RI) were delivered with two stimulating electrodes that were inserted just beneath the cuticle of left and right compound eyes, respectively. The muscle potential of the number 3 dorsal longitudinal muscle (DLM) fiber was recorded with tungsten electrodes inserted beneath the cuticle at the middle point between the midline and the root of the anterior dorso-centrals. A ground electrode was inserted into the abdomen. Muscle responses were amplified by a DAM50 DC amplifier (World Precision Instrument, Inc., Sarasota, FL) and converted to digital signal by a Digidata 1440A (Axon Instrument, Inc., Foster City, CA) coupled with Clampex 10.2 and Clamfit 10.2 software (Axon Instrument, Inc., Foster City, CA) .

The GF pathway can be triggered from different neurons by different stimulation intensities (Fig. 3-2). The time interval between the stimulus and the first muscle potential is termed the response latency. It reflects the time required

for the stimulation signal to conduct along neural circuits from the activated neuron to the innervated muscle, DLM. Based on the length of latency, the responses can be grouped into two classes, long latency (LL) and short latency (SL) responses. When a relatively low-strength stimulus (i.e., low voltage) is applied, a muscle potential with longer latency is usually elicited. As the strength of the stimulus becomes higher, the short latency muscle response is triggered. The lowest voltage by which the long latency response is elicited is termed the long latency threshold and the lowest voltage to elicit the short latency response is called the short latency threshold. If the fly was given two pulses with the same voltage amplitude and duration time but varying intervals, the longest interval at which muscle potential is elicited by the first pulse but not by the second one is termed the refractory period, which is an indication of the stability of the GF circuit (Tanouye and Wyman, 1980). The refractory period of the long latency response was tested using the mean value of the long latency threshold and the short latency threshold. The short latency refractory period was tested using stimuli at 30 volts, which is high enough to elicit the short latency in all flies examined.

3.3.7 Statistics

Student's *t*-test was used to analyze the jump phenotype during heat shock and the climbing assay results. Two-way analysis of variance (ANOVA) with Tukey's test employed as the *post hoc* test were used to analyze the data of GF recording. $P < 0.05$ was set as the criterion for statistical significance.

3.4 Results

3.4.1 *DSC1* knockout flies exhibit an abnormal jumping response during heat shock

DSC1 knockout flies exhibited normal locomotor activity at room temperature (Fig. 3-3A). However, in this study, I examined a possible role of *DSC1* in insect stress responses. First, I evaluated the sensitivity of *DSC1* knockout flies to heat shock. Flies were incubated at 40°C for 15 minutes and their responses recorded at different time points. All flies, wild-type and mutant, were paralyzed at the end of the 15-min heat shock period (Fig. 3-3B). The paralysis curves of *w*¹¹¹⁸, *DSC1*^a and *DSC1*^b overlapped, indicating that knockout of *DSC1* did not affect heat-induced paralysis kinetics. However, a distinct 'jumpy' phenotype was observed during heat shock, particularly from the fifth to tenth minutes. *DSC1* knockout flies were significantly more jumpy than *w*¹¹¹⁸ flies (Fig. 3-3C).

3.4.2 *DSC1* knockout flies showed a defect on recovery from heat shock

To test if *DSC1* knockout mutants are altered in recovery from heat shock, the vials containing paralyzed flies were returned back to room temperature at the end of the 15-min heat shock period. As shown in Fig. 3-4, wild-type flies recovered significantly faster than the *DSC1* knockout flies of both *DSC1*^a and *DSC1*^b lines. At 10-min time point, 80% of the wild-type flies, but only about 40% of *DSC1* knockout flies had resumed climbing the wall of the assay vial following heat-induced paralysis. It took another 30 min for *DSC1* knockout flies to

achieve 80% - 85% recovery (Fig 3-4).

3.4.3 Abnormal jump response and shortened life span of *DSC1* knockout flies during starvation

To test if *DSC1* knockout mutants are defective in other stress responses, we examined the response of *DSC1* knockout mutants to starvation. Flies from both *DSC1^a* and *w¹¹¹⁸* lived on 0.5% agar for three days. After 24, 48, and 72 h, the number of jumps by *DSC1^a* flies was significantly higher than those of *w¹¹¹⁸* flies (Fig. 3-5A). Beginning on day 4, both *DSC1^a* and *w¹¹¹⁸* flies began showing mortality. At day 5, 53% of the *DSC1^a* flies had died, but only 33% of the *w¹¹¹⁸* flies. Within 12 h (day 5.6), all the *DSC1^a* flies had died, yet 13% of *w¹¹¹⁸* flies were still alive, indicating a shorter life span of *DSC1^a* flies during starvation (Fig. 3-5B). To determine whether this difference was caused by differences in body mass between *DSC1^a* and *w¹¹¹⁸* flies, we weighed 40 individuals of *w¹¹¹⁸* or *DSC1^a* (20 male flies and 20 female flies). No significant difference was found in body weight between *w¹¹¹⁸* and *DSC1^a* flies (Fig. 3-5C).

3.4.4 Reduced long latency refractory period (LLRP) in response to heat shock in *DSC1* knockout flies

The abnormal jumpy phenotype of *DSC1* knockout flies during heat shock

and starvation suggests that the DSC1 channel may be involved in regulating stress-associated neuronal activities. To test this hypothesis, we examined the effects of the *DSC1* knockout on electrical signaling in the GFS. The GFS was chosen for two reasons. First, the GFS is a well-characterized and major neural circuit (Fig. 3-2) that mediates jump and flight responses in *Drosophila* (Trimarchi and Schneiderman, 1993). Second, DSC1 proteins are densely expressed in GF neurons (Castella et al., 2001). In this study, I measured the long latency and short latency responses of DLMs evoked by brain stimulation of different intensities (see the Materials and Methods for the details). No differences were detected in the latencies or the refractory period of long or short latency pathways between *w*¹¹¹⁸ and *DSC1* knockout flies at room temperature (Fig. 3-6, Table 3-1, 3-2, 3-3, 3-4.).

To examine whether the abnormal jumpy phenotype in the *DSC1* knockout flies is caused by altered electrical activities of the giant fiber circuit, I compared the activities of the GFS of *DSC1*^a, and *w*¹¹¹⁸ flies. Specifically, I measured the long latency and short latency responses of DMLs at 5 min, 10 min and 15 min of the 15-min heat shock and determined the response latency and refractory period of both short and long latency pathways.

The SL was significantly shortened after 5 min of the heat shock, but gradually increased over the rest of the heat shock period for both mutant and wild-type flies (Fig. 3-6A, Table 3-1.). The short latency refractory period (SLRP) was gradually increased for the duration of heat shock. The SLRP was significantly greater after 15 min of heat shock than it was at RT for both *w*¹¹¹⁸ and *DSC1*^a flies. However,

no differences in the response latency or refractory period of the short latency pathway were detected between w^{1118} flies and $DSC1^a$ flies (Fig. 3-6B, Table 3-2.).

The LL was also shortened after 15 min of heat shock for both $DSC1^a$ and w^{1118} flies; but no difference was found between w^{1118} flies and $DSC1^a$ flies (Fig. 3-6C, Table 3-3.). The long latency refractory period (LLRP) of $DSC1^a$ and w^{1118} were reduced by heat shock. Interestingly, the LLRP of $DSC1^a$ flies was significantly shorter than that of w^{1118} flies, measured at the fifth and tenth minutes of the heat shock treatment (Fig. 3-6D, Table 3-4.).

3.4.5 The heat-induced reduction of LLRP was rapidly reversed for w^{1118} flies, but not for $DSC1^a$ flies

The heat stress-induced changes in the latency and refractory periods of the short latency pathway (Fig. 3-7A and B) and the latency of the long latency pathway (Fig. 3-7C) were readily reversed when $DSC1^a$ and w^{1118} flies were returned to room temperature (Fig. 3-7A, B, C, Table 3-5, 3-6, 3-7). Similarly, the heat stress-induced LLRP reduction of w^{1118} flies was almost completely reversed during the first 10 min of recovery at room temperature (Fig. 3-7D, Table 3-8). However, the recovery of LLRPs of $DSC1^a$ flies following heat shock

lagged significantly behind that of w^{1118} flies. Furthermore, LLRPs for $DSC1^a$ flies did not recover fully from heat stress by the end of the 40 min recovery period at room temperature (Fig. 3-7D, Table 3-8).

Based on my behavioral assay (Fig. 3-4), at the 40-min time point, the locomotor activities of $DSC1^a$ flies seem to be fully recovered from the heat shock. To determine whether the remaining LLRP reduction at the end of the 40 min recovery from heat shock could alter the locomotor activity of $DSC1^a$ flies, we vortexed flies in vials for 1 min at the highest speed and then immediately examined the locomotor activity. We reasoned that the stimulation introduced by a brief tapping of the vial in the locomotor activity assay (See 3.3.4) may not have been sufficient to reveal subtle behavioral defects. Indeed, the climbing scores of $DSC1^a$ flies were significantly lower than that of w^{1118} flies (Fig. 3-7E) indicating that stress-induced deficits in locomotor activity of $DSC1^a$ flies had not fully recovered to the level of w^{1118} flies even after 40 min of recovery at room temperature.

3.4.6 The long latency refractory period (LLRP) of $DSC1$ knockout flies was reduced by starvation

Both w^{1118} and $DSC1$ knockout flies did not exhibit mortality in the first three days of starvation. From the 4th day, both genotypes started showing some mortality. Therefore, for my experiments to examine the GFS, I used flies that

had been starved for 3 days. No difference in the short latency pathway was found between w^{1118} and $DSC1^a$ flies following starvation (Fig. 3-8A and 3-8B). A slight, but significant reduction in the long latency was detected for w^{1118} and $DSC1^a$ flies as a result of starvation, however, there was no difference between the two lines (Fig. 3-8C). Interestingly, the LLRP was significantly shortened by starvation for $DSC1^a$ flies, but not for w^{1118} flies (Fig. 3-8D, Table 3-9.).

3.5 Discussion

DSC1 was identified as a putative sodium channel gene more than two decades ago based on sequence similarity to mammalian and insect voltage sensitive sodium channels (Salkoff et al., 1987). Functional characterization, however, revealed that the *DSC1* channel is a novel voltage-gated cation channel (Chapter 2). Despite this exciting finding, the physiological role of the *DSC1* channel in insects remains a mystery. The successful generation of two *DSC1* knockout lines, using gene targeting via homologous recombination, made it possible for me to address the physiological role of *DSC1* in *Drosophila*. In this chapter, I described several behavioral and electrophysiological characteristics of the *DSC1* knockout lines.

Under standard laboratory rearing conditions *DSC1* knockout flies are viable and exhibit no obvious behavioral defects, indicating that the *DSC1* channel does not play an indispensable role in electrical signaling under these conditions. To determine whether *DSC1* knockout flies can tolerate adverse environmental

conditions, I examined their responses to heat shock and starvation. Interestingly, I observed abnormal behavior of the *DSC1* knockout flies in response to both heat shock and starvation. The *DSC1* knockout flies jumped more frequently than *w*¹¹¹⁸ flies under these conditions. To understand the mechanism underlying this behavioral defect, I examined the GFS that expresses the *DSC1* channel and mediates jump response, specifically the long and short latency pathways of DLMS. The neuronal activities of the GFS were examined at room temperature, after heat shock for 5 min, 10 min, and at the end of the 15-min heat shock. Consistent with the behavioral results, no difference in the neuronal activities of the GFS was detected between *w*¹¹¹⁸ and *DSC1* knockout flies at room temperature. The LLRP was reduced in wild-type flies following heat shock at 40°C, in agreement with a previously published report (Elkins and Ganetzky, 1990). Interestingly, the LLRP of the *DSC1* knockout flies is significantly shorter than that of *w*¹¹¹⁸ flies at 5 min and 10 min during heat shock. The reduction in LLRPs in *DSC1* knockout flies during the heat shock correlates well with the occurrence of the abnormal jumpy phenotype. Refractory period controls the frequency of action potentials; therefore the reduction of LLRP could increase the frequency of firing in the long latency pathway. Therefore, I predict that the reduction in the LLRP could enhance thoracic jump muscle activities, which could lead to the jumpy behavior of *DSC1* knockout flies. The reduction in LLRP was also observed in starved *DSC1* knockout flies that exhibit the jumpy phenotype, further supporting my prediction.

Although at the end of the 15-min heat shock, the LLRPs of both *w*¹¹¹⁸ and *DSC1* knockout flies were reduced to the same level, the LLRP of *w*¹¹¹⁸ flies returned to the initial level within a few minutes after the flies were transferred back to room temperature. In contrast, the recovery of LLRP of *DSC1* knockout flies lagged significantly behind that of *w*¹¹¹⁸ flies. In fact, after a 40-min recovery from heat shock, although the locomotor activity of the *DSC1* knockout flies was recovered, the LLRP of *DSC1* knockout flies was restored to only 75% of the original level before the heat shock. These results indicate that recovery from heat shock is mediated by neural circuits other than the GFS, suggesting the involvement of the *DSC1* channel in other neural circuits as well.

The requirement of the *DSC1* channel for maintaining the neuronal excitability under heat shock highlights an important role of *DSC1*-regulated neuronal circuits (and possibly other cellular processes) in insect stress responses. In this study, I also observed jump behavior and reduced tolerance of *DSC1* knockout flies when they were challenged with another stressful condition, starvation, although there is no difference in the biomass between *w*¹¹¹⁸ flies and *DSC1* knockout flies.

In the past several decades, extensive studies have been carried out to understand the starvation responses, mainly focusing on metabolic pathways (Piper et al., 2005; Rion and Kawecki, 2007). Little information is available regarding the involvement of ion channels in regulating tolerance to starvation. Shahidullah et. al. (2009) showed that a *Drosophila* potassium channel binding protein, Slob, modulates fly tolerance to starvation, probably through regulating

neuronal excitability (Shahidullah et al., 2009). I found in this study that the LLRP of *DSC1* knockout flies was shorter than that of *w¹¹¹⁸* flies after 3 days of starvation, indicating a relationship between enhanced neuronal excitability and reduced starvation resistance in *DSC1* knockout flies. However, how starvation shortens the LLRP and whether there is a direct connection between the shortened LLRP and altered starvation tolerance requires further investigation.

In summary, heat shock and starvation both enhance the neuronal excitability of the GFS in *D. melanogaster*. These stress conditions affect *DSC1* knockout flies more than to *w¹¹¹⁸* flies, highlighting the important role of the *DSC1* channel in dampening neuronal excitability under these extreme conditions. How the *DSC1* channel modulate neuronal excitability is not clear. It has been shown that expression of *para* and *DSC1* transcripts completely overlap in the CNS of *Drosophila* adults (Hong and Ganetzky, 1994), suggesting that the *DSC1* channel may function along with the *Para* channel in regulating neuronal activities. Sodium channels are responsible for the rising phase of the action potential. Because the *DSC1* channel requires high depolarization voltage to be activated (Chapter 2), it is possible that this channel could be activated only during the rising phase of an action potential. If so, the *DSC1* channel may prolong or enhance depolarization of the membrane potential during the rising phase of the action potential. It is possible that the modification of the action potential by the *DSC1* channel is too subtle to be detected at room temperature. However, in response to stress conditions when the conductance of the sodium channel and the potassium channel are altered (Huxley, 1959), the modulating role of the *DSC1* channel

becomes evident. Future experiments recording the action potential of the GF neuron from both *w¹¹¹⁸* and *DSC1* knockout flies will be able to test this hypothesis. Interestingly, a Ca^{2+} -activated plateau action potential has been detected in dorsal paired median neurons from the terminal abdominal ganglion of the cockroach *Periplaneta americana*, but the ion channel responsible for the action potential has remained elusive (Amat et al., 1998). It is possible that the *DSC1* channel is involved in the generation of the Ca^{2+} -activated plateau action potential. Direct measurement of the action potential in dorsal paired median neurons in the *DSC1* mutant using voltage clamp could test this prediction. Therefore, I predict that the *DSC1* channel dampens the neuronal excitability by modulating the initiation and propagation of the action potential mediated by the sodium channel.

Table 3-1. Response latencies (ms) of the short latency pathway of w^{1118} and $DSC1^a$ flies measured at different time points of heat shock process (mean \pm SD)

	Heat Shock Time			
	RT ¹	5 min	10 min	15 min
w^{1118}	1.2 \pm 0.2 (n=17)	1.0 \pm 0.1 (n=5) ²	1.0 \pm 0.1 (n=5)	1.5 \pm 0.2 (n=10) ⁴
$DSC1^a$	1.2 \pm 0.2 (n=17)	1.0 \pm 0.2 (n=5) ³	1.2 \pm 0.0 (n=5)	1.4 \pm 0.1 (n=10) ⁵

Note:

SL - short latency

1 0 min (Response latency measured at room temperature before heat shock).

2 $p < 0.05$, compared with the SL value of w^{1118} recorded before heat shock, Two-way ANOVA.

3 $p < 0.05$, compared with the SL value of $DSC1^a$ recorded before heat shock, Two-way ANOVA.

4 $p < 0.05$, compared with the SL value of w^{1118} recorded at five-minute time point of heat shock process, Two-way ANOVA.

5 $p < 0.05$, compared with the SL value of $DSC1^a$ recorded at five-minute time point of heat shock process, Two-way ANOVA.

Table 3-2. Refractory periods (ms) of the short latency pathway of w^{1118} and $DSC1^a$ flies measured at different time points of heat shock process (mean \pm SD)

	Heat Shock Time			
	RT ¹	5 min	10 min	15 min
w^{1118}	5.9 \pm 1.2 (n=20)	7.6 \pm 0.9 (n=5)	8.0 \pm 1.6 (n=5)	8.5 \pm 1.9 (n=11) ²
$DSC1^a$	6.5 \pm 1.0 (n=23)	6.2 \pm 1.6 (n=5)	8.8 \pm 1.6 (n=5)	9.8 \pm 2.3 (n=11) ³

Note:

SLRP - short latency refractory period

1 0 min (i.e. Refractory period measured at room temperature before heat shock).

2 $p < 0.05$, compared with the value of w^{1118} recorded before heat shock, Two-way ANOVA.

3 $p < 0.05$, compared with the value of $DSC1^a$ recorded before heat shock, Two-way ANOVA.

Table 3-3. Response latencies (ms) of the long latency pathway of w^{1118} and $DSC1^a$ flies measured at different time points of heat shock process (mean \pm SD)

	Heat Shock Time			
	RT ¹	5 min	10 min	15 min
w^{1118}	3.8 \pm 0.4 (n=22)	3.8 \pm 0.3 (n=7)	3.9 \pm 0.4 (n=9)	3.5 \pm 0.1 (n=7) ²
$DSC1^a$	3.8 \pm 0.3 (n=24)	3.6 \pm 0.2 (n=5)	3.9 \pm 0.3 (n=8)	3.4 \pm 0.1 (n=11) ³

Note:

LL - long latency

1 0 min (i.e. response latency measured at room temperature before heat shock).

2 $p < 0.05$, compared with the value of w^{1118} recorded before heat shock, Two-way ANOVA.

3 $p < 0.05$, compared with the value of $DSC1^a$ recorded before heat shock, Two-way ANOVA.

Table 3-4. Refractory periods (ms) of the long latency pathway of w^{1118} and $DSC1^a$ flies measured at different time points of heat shock process (mean \pm SD)

	Heat Shock Time			
	RT ¹	5 min	10 min	15 min
w^{1118}	46.0 \pm 9.3 (n=21)	39.1 \pm 5.2 (n=9)	44.3 \pm 8.0 (n=9)	26.9 \pm 7.0 (n=7) ²
$DSC1^a$	46.8 \pm 15.9 (n=25)	31.0 \pm 4.8 (n=8) ⁴	23.4 \pm 2.8 (n=8) ⁵	23.6 \pm 3.1 (n=11) ³

Note:

LLRP - long latency refractory period

1 0 min (i.e. Refractory period measured at room temperature before heat shock).

2 $p < 0.05$, compared with the LLRP of w^{1118} recorded before the heat shock, Two-way ANOVA.

3 $p < 0.05$, compared with the LLRP of $DSC1^a$ recorded before the heat shock, Two-way ANOVA.

4 $p < 0.05$, compared with the LLRP of w^{1118} recorded at the same time point (five-minute), Two-way ANOVA

5 $p < 0.05$, compared with the LLRP of w^{1118} recorded at the same time point (10-minute), Two-way ANOVA

Table 3-5. Response latencies (ms) of the short latency pathway of w^{1118} and $DSC1^a$ flies measured at different time points of recovery process (mean \pm SD)

	Recovery Time			
	10 min	20 min	30 min	40 min
w^{1118}	1.2 \pm 0.1 (n=12)	1.1 \pm 0.1 (n=5)	1.1 \pm 0.1 (n=5)	1.2 \pm 0.1 (n=9) ¹
$DSC1^a$	1.2 \pm 0.1 (n=10)	1.1 \pm 0.1 (n=6)	1.1 \pm 0.1 (n=6)	1.2 \pm 0.1 (n=11) ²

Note:

SL - short latency

1 $p < 0.05$, compared with the SL of w^{1118} recorded at the end of the heat shock, Two-way ANOVA.

2 $p < 0.05$, compared with the SL of $DSC1^a$ recorded at the end of the heat shock, Two-way ANOVA.

Table 3-6. Refractory periods (ms) of the short latency pathway of w^{1118} and $DSC1^a$ flies measured at different time points of recovery process (mean \pm SD)

	Recovery Time			
	10 min	20 min	30 min	40 min
w^{1118}	7.5 \pm 2.1 (n=12)	6.2 \pm 1.3 (n=5)	6.6 \pm 1.5 (n=5)	6.5 \pm 1.3 (n=10) ¹
$DSC1^a$	7.6 \pm 1.9 (n=10)	8.2 \pm 1.2 (n=6)	8.7 \pm 1.2 (n=6)	6.9 \pm 0.9 (n=11) ²

Note:

SLRP - short latency refractory period

1 $p < 0.05$, compared with the SLRP of w^{1118} recorded at the end of the heat shock, Two-way ANOVA.

2 $p < 0.05$, compared with the SLRP of $DSC1^a$ recorded at the end of the heat shock, Two-way ANOVA.

Table 3-7. Response latencies (ms) of the long latency pathway of w^{1118} and $DSC1^a$ flies measured at different time points of recovery process (mean \pm SD)

	Recovery Time			
	10 min	20 min	30 min	40 min
w^{1118}	4.0 \pm 0.1 (n=12)	4.1 \pm 0.2 (n=11)	3.9 \pm 0.2 (n=6)	3.9 \pm 0.2 (n=7) ¹
$DSC1^a$	3.8 \pm 0.2 (n=9)	3.9 \pm 0.1 (n=8)	3.6 \pm 0.2 (n=8)	3.7 \pm 0.2 (n=9) ²

Note:

LL - long latency

1 $p < 0.05$, compared with the LL of w^{1118} recorded at the end of the heat shock, Two-way ANOVA.

2 $p < 0.05$, compared with the LL of $DSC1^a$ recorded at the end of the heat shock, Two-way ANOVA.

Table 3-8. Refractory periods (ms) of the long latency pathway of w^{1118} and $DSC1^a$ flies measured at different time points of recovery process (mean \pm SD)

	Recovery Time			
	10 min	20 min	30 min	40 min
w^{1118}	44.6 \pm 7.8 (n=12)	48.7 \pm 8.6 (n=11)	44.8 \pm 6.0 (n=6)	49.7 \pm 10.0 (n=7) ¹
$DSC1^a$	26.3 \pm 2.1 (n=9) ³	32.6 \pm 5.6 (n=8) ⁴	30.1 \pm 4.3 (n=8) ⁵	31.4 \pm 4.8 (n=9) ^{2,6}

Note:

LLRP - long latency refractory period

1 $p < 0.05$, compared with the LLRP of w^{1118} recorded at the end of the heat shock, Two-way ANOVA.

2 $p < 0.05$, compared with the LLRP of $DSC1^a$ recorded at the end of the heat shock, Two-way ANOVA.

3 $p < 0.05$, compared with the LLRP of w^{1118} recorded at the same time point (10-minute), Two-way ANOVA

4 $p < 0.05$, compared with the LLRP of w^{1118} recorded at the same time point (20-minute), Two-way ANOVA

5 $p < 0.05$, compared with the LLRP of w^{1118} recorded at the same time point (30-minute), Two-way ANOVA

6 $p < 0.05$, compared with the LLRP of w^{1118} recorded at the same time point (40-minute), Two-way ANOVA

Table 3-9. Response latencies and refractory periods of *w¹¹¹⁸*, and *DSC1^a* flies after 72 hours starvation (mean \pm SD)

	SL (ms)	SLRP (ms)	LL (ms)	LLRP (ms)
<i>w¹¹¹⁸</i>	1.1 \pm 0.1 (n=13)	5.5 \pm 0.6 (n=13)	3.5 \pm 0.2 (n=13) ¹	49.2 \pm 13.8 (n=13)
<i>DSC1^a</i>	1.1 \pm 0.1 (n=12)	6.0 \pm 1.6 (n=12)	3.3 \pm 0.2 (n=12) ²	35.3 \pm 5.8 (n=12) ³

Note:

SL- short latency

SLRP- short latency refractory period

LL- long latency

LLRP- long latency refractory period

1 $p < 0.05$, compared with the LLRP of *w¹¹¹⁸* recorded before starvation, Two-way ANOVA.

2 $p < 0.05$, compared with the LLRP of *DSC1^a* recorded before starvation, Two-way ANOVA.

3 $p < 0.05$, compared with the LLRP of *w¹¹¹⁸* recorded after starved for 72 hours, Two-way ANOVA.

Figure 3-1. Generation of *DSC1* knockout *D. melanogaster* lines. **A.** Schematic illustration of the targeting strategy. Stop codons (ST) were introduced in upstream and downstream homologue regions. A wild type genomic DNA fragment containing part of the *DSC1* gene was replaced through ends-out homologous recombination. The mini w^+ gene was used as a marker to indicate the successful replacement. **B.** Southern blot analysis of the genomic DNA of *DSC1* knockout flies. Kpn I was used to digest genomic DNA for Southern blot analysis. The positions of Kpn I sites are labeled and sizes of DNA fragments are shown in A. Sizes of DNA fragments are demonstrated. *DSC1* KO: *DSC1* knockout line.

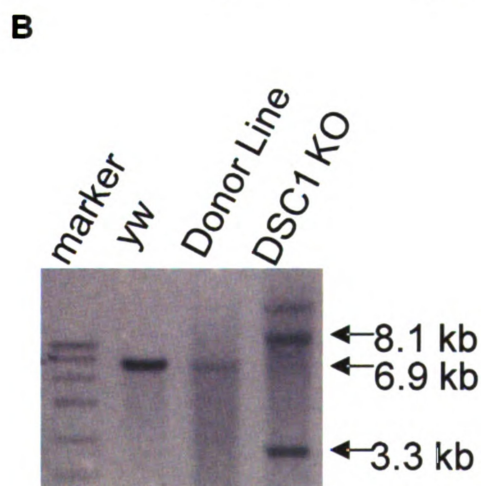
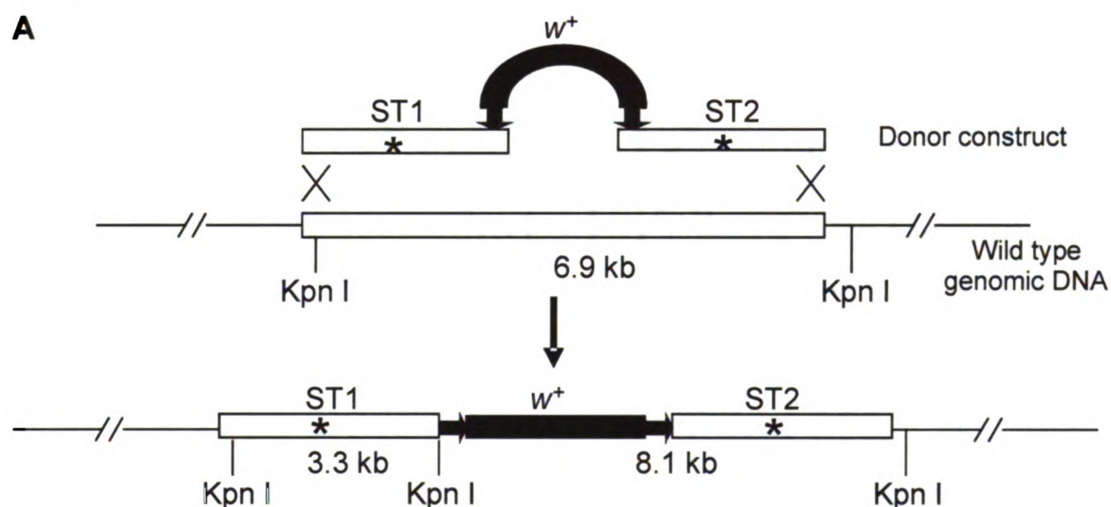


Figure 3-2. Schematic illustration of the giant fiber pathway (one side shown). High-voltage stimulation (high) activates the cervical giant fiber (CGF) to induce a short-latency response, whereas low voltage stimulation (low) excites brain afferent neurons to trigger a long-latency response. (TTM) Tergotrochanteral muscle; (TTMn) TTM motoneuron; (DLM) dorsal longitudinal muscle; (DLMn) DLM motoneuron; (PSI) peripherally synapsing interneuron. (modified from Engel et al.2000)

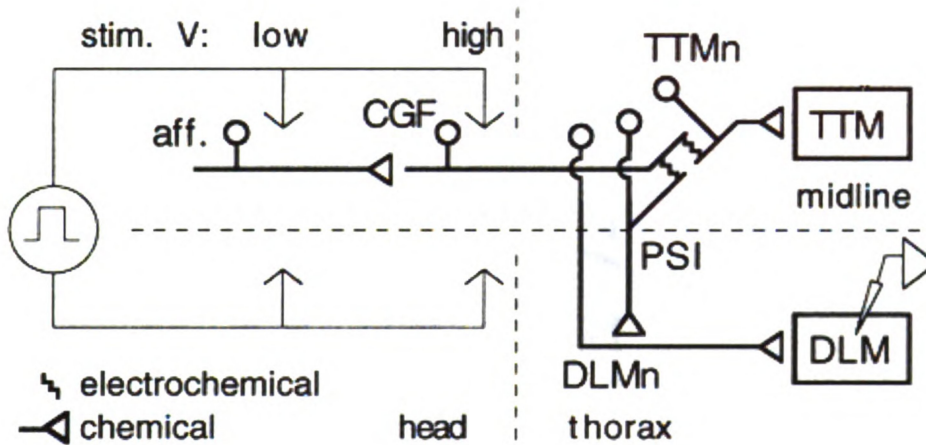
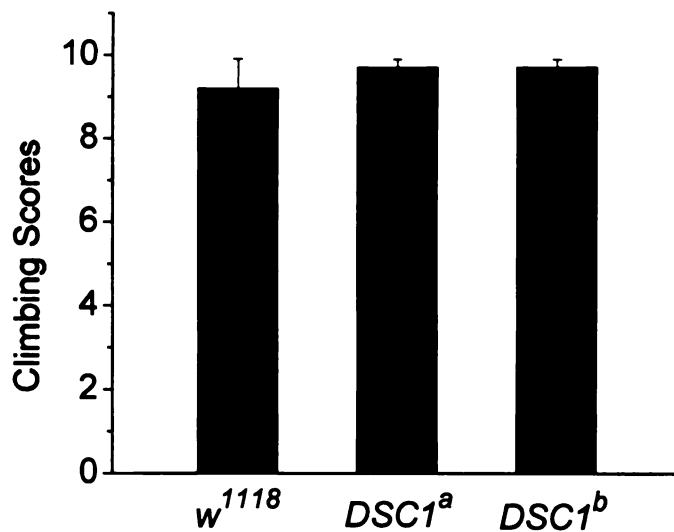


Figure 3-3. *DSC1* knockout flies have normal locomotor activity but are more jumpy than *w¹¹¹⁸* flies. **A.** Climbing assay carried out on *w¹¹¹⁸* flies (n=5), *DSC1^a* (n=5), and *DSC1^b* (n=5) flies at room temperature. **B.** Time course of paralysis in response to heat shock (40°C) of *w¹¹¹⁸* (n=5), *DSC1^a* (n=5) and *DSC1^b* (n=5) flies. **C.** The number of jumps of *w¹¹¹⁸* (n=5), *DSC1^a* (n=5) or *DSC1^b* (n=5) flies from the fifth to tenth minutes during heat shock (mean \pm SD, * $p < 0.05$, Student's *t*-test). The values are the averages of a total number of jump of 10 flies per vial.

A



B

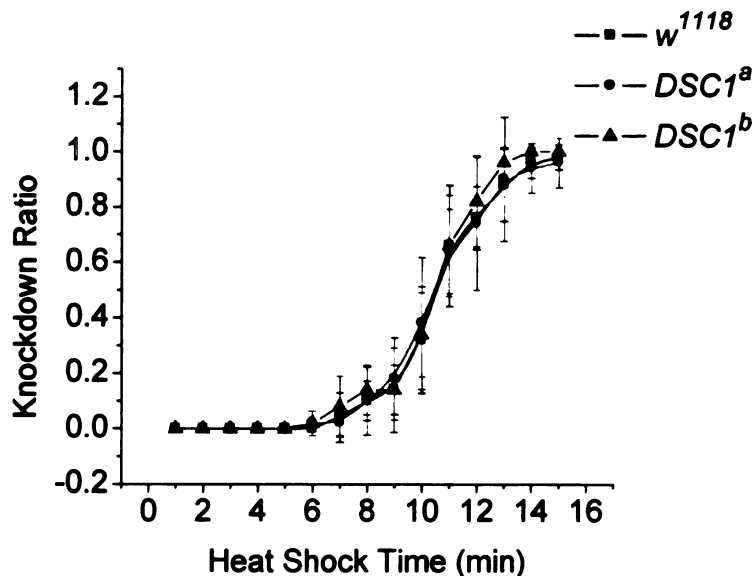


Figure 3-3 (continued)

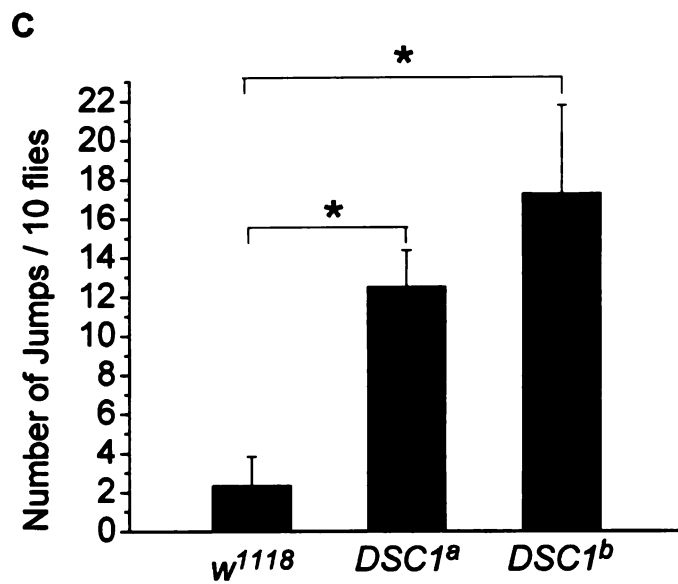


Figure 3-4. *DSC1* knockout flies recovered more slowly from heat shock than *w¹¹¹⁸* flies. The recovery from heat shock was determined using a climbing assay to measure the locomotor activity of *w¹¹¹⁸* (n=5), *DSC1^a* (n=5), and *DSC1^b* (n=5) flies. (mean \pm SD)

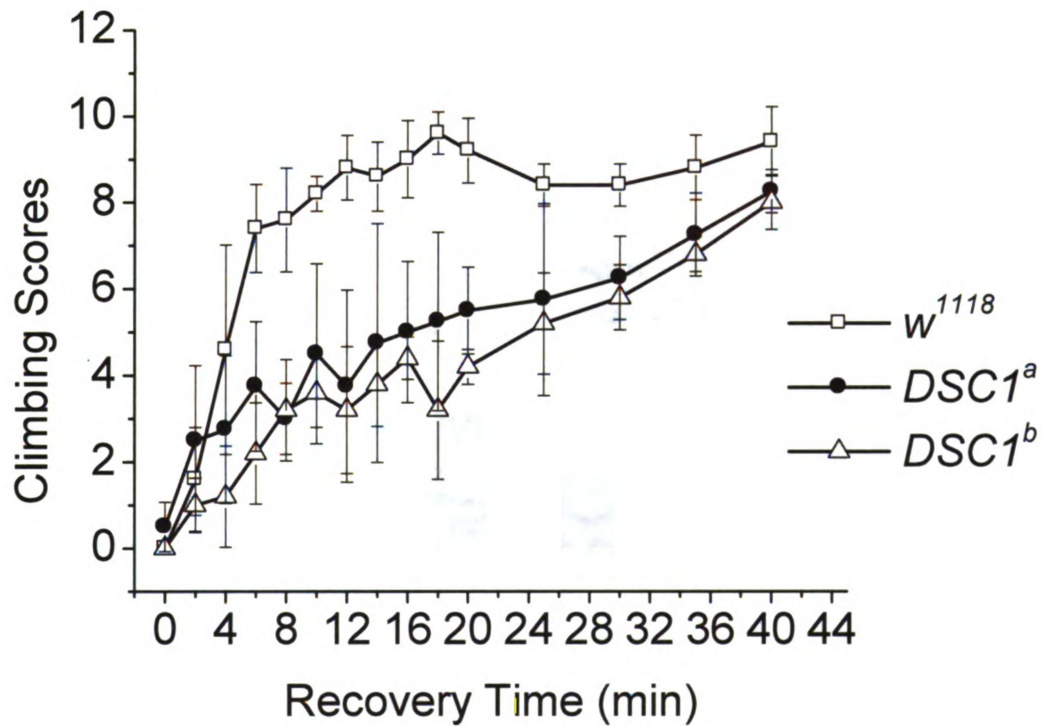
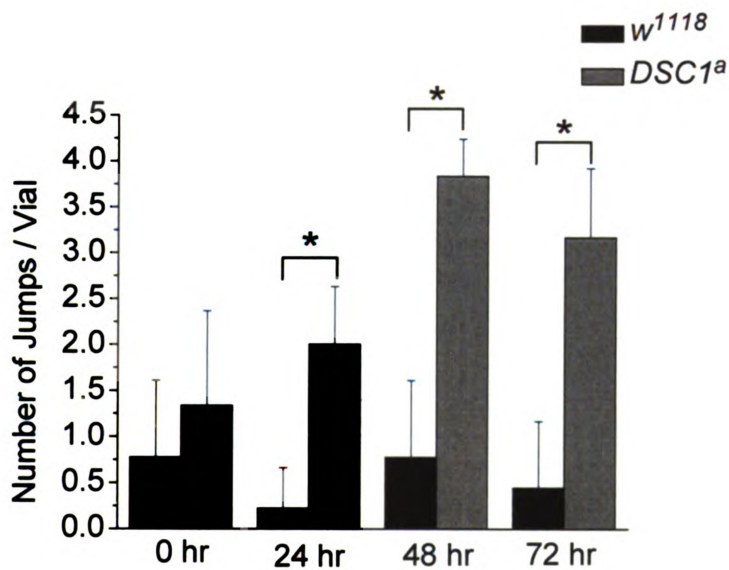


Figure 3-5. *DSC1* knockout flies jumped more and died earlier during starvation.

A. Number of jumps of *w¹¹¹⁸* (n=10) and *DSC1^a* (n=10) flies counted during the first three days of starvation. A jumpy phenotype similar to that induced during the heat shock was observed by a brief tapping of vials and videotaping. The number of jump per vial (five flies) was counted during the second to tenth seconds after tapping. (mean \pm SD, * $p < 0.05$, Two-way ANOVA). **B.** Survival curves of *w¹¹¹⁸* (n=6) and *DSC1^a* (n=6) flies. (mean \pm SD) **C.** Weights of individual fly of *w¹¹¹⁸* (n=40) and *DSC1^a* (n=40) line.

A



B

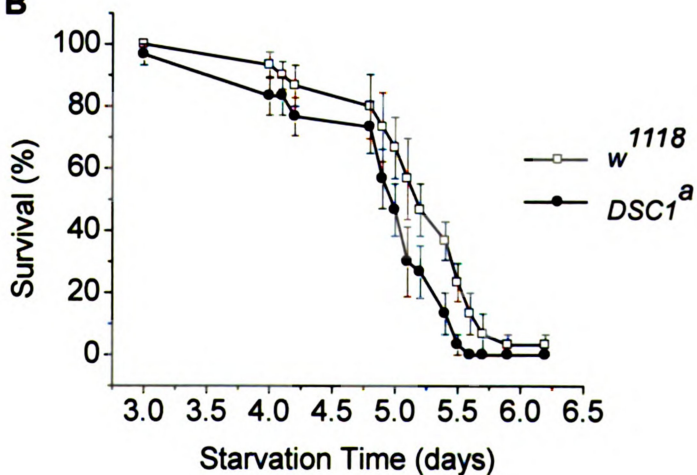


Figure 3-5 (continued)

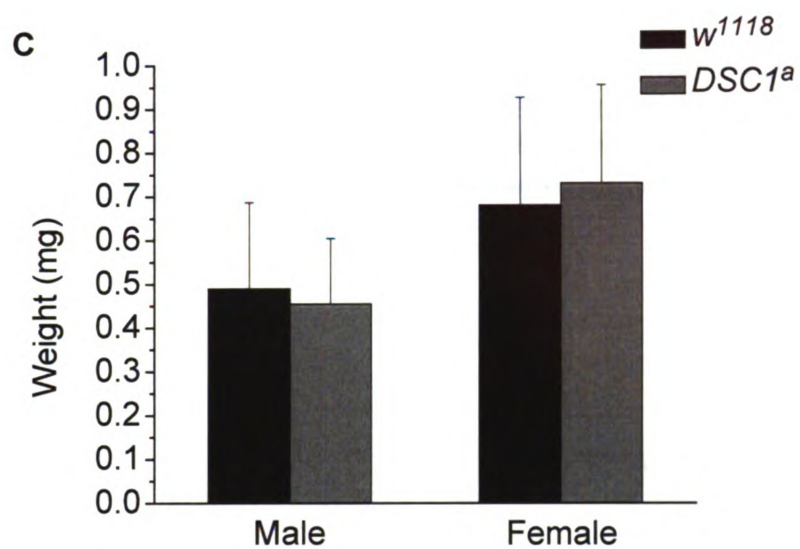


Figure 3-6. Giant fiber recording of the short latency pathway (**A. B.**) and the long latency pathway (**C. D.**) carried out on w^{1118} and $DSC1^a$ flies at different time points during heat shock. The latencies and refractory periods measured at room temperature before heat shock were included for comparison (RT). SL: short latency; SLRP: short latency refractory period; LL: long latency; LLRP: long latency refractory period; RT: room temperature. (mean \pm SD, * $p < 0.05$, Two-way ANOVA)

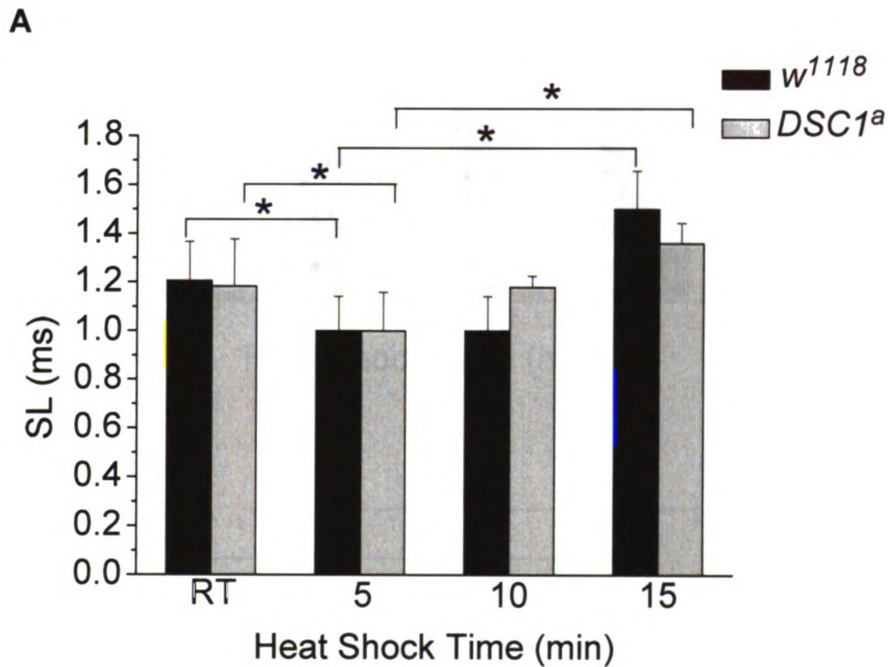
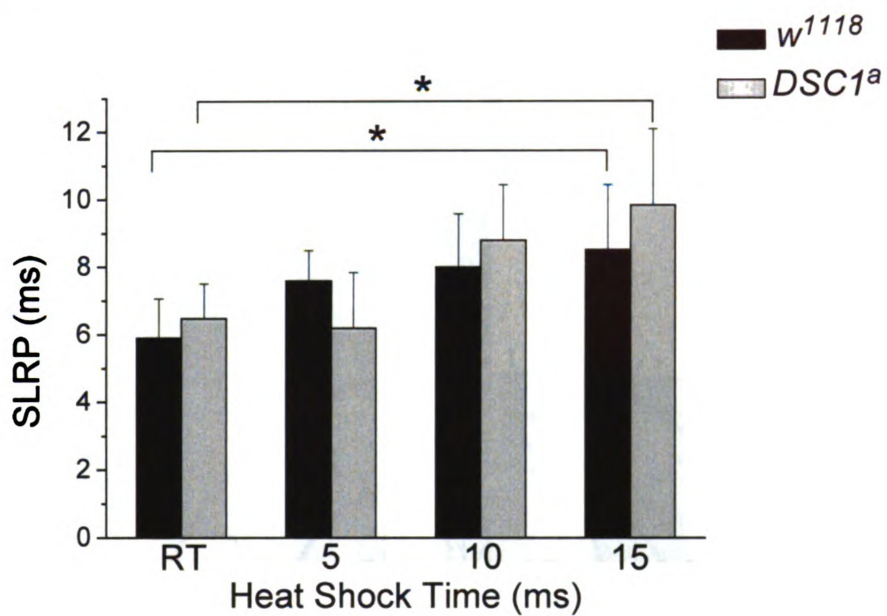


Figure 3-6 (continued)

B



C

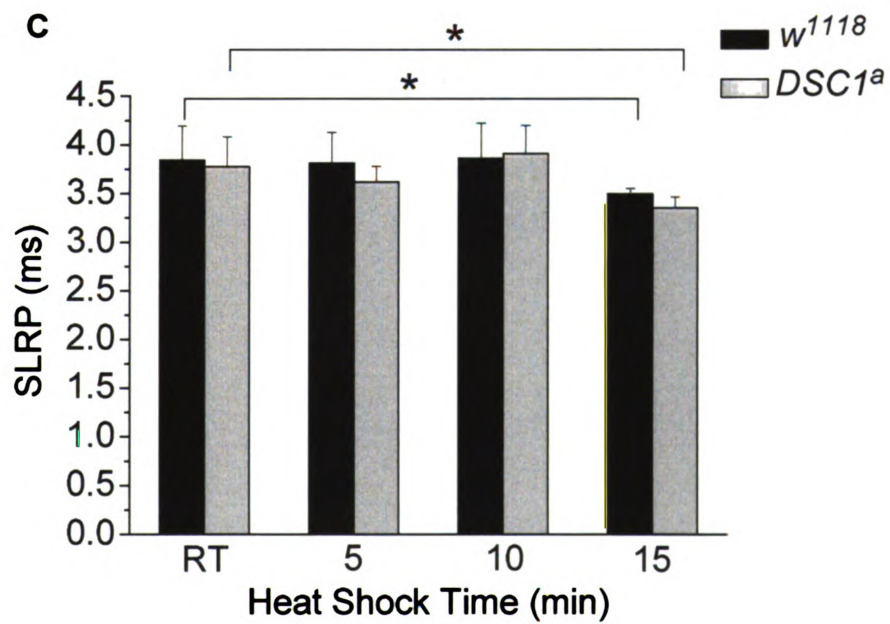


Figure 3-6 (continued)

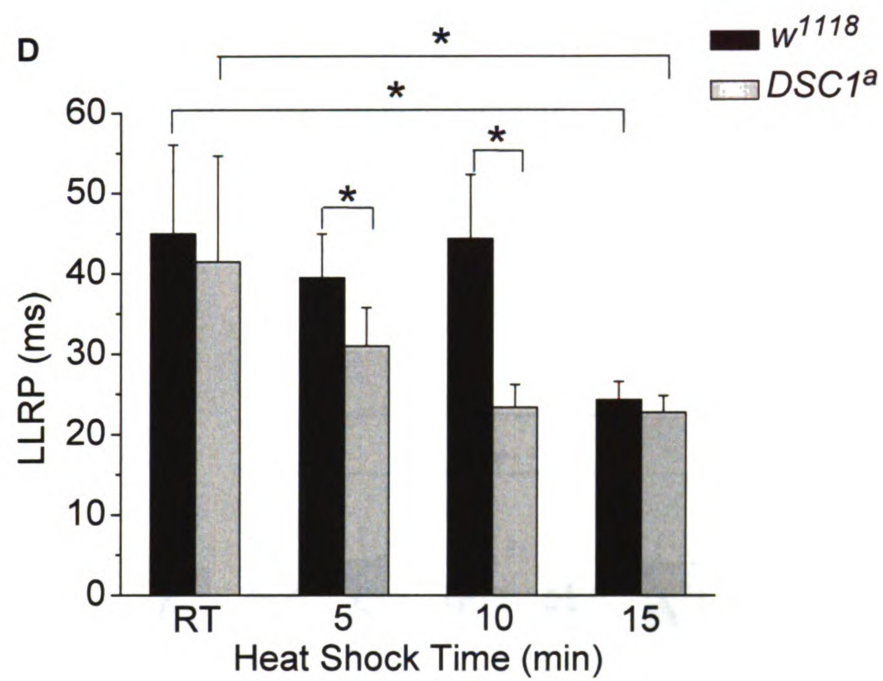


Figure 3-7. Giant fiber recording of the short latency pathway (A. B.) and the long latency pathway (C. D.) carried out on w^{1118} and $DSC1^a$ flies at different time points during a recovery process after heat shock. The latencies and refractory periods measured at room temperature before heat shock were included for comparison (RT). SL: short latency; SLRP: short latency refractory period; LL: long latency; LLRP: long latency refractory period; RT: room temperature. (mean \pm SD, * $p < 0.05$, two-way ANOVA) E. Locomotor activity of w^{1118} (n=60) and $DSC1^a$ (n=60) flies tested at the end of recovery process with a vortex. (mean \pm SD, # $p < 0.05$, Student's t -test)

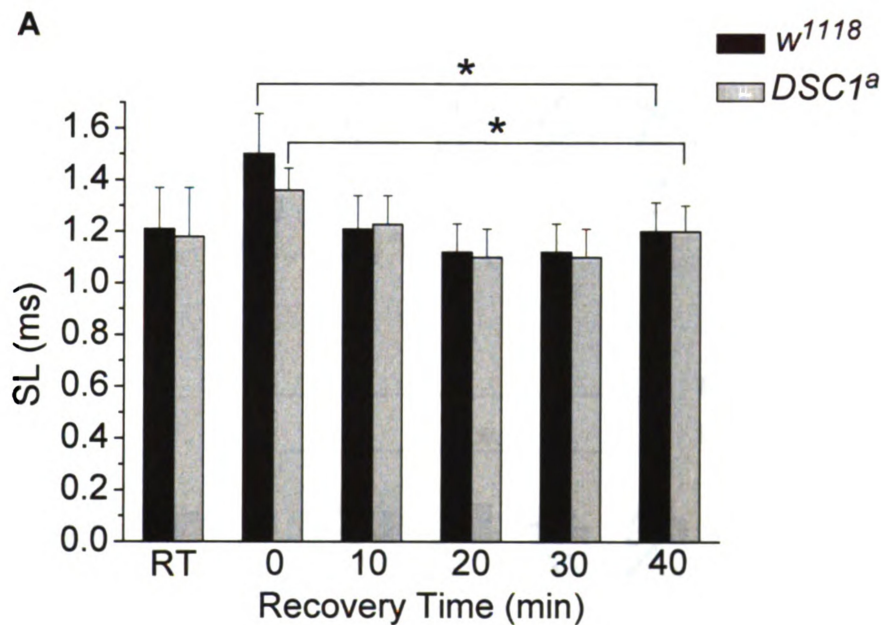


Figure 3-7 (continued)

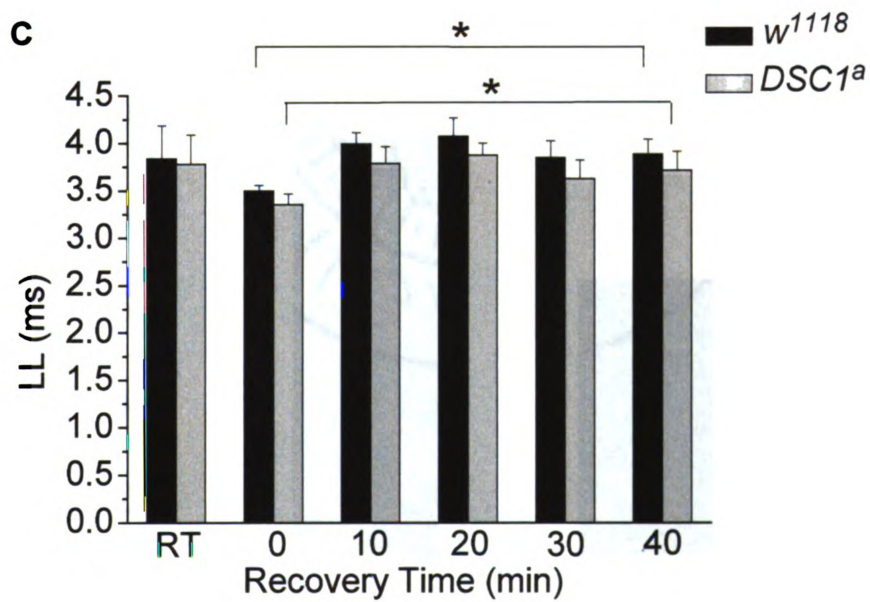
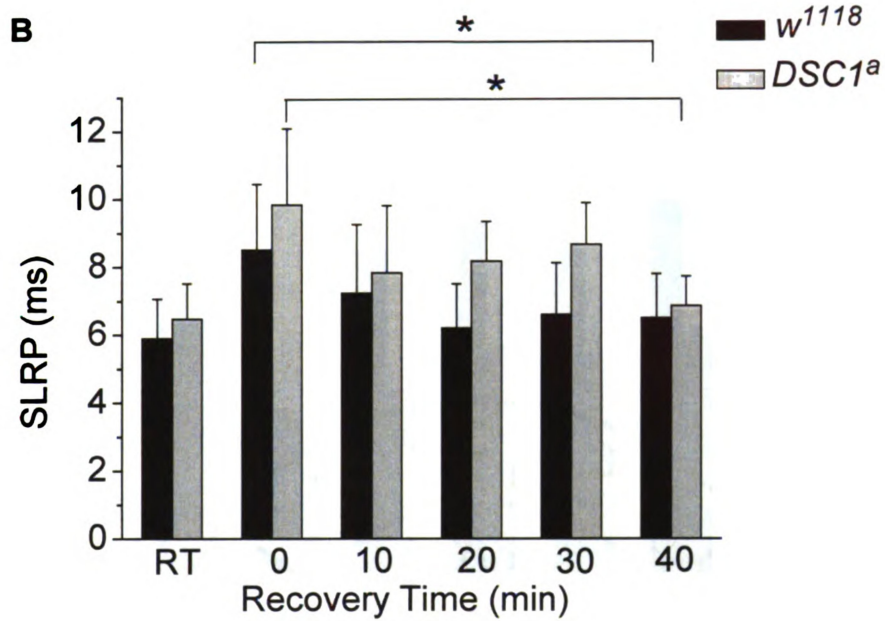


Figure 3-7 (continued)

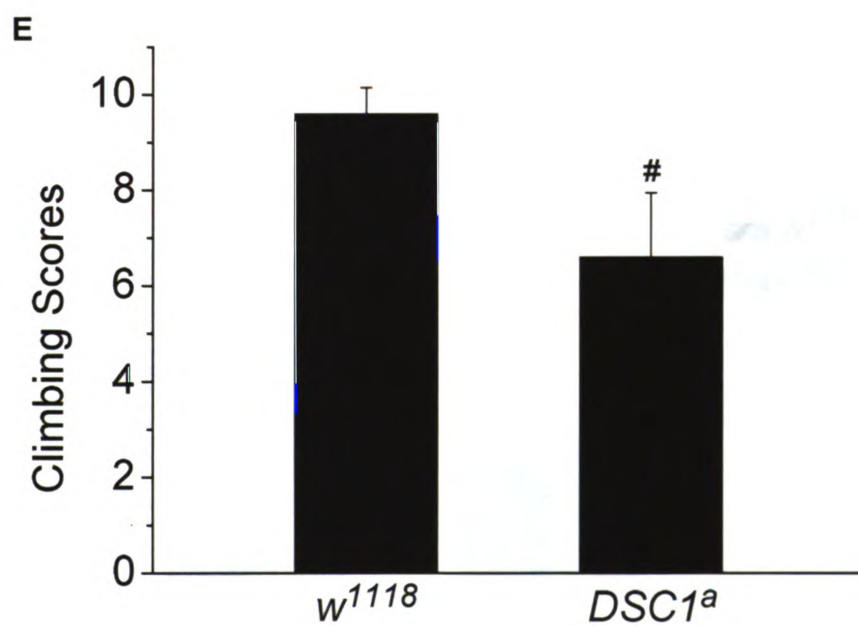
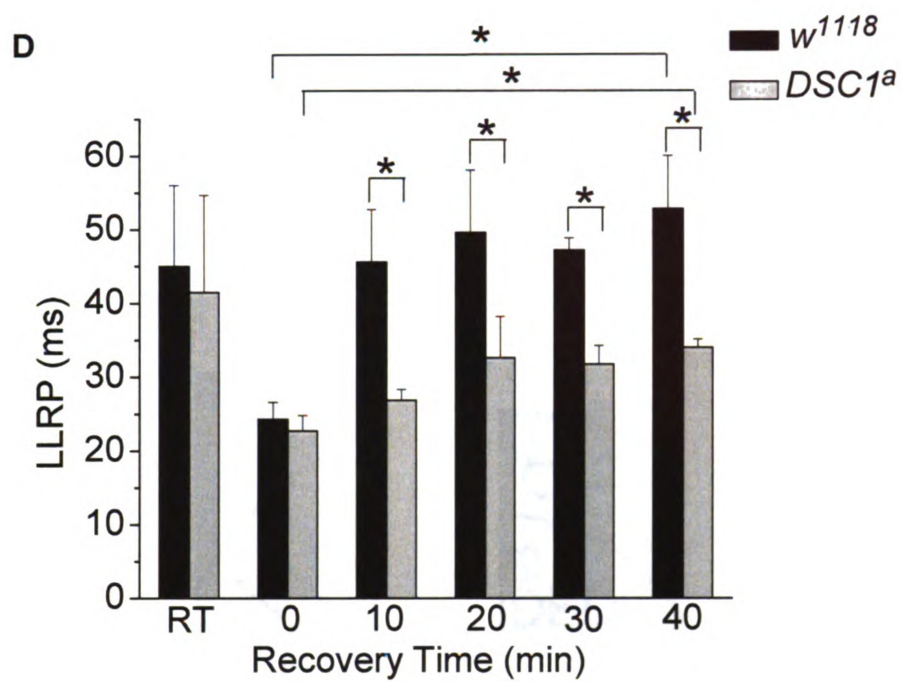


Figure 3-8. Giant fiber recording of the short latency pathway (A. B.) and the long latency pathway (C. D.) in w^{1118} and $DSC1^a$ flies after 72 hours of starvation. SL: short latency; SLRP: short latency refractory period; LL: long latency; LLRP: long latency refractory period; CT: values recorded before starvation. (mean \pm SD, * $p < 0.05$, Two-way ANOVA)

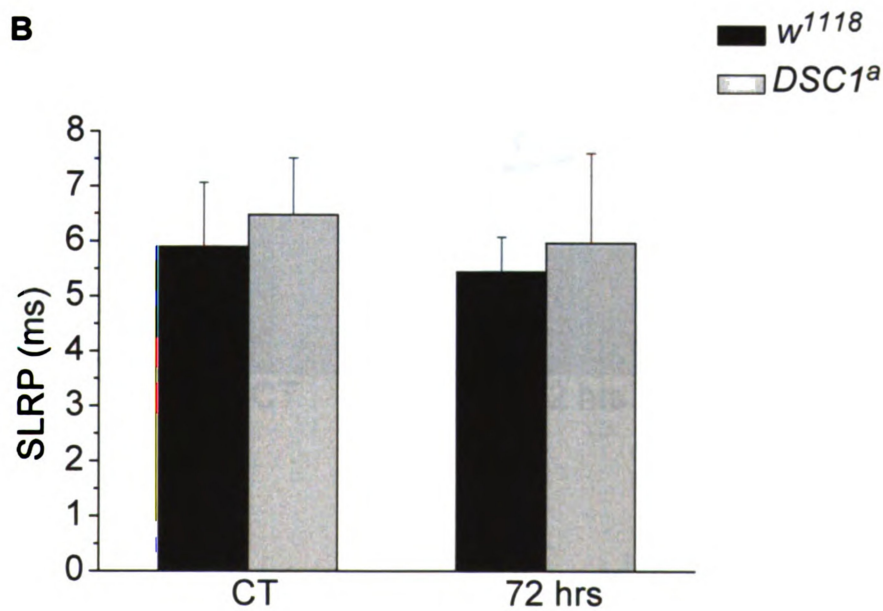
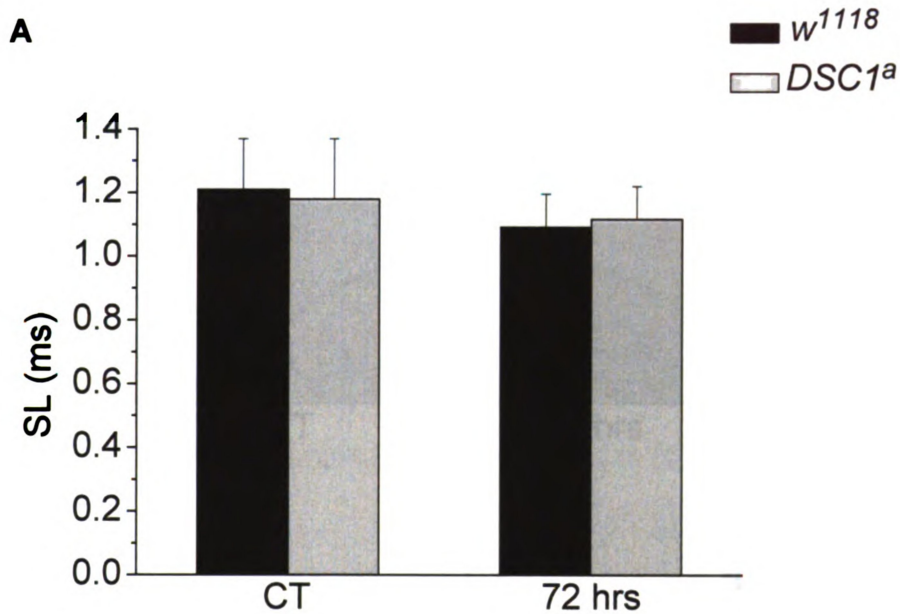
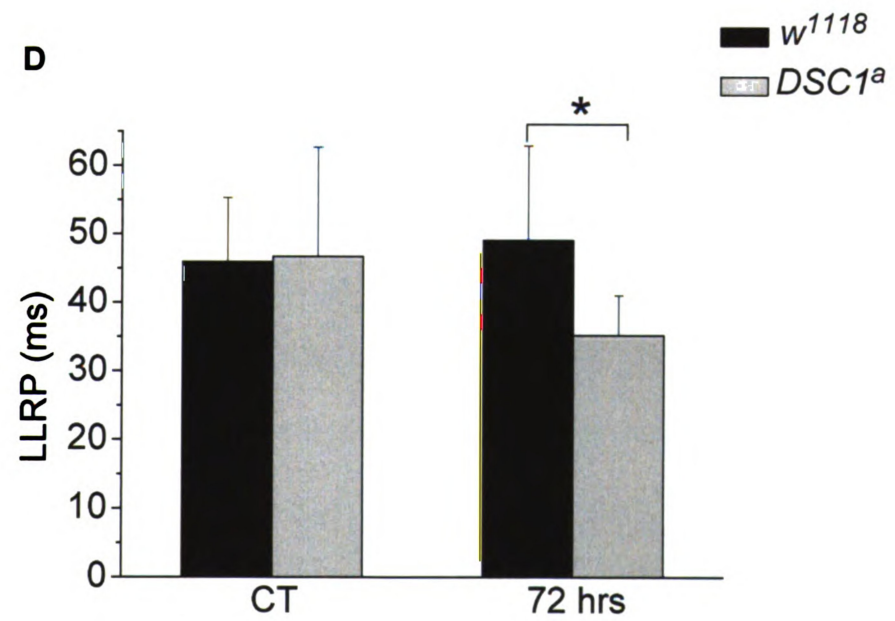
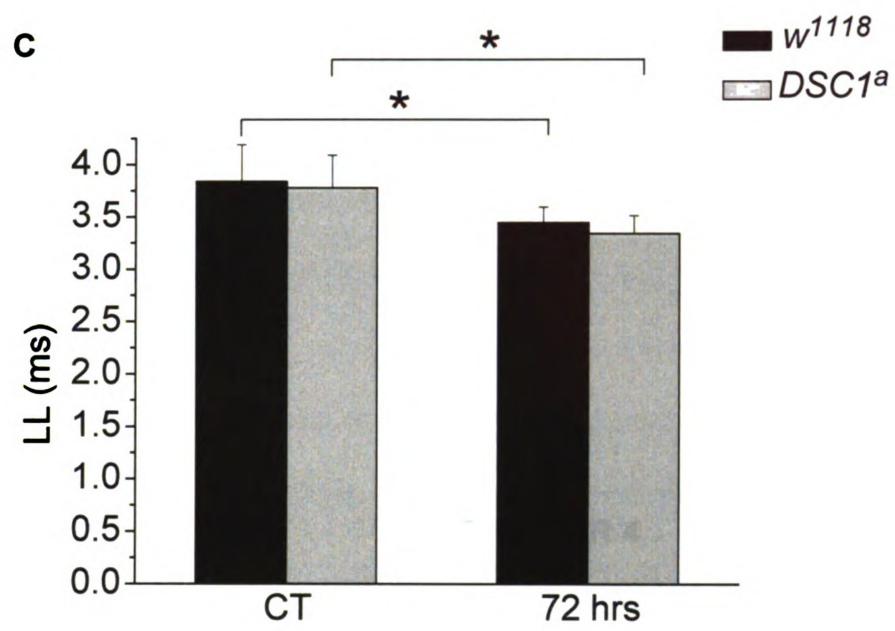


Figure 3-8 (continued)



CHAPTER 4

***DSC1* KNOCKOUT MUTANTS ARE MORE SUSCEPTIBLE TO PYRETHROID INSECTICIDES**

4.1 Abstract

Voltage- or ligand-gated ion channels are transmembrane proteins that mediate critical neuronal functions, such as action potential (AP) and neurotransmitter release. They are often the molecular targets of natural or synthetic neurotoxins, including insecticides. Voltage-gated sodium channels are the primary targets of two important classes of insecticides: sodium channel-gating modifying pyrethroid insecticides and sodium channel blocker insecticides (SCBIs). The DSC1 channel shares up to 50% identity in the transmembrane domains with Para sodium channels. However, whether the DSC1 channel is involved in the toxicology of pyrethroids and/or SCBIs remains unclear. In this study, using both contact and topical bioassays, I examined the susceptibility of adult *DSC1* knockout flies to four pyrethroids (permethrin, bioresmethrin, deltamethrin and fenvalerate), N-decarbomethoxyllated JW062 (DCJW), a potent metabolite of a SCBI, indoxacarb, and fipronil, a γ -aminobutyric acid (GABA)-gated chloride channel blocker insecticide. I found that *DSC1* knockout flies were more susceptible to all pyrethroids tested, but remain as susceptible as wild-type flies to DCJW and fipronil. To determine whether the increased susceptibility to pyrethroids is due to enhanced sensitivity of the nervous system, I examined the response of a well-defined neural circuit, the giant fiber system, to deltamethrin. Indeed, compared with that of wild-type flies, the giant fiber system of *DSC1* knockout flies was more sensitive to pyrethroids. These results indicate that the DSC1 channel is involved in dampening the neuronal excitability induced by pyrethroids, which is reminiscent of the role of the

DSC1 channel in modulating neuronal excitability in response to heat shock and starvation reported in the Chapter 3.

4.2 Introduction

Voltage-gated ion channels (VGICs) are transmembrane proteins located on the surface of every excitable cell. Opening and closure of these channels are regulated by the membrane potential. Opening of VGICs leads to either outward or inward currents, which in turn may either depolarize or hyperpolarize the membrane potential to facilitate critical cellular functions such as initiation and propagation of APs and neurotransmitter release.

VGICs can be classified into several groups based on their ion selectivity and play different roles in modulating specific cellular functions (Yu et al., 2005; Catterall et al., 2007). For example, voltage-gated sodium channels are responsible for the rising phase of an AP, whereas voltage-gated potassium channels mediate the falling phase of an AP. There are more than nine voltage-gated sodium channel genes identified in mammals by far, but only one confirmed sodium channel gene in insects, such as *para* in *Drosophila melanogaster*. The *Drosophila sodium channel 1* (*DSC1*) gene was discovered in 1987, and was initially predicted to encode a sodium channel based on its high sequence similarity with sodium channels. However, functional characterization in *Xenopus* oocytes showed that *DSC1* encodes a novel voltage-gated cation channel, instead of a conventional voltage-gated sodium channel (Chapter 2).

VGICs are some of the most important targets of insecticides (Soderlund and

Bloomquist, 1989; Soderlund, 1990; Narahashi, 1996; Narahashi, 2000; Ray and Fry, 2006). In particular, sodium channels are a well-known target of two widely used classes of insecticides, pyrethroids (Narahashi, 1996; Narahashi, 2000; Narahashi et al., 2007) and SCBIs (Silver and Soderlund, 2005). The modes of action of pyrethroids and SCBIs are different. Pyrethroids inhibit channel deactivation and inactivation, causing persistent activation of sodium channels (Narahashi, 1996; Narahashi, 2000), whereas SCBIs block sodium channels in a state-dependent manner (Zhao et al., 2003). Pyrethroids are classified into type I and type II pyrethroids based on the absence (type I) or presence (type II) of a α -cyano-3-phenoxybenzyl alcohol (See Fig. 1-3) (Soderlund and Bloomquist, 1989). Although both type I and type II pyrethroids are sodium channel gating modifiers, type II pyrethroids alter gating kinetics more drastically than type I pyrethroids, causing a much slower decaying tail current upon repolarization. At the cellular level, type I pyrethroids produce repetitive discharges, whereas type II compounds do not (Soderlund and Bloomquist, 1989). Instead, type II pyrethroids cause stimulus-dependent membrane depolarization and block of nerve conductance (Narahashi, 1988; Soderlund and Bloomquist, 1989; Narahashi, 1992).

The predicted topology of the DSC1 protein is highly similar to that of the sodium channel, and DSC1 shares the highest amino acid sequence similarity to the Para sodium channel, with up to 50% identity in the four transmembrane domains. However, it is not known whether DSC1 is involved in the toxicology of pyrethroids and/or SCBIs. In this study, I evaluated the susceptibility of adult *w*¹¹¹⁸

and *DSC1* knockout flies using both contact and topical bioassays to four pyrethroids, as well as DCJW, a potent metabolite of indoxacarb, and a GABA-gated chloride channel blocker, fipronil.

4.3 Materials and Methods

4.3.1 Fly stocks

Two initial *DSC1* knockout *D. melanogaster* founder lines, *DSC1-3* and *DSC1-6*, were generated by Dr. Ningguang Luo, a former post-doc associate in our lab, using homologous recombination-mediated gene disruption (Gong and Golic, 2003). *DSC1-6* was backcrossed to w^{1118} for five generations to generate *DSC1^a*, while *DSC1-3* was backcrossed to w^{1118} for five generations to generate *DSC1^b*. *DSC1^b* was further back crossed to w^{1118} for four generations to generate *DSC1^c*. *DSC1^a* and *DSC1^c* were used in insecticide bioassays. w^{1118} was used as a wild-type control in all experiments. All these lines were raised on regular cornmeal-molasses-agar medium at room temperature.

4.3.2 Contact bioassay:

A 0.5-ml insecticide solution dissolved in acetone was delivered into a 25-ml glass scintillation vial. To coat the inner surface of the vial with insecticide, the vial was rolled on the side in a chemical fume hood for 3 to 5 min. Vials were kept in the hood for another 30 min to evaporate residual acetone. Twenty flies at the age

of two to three days old were slightly immobilized by CO₂ and put into the insecticide-coated scintillation vials. Vials were plugged with a cotton ball and 3 ml of 20% sugar water was then added on the cotton ball. The vials were then kept at room temperature and the number of dead flies was counted 24 hours later. Three to five replicates were carried out for each concentration. The bioassay was repeated at least three times. The median lethal concentration (LC₅₀) and 95% confidential interval were calculated using the POLOplus software (LeOra Software Company, Petaluma, CA). The LC₅₀ ratio is defined as the LC₅₀ of *w*¹¹¹⁸ flies divided by the LC₅₀ of *DSC1* knockout flies.

4.3.3 Topical bioassay:

For topical bioassay, 2- to 3-day-old male flies were slightly immobilized by CO₂ and 0.2 µl insecticide acetone solution was delivered onto the dorsal side of thorax of individual flies. The treated flies were held in disposable plastic Petri dishes (6-cm diameter × 1-cm height) lined with a moistened filter paper (Whatman, Clifton, NJ) at room temperature for 15 minutes. Two toxicity-associated phenotypes, abdomen elongation and knockdown, were recorded. The abdomen elongation phenotype was defined as rigid, elongated abdomen (See Fig. 4-2B) in comparison with shorter, flexible abdomen (See Fig. 4-2A) before insecticide exposure. The knockdown phenotype was defined as losing the ability to walk. The median effective dose (ED₅₀) and 95% confidential

interval for both phenotypes were calculated using the POLOplus software (LeOra Software Company, Petaluma, CA).

4.3.4 Giant fiber recording

A dose of 0.4 ng deltamethrin (i.e., ED₉₅ of knockdown of *w*¹¹¹⁸ flies) or 4 ng bioresmethrin was topically delivered to individual 2- or 3-day old male flies. The dose of bioresmethrin was chosen based on contact bioassay results which show that the LC₅₀ of bioresmethrin was about 10 times higher than that of deltamethrin. The activities in the giant fiber system (GFS) were recorded 15 min after pyrethroid exposure. The methods for recording the response latency and refractory period are the same as those described in Chapter 3.

To examine the stability of the GFS, I used a protocol modified from those described in (Tanouye and Wyman, 1980; Fayyazuddin et al., 2006). A train of 50 pulses of 30 V was delivered at the frequency of 100 Hz. The response (i.e., muscle potentials) of dorsal longitudinal muscles (DLMs) to this stimulation was recorded. The 50 pulses were divided into 5 groups with 10 pulses in each group; and the number of muscle potentials in each group was counted.

4.3.5 Statistics

Student's *t*-test was used to analyze the data of muscle potentials elicited by high frequency stimulus. Log-rank test was used to analyze the data of the percentage of knockdown that are obtained after being exposed to deltamethrin

for various periods. Two-way analysis of variance (ANOVA) with Tukey's test employed as the *post hoc* test were used to analyze the other GF recording data. $P < 0.05$ was set as the criterion for statistical significance.

4.4 Results

4.4.1 *DSC1* knockout flies are more sensitive to pyrethroids, but not to DCJW and fipronil

To determine whether the *DSC1* channel could be involved in the toxicity of pyrethroids, a contact bioassay was performed using w^{1118} , *DSC1^a*, and *DSC1^c* flies. *DSC1^a* flies and *DSC1^c* were about 2-fold more susceptible, measured by lethality, than w^{1118} to all four pyrethroids tested: two type I pyrethroids, permethrin and bioresmethrin, and two type II pyrethroids, deltamethrin and fenvalerate (Table 4-1, 4-2, 4-3, 4-4). In contrast, w^{1118} and *DSC1* knockout flies exhibited similar susceptibility to DCJW and fipronil (Table 4-5, 4-6).

4.4.2 *DSC1* knockout flies are more sensitive to knockdown by deltamethrin

Being extremely lipophilic, pyrethroids can be taken up by insects easily and affect sodium channels yielding the acute knockdown symptom, which is an important characteristics of pyrethroid intoxication (Narahashi, 1996). To study if *DSC1* knockout flies are also more easily knocked down by pyrethroids, I performed a topical bioassay using deltamethrin on w^{1118} and *DSC1^a* flies.

Results showed that *DSC1^a* flies were more susceptible to deltamethrin than *w¹¹¹⁸* flies (Fig. 4-1, Table 4-7). During these experiments, I noticed another phenotype. After being exposed to deltamethrin for 15 minutes, the shape of the abdomen of some flies changed from a smooth and soft state (Fig. 4-2A) to an elongated and rigid state (Fig. 4-2B). *DSC1^a* flies more frequently displayed this deltamethrin-induced abdomen elongation phenotype (Fig. 4-2C, Table 4-8).

To compare the kinetics of intoxication of *w¹¹¹⁸* and *DSC1^a* lines, I topically applied 0.04 ng deltamethrin, which is close to the ED₅₀ of *DSC1^a* flies, to individual fly and observed the knockdown phenotype for two hours. The number of flies that were knocked down was recorded every 15 minutes during the first hour and every 30 minutes during the second hour. A time-response curve was generated (Fig. 4-3). *w¹¹¹⁸* flies began to exhibit the knockdown phenotype at about 15 minutes after pyrethroid exposure, and the percentage of knockdown peaked at 90 minutes and then decreased. The kinetics of knockdown of *DSC1^a* flies was parallel to that of *w¹¹¹⁸* flies. However, at 30, 45, and 60 minutes after pyrethroid exposure, the percentage of knockdown of *DSC1^a* flies was significantly higher than that of *w¹¹¹⁸* flies ($p < 0.05$, Log-rank test).

4.4.3 Pyrethroids destabilized the GFS of *DSC1*^a knockout flies to a greater extent

To investigate whether the enhanced pyrethroid susceptibility of *DSC1*^a flies is correlated with an enhanced sensitivity of the nervous system to pyrethroids, we examined the response of a well-defined neuronal circuit, the GFS, to bioresmethrin (a type I pyrethroid) and deltamethrin (a type II pyrethroid). I first examined the activities of short and long latency pathways of *DSC1*^a and *w*¹¹¹⁸ flies 15-min after topical application of bioresmethrin (type I) and deltamethrin (type II). Unexpectedly, bioresmethrin had no effect on the long or short latency pathways of *w*¹¹¹⁸ flies (Fig. 4-4). However, bioresmethrin increased the short latency (Table 4-9, Fig. 4-4 A), but reduced the short latency refractory period (SLRP) of *DSC1*^a flies (Fig. 4-4 B). Bioresmethrin also did not affect the latency or the refractory period of the long latency pathway of *DSC1*^a flies (Fig. 4-4 C, D). In contrast to bioresmethrin, deltamethrin did not alter the latency or the refractory period of the short latency pathway of either line (Table 4-10, Fig 4-5 A, B). However, deltamethrin shortened both the latency and the refractory period of the long latency pathway of both *w*¹¹¹⁸ and *DSC1*^a flies, but there was no difference between the two lines (Fig. 4-5 C, D).

In wild-type *Drosophila* flies, the short latency pathway to the DLM can follow stimuli at frequencies as high as 100 Hz (Tanouye and Wyman, 1980). To further characterize the function (i.e., stability) of the GFS, we examined the response of

both w^{1118} and $DSC1^a$ flies to high frequency stimulation in the absence and presence of pyrethroids. In response to a train of 50 pulses delivered at 100 Hz at the amplitude of 30 V, each stimulus evoked a muscle potential from the DLM and a total of 50 muscle potentials were recorded. A recording trace of 10 muscle potentials in response to the first 10 pulses is shown in Fig. 4-6 A. No difference was observed between w^{1118} and $DSC1^a$ flies after topically applying 0.2 μ l acetone (Fig. 4-6 B). In the presence of deltamethrin, the number of muscle potentials was reduced to about seven in the fifth 10 stimuli in w^{1118} flies, indicating that deltamethrin destabilizes the function of the GFS. Interestingly, in $DSC1^a$ flies the reduction in muscle potentials was already evident in the second 10 stimuli and this reduction progressed in the remaining three groups of 10 stimuli (Fig. 4-6 C). Bioresmethrin affected the function of the GFS more drastically than deltamethrin. In w^{1118} flies, the number of muscle potentials during the third 10 stimuli was reduced to about 3; and no muscle potentials were elicited in the remaining two groups of 10 stimuli (Fig. 4-6 D). Again, the function of the GFS in $DSC1^a$ flies was more sensitive to bioresmethrin; a reduction in muscle potential number was observed in the second 10 stimuli (Fig. 4-6 D). Thus, both type I and type II pyrethroids affect the GFS, with bioresmethrin being more potent than deltamethrin. The $DSC1^a$ flies are hypersensitive to pyrethroids, compared with w^{1118} flies.

4.5 Discussion

Ion channels are transmembrane proteins that are essential for neuronal functions. Many natural or synthetic neurotoxins and insecticides target ion channels. For example, voltage-gated sodium channels are the primary targets of pyrethroid insecticides and sodium-channel-blocker insecticides, such as DCJW. Synthetic pyrethroids are a group of environmentally friendly, highly effective, and very selective insecticides used globally for pest control. Unfortunately, with intensive application, insecticide resistance has emerged in numerous insect populations, resulting in reduced efficacy of insecticides. As a result, pest control often requires higher insecticide dosages, which poses greater risks to humans, wildlife, and environment (Jeyaratnam, 1990; Konradsen, 2007). There is a great need to enhance the effectiveness of available insecticides and also to discover new insecticides that are highly selective against insects. In this study, I found that *DSC1* knockout flies were more susceptible to both type I and type II pyrethroids, compared with *w¹¹¹⁸* flies. The effects of the *DSC1* channel on the toxicity of pyrethroids are evident in both short- and long-duration exposures since *DSC1* knockout flies are sensitive to both pyrethroid-induced rapid knockdown and eventual lethality. I predict that an inhibitor of the *DSC1* channel may enhance the efficacy of pyrethroids against pests. Therefore, this channel may be a potential target for the development of a new generation of insecticide synergists.

To gain an understanding of the involvement of the *DSC1* channel in insect susceptibility to pyrethroids, I compared the activities of the GFS in *w¹¹¹⁸* and

DSC1 knockout flies before and after pyrethroid application. The three main findings and the implications of these findings are summarized below.

First, the type II pyrethroid deltamethrin, but not type I bioresmethrin, reduced the response latency and the refractory period of the long latency pathway in both *w*¹¹¹⁸ and *DSC1* knockout flies. The effects of deltamethrin, but not bioresmethrin, on the long latency pathway may be caused by differences in the modification of sodium channel gating by type I vs. type II pyrethroids. It is known that type II pyrethroids modify the gating of sodium channels to a greater extent than type I pyrethroids, resulting in more drastic alterations in neuronal excitability (Narahashi, 1992; Bloomquist, 1993). At the cellular level, type I pyrethroids induce repetitive firing, whereas type II pyrethroids cause membrane depolarization (Narahashi, 1988; Narahashi, 1992). Splice variants with differential sensitivity to type I and type II pyrethroids have been isolated from *Blattella germanica* and *D. melanogaster* (Tan et al., 2002; Du et al., 2009b; Hu et al., unpublished data). Perhaps neurons that are important for the long latency pathway but not for the short latency pathway (e.g., those in the brain that are presynaptic to the giant fiber) express sodium channel variants that are more sensitive to deltamethrin or more resistant to bioresmethrin.

Secondly, the refractory period of the short latency pathway was reduced by bioresmethrin in *DSC1* knockout flies although neither deltamethrin nor bioresmethrin altered the latency or refractory period of the short latency pathway in *w*¹¹¹⁸ flies. Thus, knockout of the *DSC1* gene possibly potentiates the repetitive firing induced by type I pyrethroids. This finding supports my

hypothesis in Chapter 3 that the DSC1 channel dampens neuronal excitability, based on enhanced excitability of *DSC1 knockout* flies in response to heat shock and starvation. The lack of an effect of deltamethrin on the refractory period of the short latency pathway in *DSC1* knockout flies may be explained by the unique mode of action of type II pyrethroid, which does not induce repetitive firing, but mainly causes depolarization of the membrane potential.

Thirdly, both pyrethroids reduced the ability of the short latency pathway to follow stimulus at high frequency; and the effect was more pronounced on *DSC1* knockout flies than on *w¹¹¹⁸* flies. These results indicate that the nervous system of *DSC1* knockout flies is more sensitive to pyrethroids than that of *w¹¹¹⁸* flies.

The *DSC1* mutation does not alter the action of DCJW, a sodium channel blocker. I found this result intriguing because the effect of the DSC1 channel is evident only when sodium channels are activated (by pyrethroids), but not when sodium channels are blocked (by DCJW). *DSC1* knockout flies are also not more sensitive or resistant to fipronil compared with *w¹¹¹⁸*. Fipronil blocks GABA-gated chloride channels, thereby enhancing the overall excitability of the nervous system, similar to that of pyrethroids. The fact that *DSC1* knockout flies are not altered in fipronil sensitivity indicates that enhanced nerve excitability per se may not be the basis for the effect of the *DSC1* knockout. Instead, my results support the hypothesis the DSC1 channel functions specifically along with sodium channels to regulate the initiation and propagation of action potential in the

nervous system.

In conclusion, the results reported in this chapter show that the knockout of the *DSC1* gene increases the toxicity of the sodium-channel-activators insecticides pyrethroids. This effect is accompanied by an enhancement of the sensitivity of the nervous system to pyrethroids in *DSC1* knockout flies. The lack of an effect of *DSC1* knockout on the action of blockers of sodium channels or GABA-gated chloride channels indicates that the DSC1 channel dampens neuronal excitability likely by modulating the initiation and propagation of the action potential, in which activation of sodium channels is crucial.

Table 4-1 Susceptibility of w^{1118} and *DSC1* knockout flies to permethrin (contact bioassay)

	LC ₅₀ (95%CI) (µg/vial)	<i>n</i>	Slope (SE)	LC ₅₀ ratio
w^{1118}	14.00 (11.56-16.57)	1680	3.47 (0.23)	-
<i>DSC1</i> ^a	5.01 (4.37-5.75)	700	3.06 (0.25)	2.8
<i>DSC1</i> ^c	5.37 (4.17-6.68)	600	3.95 (0.34)	2.6

Note:

LC₅₀, median lethal concentration

LC₅₀ ratio = (LC₅₀ of w^{1118}) / (LC₅₀ of *DSC1* knockout line)

Table 4-2 Susceptibility of w^{1118} and *DSC1* knockout flies to bioresmethrin (contact bioassay)

	LC ₅₀ (95%CI) (µg/vial)	<i>n</i>	Slope (SE)	LC ₅₀ ratio
w^{1118}	3.80 (3.34-4.31)	640	2.68 (0.21)	-
<i>DSC1</i> ^a	2.18 (1.95-2.43)	640	3.32 (0.27)	1.7
<i>DSC1</i> ^c	2.04 (1.83-2.27)	640	3.41 (0.27)	1.9

Note:

LC₅₀, median lethal concentration

LC₅₀ ratio = (LC₅₀ of w^{1118}) / (LC₅₀ of *DSC1* knockout line)

Table 4-3 Susceptibility of *w*¹¹¹⁸ and *DSC1* knockout flies to deltamethrin (contact bioassay)

	LC ₅₀ (95%CI) (µg/vial)	<i>n</i>	Slope (SE)	LC ₅₀ ratio
<i>w</i> ¹¹¹⁸	0.46 (0.38-0.55)	2220	2.79 (0.14)	-
<i>DSC1</i> ^a	0.25 (0.21-0.30)	640	1.96 (0.15)	1.9
<i>DSC1</i> ^c	0.20 (0.16-0.25)	240	3.43 (0.62)	2.3

Note:

LC₅₀, median lethal concentration

LC₅₀ ratio = (LC₅₀ of *w*¹¹¹⁸) / (LC₅₀ of *DSC1* knockout line)

Table 4-4 Susceptibility of *w*¹¹¹⁸ and *DSC1* knockout flies to fenvalerate (contact bioassay)

	LC ₅₀ (95%CI) (µg/vial)	<i>n</i>	Slope (SE)	LC ₅₀ ratio
<i>w</i> ¹¹¹⁸	3.09 (2.73-3.37)	860	3.28 (0.32)	-
<i>DSC1</i> ^a	1.4 (0.85-1.92)	1160	2.5 (0.23)	2.2
<i>DSC1</i> ^c	1.65 (0.99-2.41)	860	2.15 (0.21)	1.9

Note:

LC₅₀, median lethal concentration

LC₅₀ ratio = (LC₅₀ of *w*¹¹¹⁸) / (LC₅₀ of *DSC1* knockout line)

Table 4-5 Susceptibility of *w*¹¹¹⁸ and *DSC1*^a flies to DCJW (contact bioassay)

	LC ₅₀ (95%CI) (µg/vial)	<i>n</i>	Slope (SE)	LC ₅₀ ratio
<i>w</i> ¹¹¹⁸	2.10 (1.69-2.53)	720	1.48 (0.15)	-
<i>DSC1</i> ^a	1.93 (1.53-2.34)	720	1.43 (0.15)	1.1

Note:

LC₅₀, median lethal concentration

LC₅₀ ratio = (LC₅₀ of *w*¹¹¹⁸) / (LC₅₀ of *DSC1* knockout line)

Table 4-6 Susceptibility of *w*¹¹¹⁸ and *DSC1*^a flies to fipronil (contact bioassay)

	LC ₅₀ (95%CI) (µg/vial)	<i>n</i>	Slope (SE)	LC ₅₀ ratio
<i>w</i> ¹¹¹⁸	1.58 (0.71-5.49)	420	1.58 (0.15)	-
<i>DSC1</i> ^a	1.13 (0.77-1.91)	480	1.74 (0.16)	1.4

Note:

LC₅₀, median lethal concentration

LC₅₀ ratio = (LC₅₀ of *w*¹¹¹⁸) / (LC₅₀ of *DSC1* knockout line)

Table 4-7 ED₅₀ of *w*¹¹¹⁸ and *DSC1*^a flies to knockdown phenotype

	ED ₅₀ (95% CI) (ng/fly)	ED ₉₅ (95% CI) (ng/fly)	<i>n</i>	Slope (SE)
<i>w</i> ¹¹¹⁸	0.067 (0.055-0.083)	0.376 (0.262-0.638)	240	2.20 (0.24)
<i>DSC1</i> ^a	0.034 (0.026-0.044)	0.298 (0.195-0.568)	240	1.75 (0.21)

ED₅₀, median effective dose**Table 4-8** ED₅₀ of *w*¹¹¹⁸ and *DSC1*^a flies to abdomen elongation phenotype

	ED ₅₀ (95% CI) (ng/fly)	ED ₉₅ (95% CI) (ng/fly)	<i>n</i>	Slope (SE)
<i>w</i> ¹¹¹⁸	0.029 (0.027-0.031)	0.055 (0.049-0.065)	300	5.89 (0.61)
<i>DSC1</i> ^a	0.024 (0.022-0.025)	0.044 (0.040-0.051)	300	6.12 (0.59)

ED₅₀, median effective dose

Table 4-9. Response latencies and refractory periods of male *w¹¹¹⁸* and *DSC1^a* flies before and after exposure to 4ng/fly bioresmethrin for 15 minutes (mean \pm SD)

	Before		After	
	<i>w¹¹¹⁸</i>	<i>DSC1^a</i>	<i>w¹¹¹⁸</i>	<i>DSC1^a</i>
SL (ms)	1.2 \pm 0.2 (n=9)	1.2 \pm 0.2 (n=12)	1.3 \pm 0.1 (n=6)	1.5 \pm 0.1 (n=6) ¹
SLRP (ms)	5.9 \pm 1.4 (n=7)	6.0 \pm 1.0 (n=12)	5.1 \pm 0.6 (n=6)	4.9 \pm 0.5 (n=6) ²
LL (ms)	4.1 \pm 0.3 (n=8)	3.9 \pm 0.2 (n=12)	3.9 \pm 0.2 (n=6)	4.1 \pm 0.3 (n=6)
LLRP (ms)	45.4 \pm 10.1 (n=12)	43.5 \pm 8.7 (n=12)	42.7 \pm 6.2 (n=6)	41.3 \pm 4.4 (n=6)

Note:

SL - short latency

SLRP - short latency refractory period

LL - long latency

LLRP - long latency refractory period

1 $p < 0.05$, in comparison with the SL of *DSC1^a* before bioresmethrin application, Two-way ANOVA.

2 $p < 0.05$, in comparison with the SLRP of *DSC1^a* before bioresmethrin application, Two-way ANOVA.

Table 4-10. Response latencies and refractory periods of male *w¹¹¹⁸* and *DSC1^a* flies recorded before and after exposure to 0.4ng/fly deltamethrin for 15 minutes (mean±SD)

	Before		After	
	<i>w¹¹¹⁸</i>	<i>DSC1^a</i>	<i>w¹¹¹⁸</i>	<i>DSC1^a</i>
SL (ms)	1.2 ± 0.2 (n=9)	1.2 ± 0.2 (n=12)	1.2 ± 0.1 (n=9)	1.2 ± 0.2 (n=9)
SLRP (ms)	5.9 ± 1.4 (n=7)	6.0 ± 1.0 (n=12)	6.3 ± 1.0 (n=8)	6.1 ± 0.9 (n=9)
LL (ms)	4.1 ± 0.3 (n=8)	3.9 ± 0.2 (n=12)	3.6 ± 0.2 (n=8) ¹	3.6 ± 0.2 (n=6) ²
LLRP (ms)	45.4 ± 10.1 (n=12)	43.5 ± 8.7 (n=12)	38.6 ± 3.4 (n=8) ³	33.2 ± 6.1 (n=6) ⁴

Note:

SL - short latency

SLRP - short latency refractory period

LL - long latency

LLRP - long latency refractory period

1 $p < 0.05$, in comparison with the LL of *w¹¹¹⁸* before deltamethrin application, Two-way ANOVA.

2 $p < 0.05$, in comparison with the LL of *DSC1^a* before deltamethrin application, Two-way ANOVA.

3 $p < 0.05$, in comparison with the LLRP of *w¹¹¹⁸* before deltamethrin application, Two-way ANOVA.

4 $p < 0.05$, in comparison with the LLRP of *DSC1^a* before deltamethrin application, Two-way ANOVA.

Figure 4-1. Deltamethrin dose-response relation to knockdown phenotype of w^{1118} and $DSC1^a$ flies. Probit values were calculated using software SAS and plotted using software Originlab 8.0. ED₅, ED₅₀, and ED₉₅ were marked by dash lines.

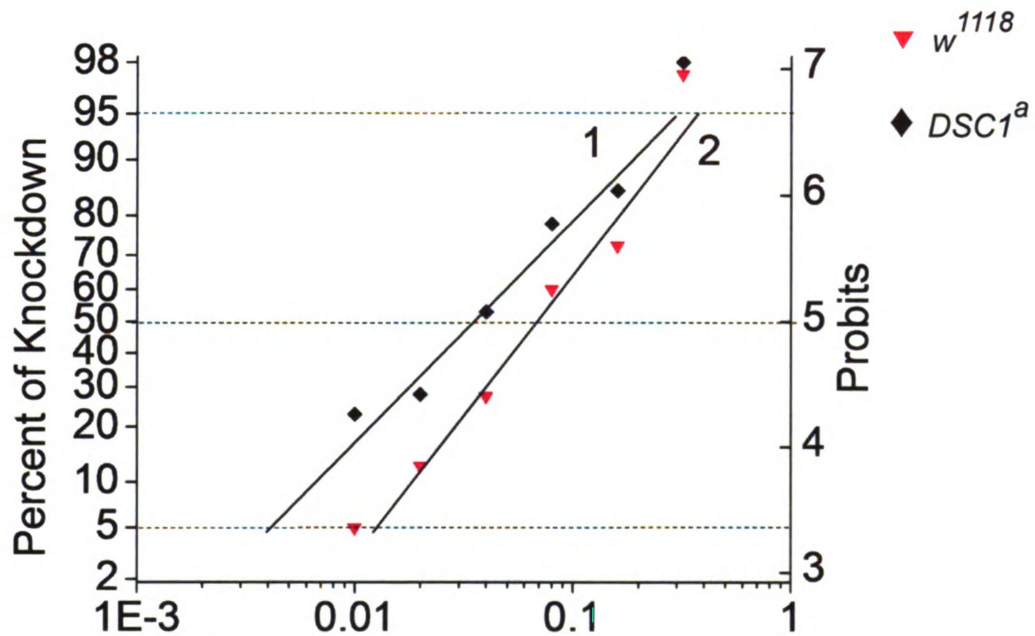


Figure 4-2. Abdomen elongation phenotype of w^{1118} and $DSC1^a$ flies. **A.** Abdomen of a $DSC1^b$ fly before deltamethrin exposure. **B.** Abdomen of the same $DSC1^b$ fly after deltamethrin exposure. The abdomen is elongated and rigid. **C.** Deltamethrin dose-response relation to abdomen elongation phenotype w^{1118} and $DSC1^a$ flies. Probit values were calculated using software SAS and plotted using software Originlab 8.0. ED₅, ED₅₀, and ED₉₅ were marked by dash lines.

A



B



Figure 4-2 (continued)

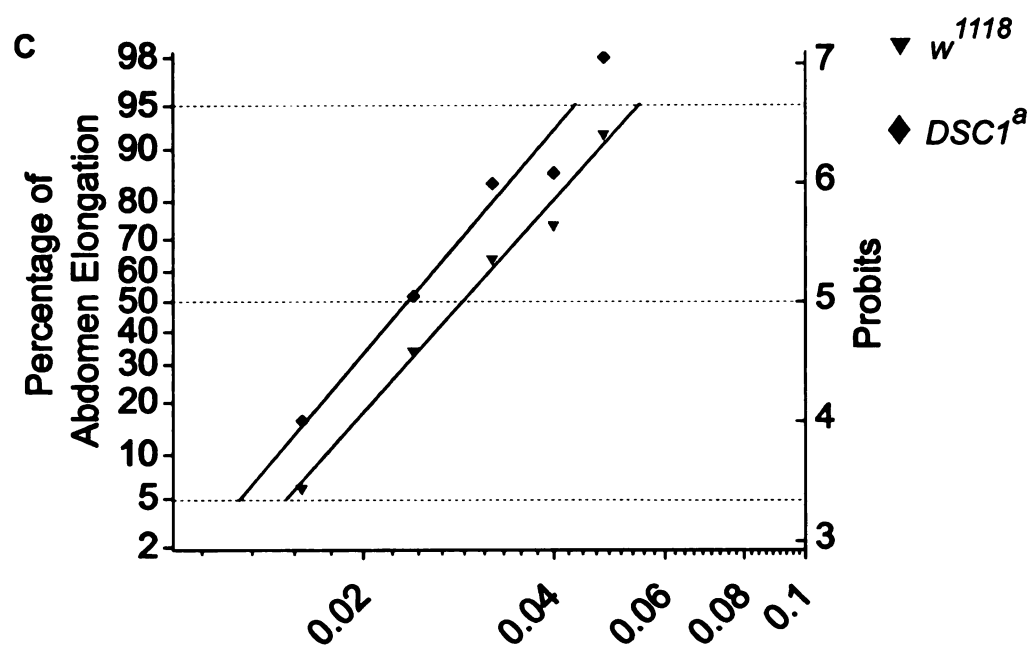


Figure 4-3. Time-response curves of knockdown phenotype of w^{1118} and $DSC1^a$ flies. The dose of deltamethrin applied was 0.04ng/fly. (mean \pm SD, $p < 0.05$, Log-rank test).

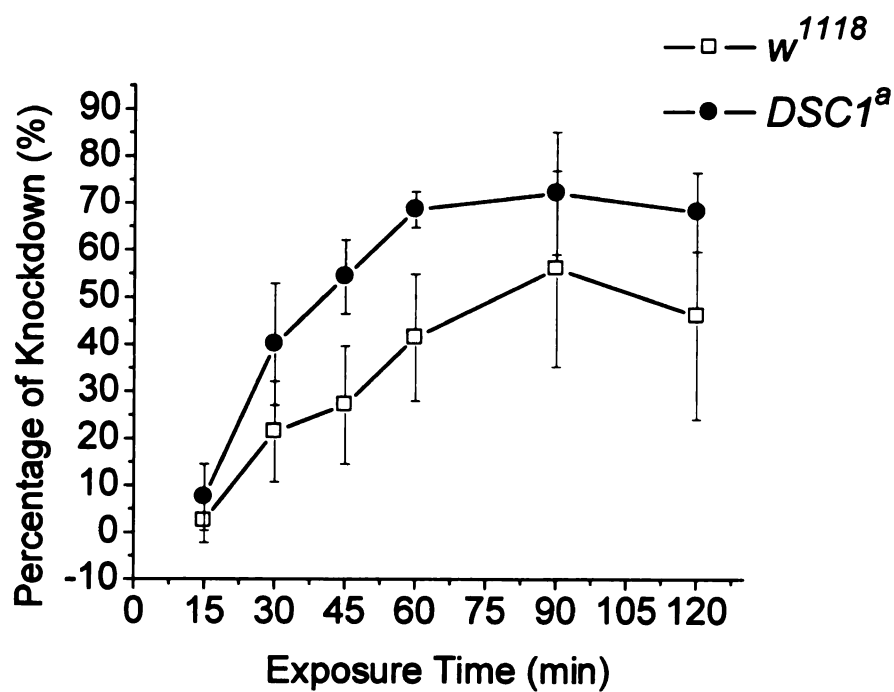


Figure 4-4. The GFSs of w^{1118} and $DSC1^a$ flies response differently to bioresmethrin. Response latencies and refractory periods were measured in w^{1118} and $DSC1^a$ male flies before and after exposed to 4 ng/fly bioresmethrin for 15 minutes. SL, short latency; SLRP, short latency refractory period; LL, long latency; LLRP, long latency refractory period. (* $p < 0.05$, Two-way ANOVA)

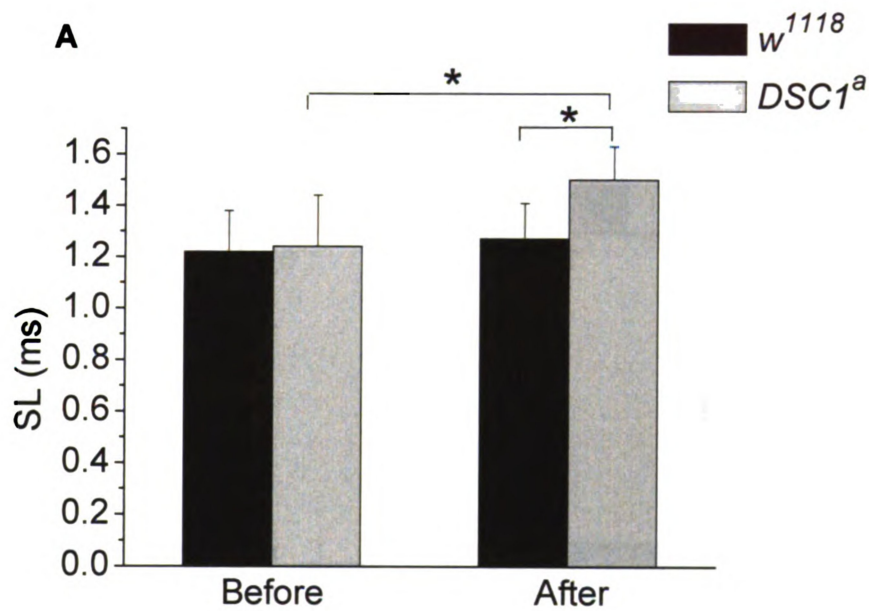
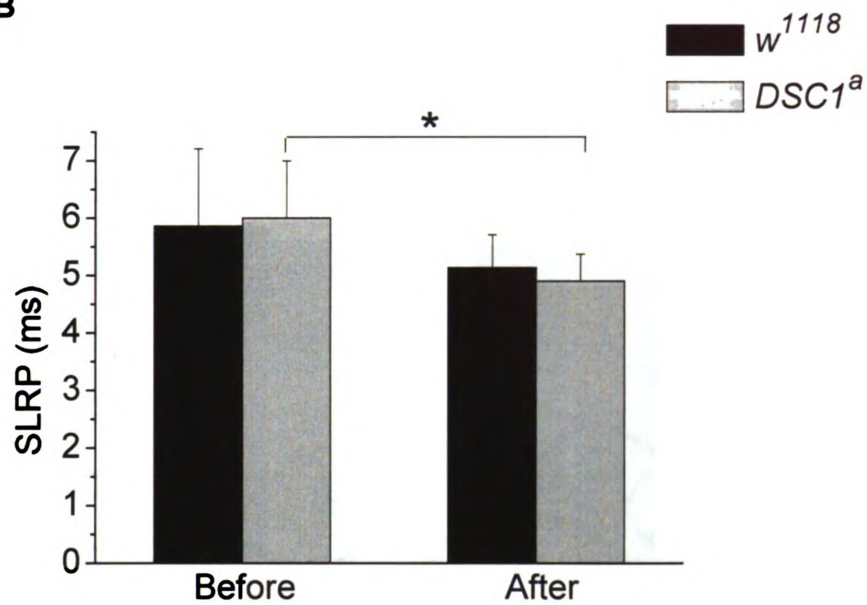


Figure 4-4 (continued)

B



C

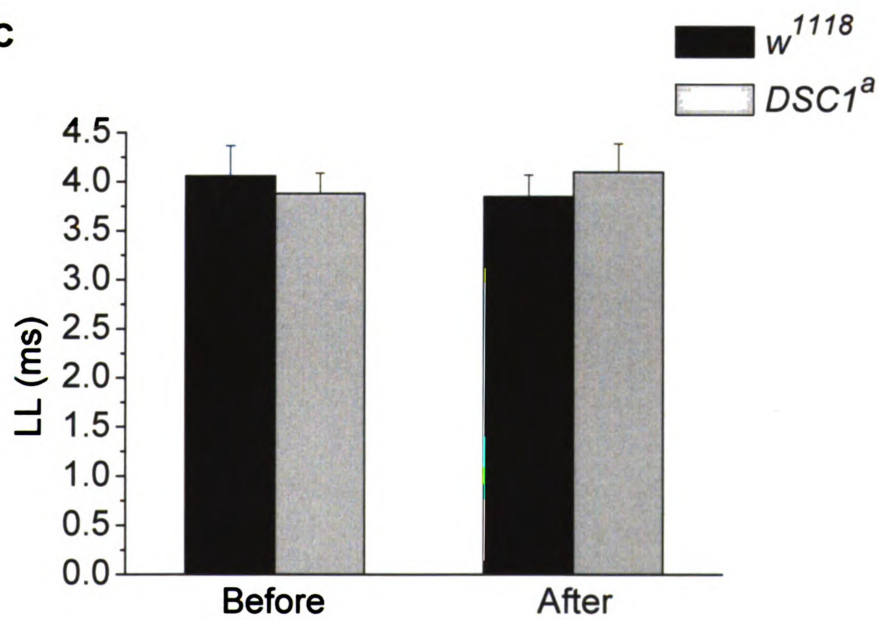


Figure 4-4 (continued)

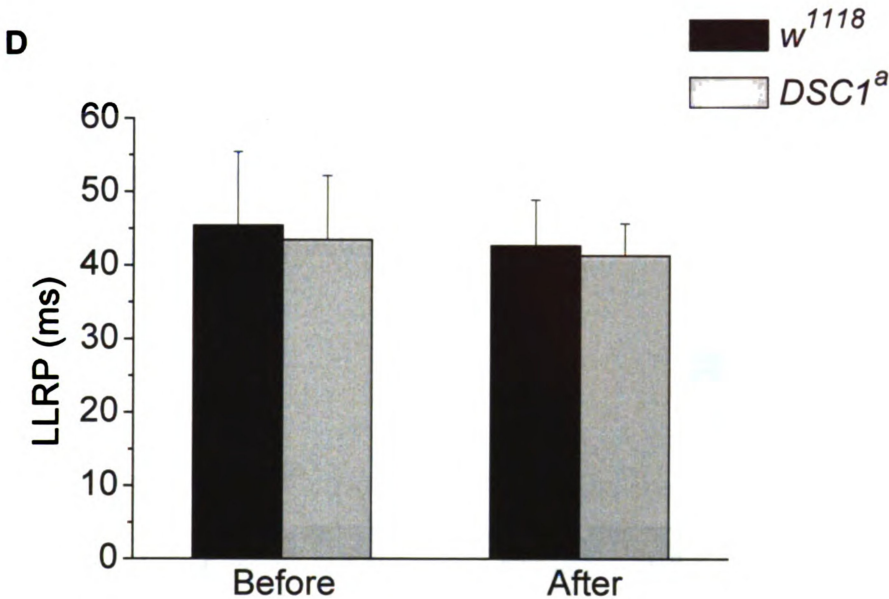


Figure 4-5. The GFSs of w^{1118} and $DSC1^a$ flies response differently to deltamethrin. Response latencies and refractory periods were measured in w^{1118} and $DSC1^a$ male flies before and after exposed to 0.4ng/fly deltamethrin for 15 minutes. SL, short latency; SLRP, short latency refractory period; LL, long latency; LLRP, long latency refractory period. (* $p < 0.05$, Two-way ANOVA)

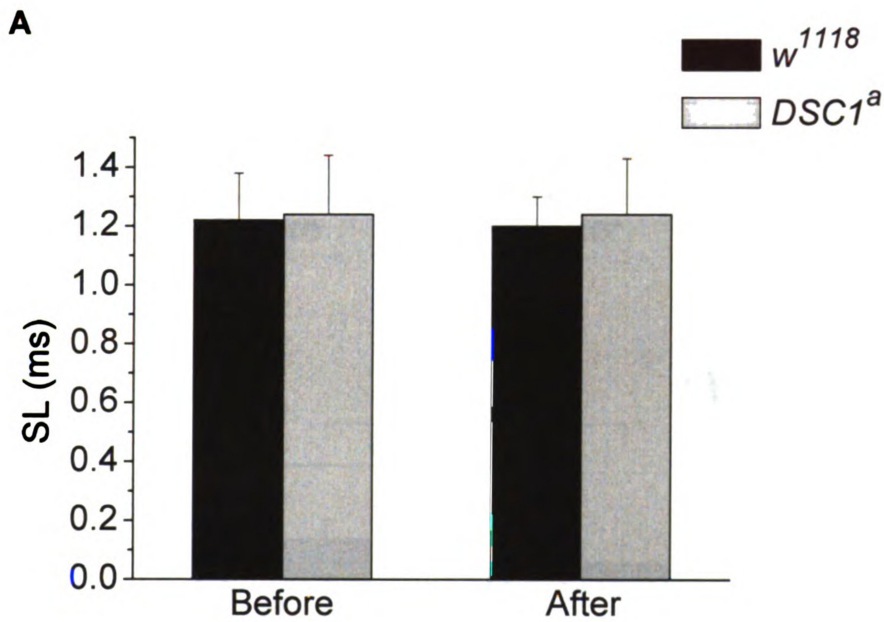


Figure 4-5 (continued)

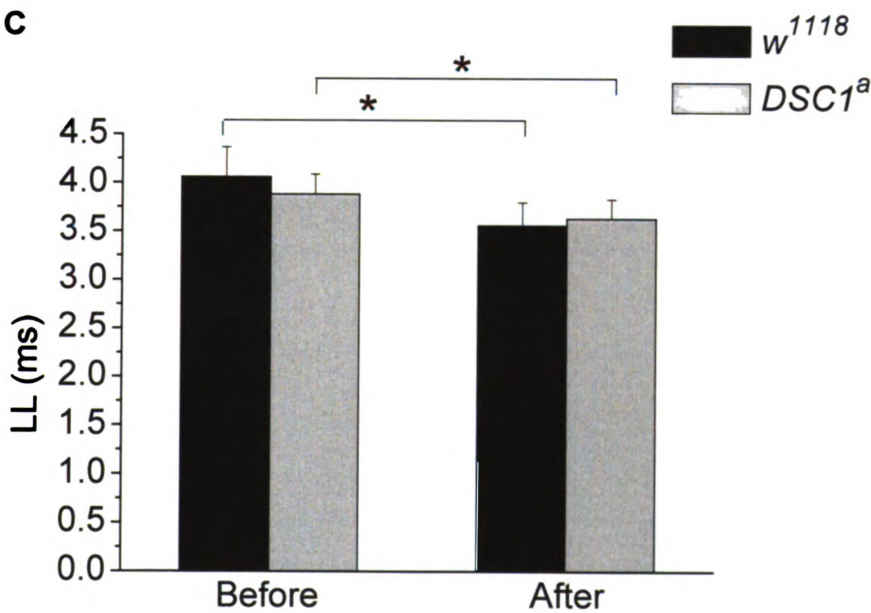
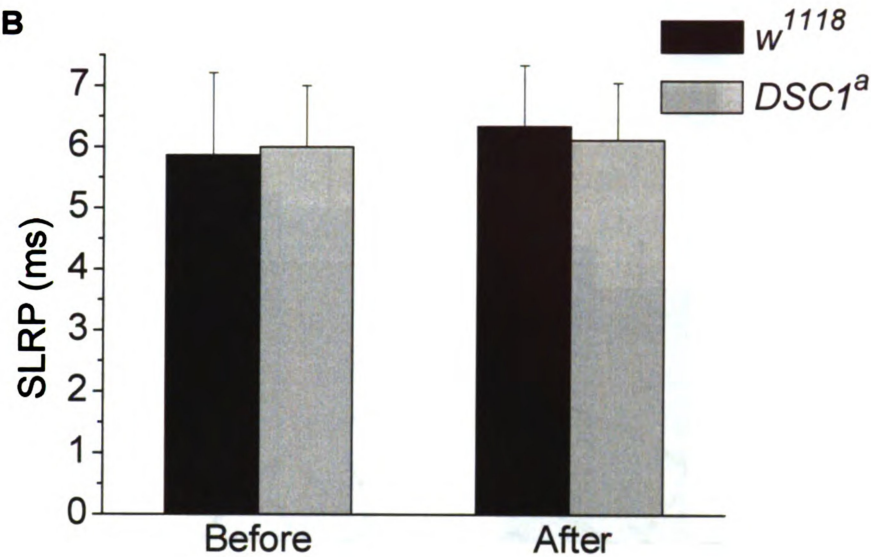


Figure 4-5 (continued)

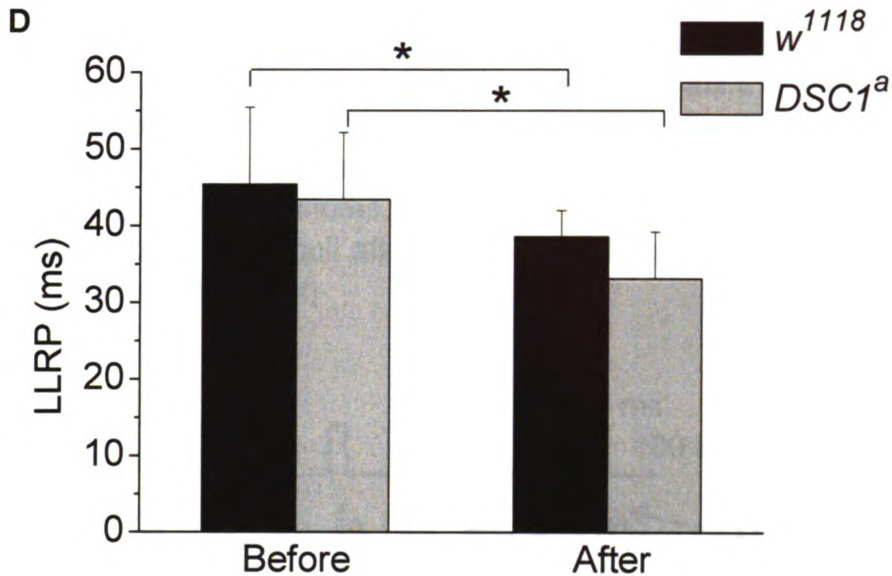


Figure 4-6. Pyrethroids destabilized the GFS of *DSC1* knockout flies to a greater extent. **A.** Representative traces of DLM muscle potentials elicited by a train of stimuli before pyrethroid application. The frequency of the train pulse is 100 Hz. The amplitude and duration of each pulse are 30 volts and 0.1 ms respectively. **B.** Number of DLM muscle potentials triggered by each of groups of stimuli after exposed to 0.2 μ l acetone for 15 minutes. **C.** Number of DLM muscle potentials triggered by each of groups of stimuli after exposed to 0.4 ng deltamethrin for 15 minutes. **D.** Number of DLM muscle potentials triggered by each of groups of stimuli after exposed to 4 ng bioresmethrin for 15 minutes. (* $p < 0.05$, Student's *t*-test)

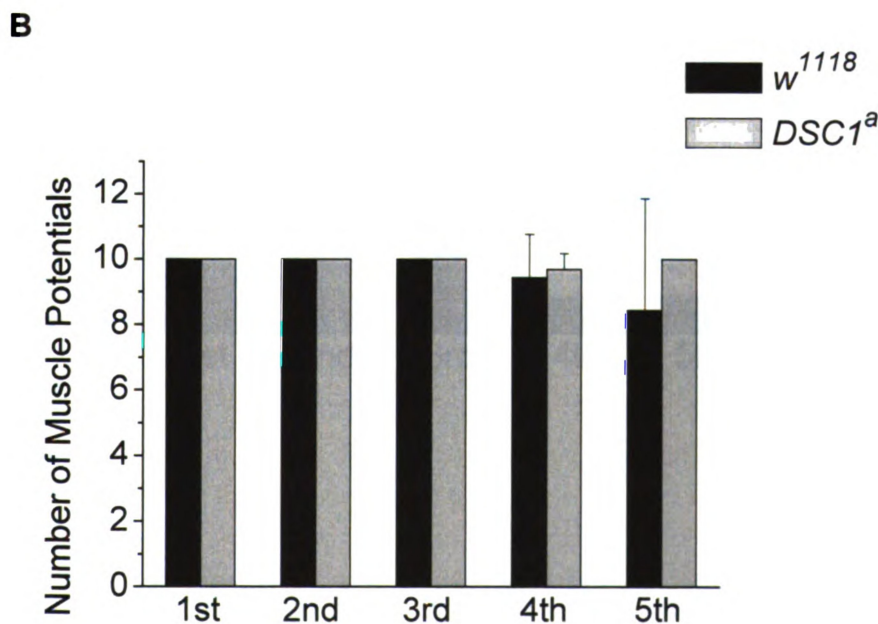
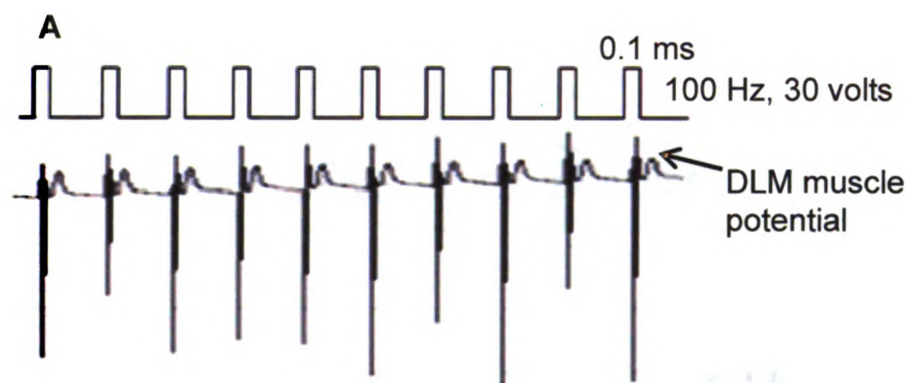
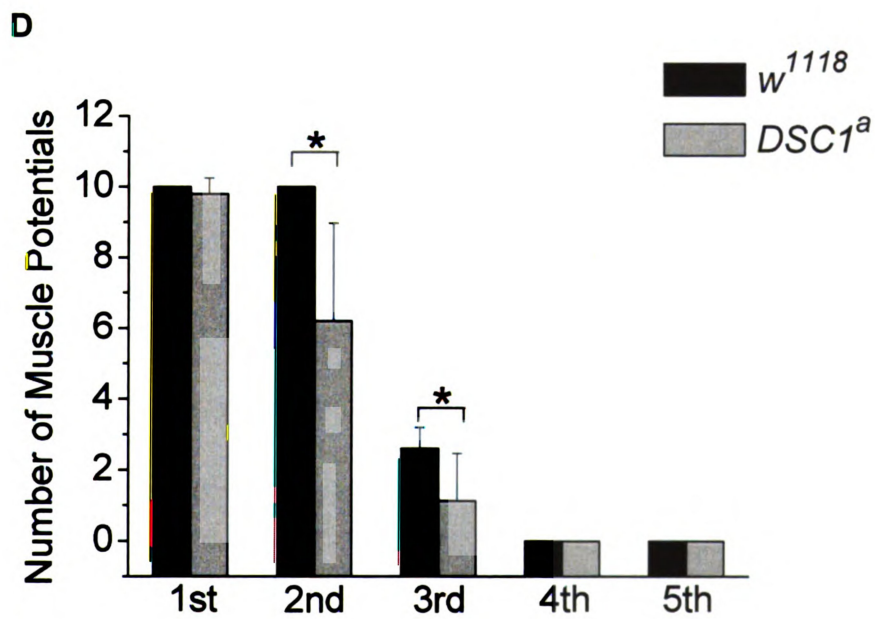
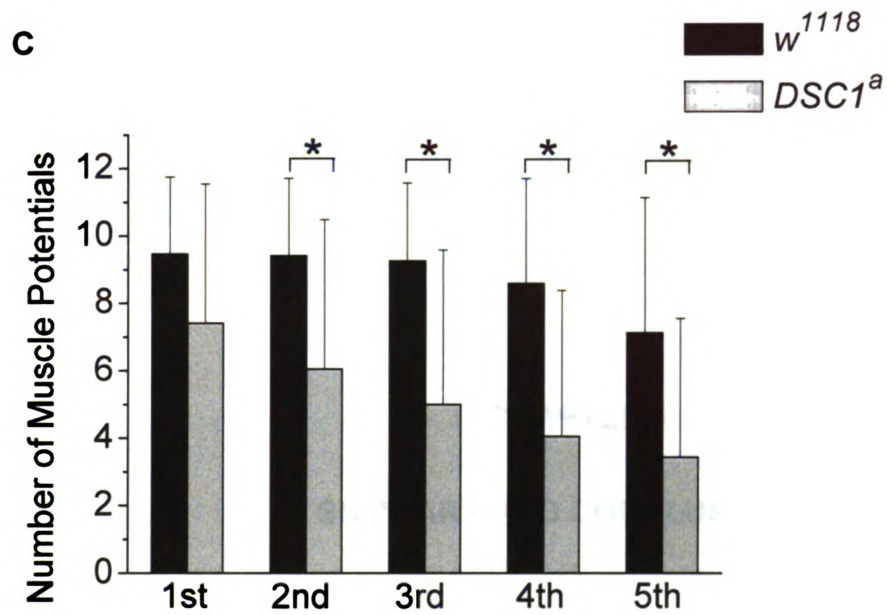


Figure 4-6 (continued)



CHAPTER 5

SUMMARY AND CONCLUSIONS

5.1 Summary and conclusions

The goal of this project was to investigate the role of the DSC1 channel in neurophysiology in *Drosophila melanogaster*. Two *DSC1* knockout *D. melanogaster* lines were studied for behavioral defects under both normal and stressful conditions (heat shock and starvation). The *DSC1* knockout flies were also evaluated for their susceptibilities to several classes of insecticides. The activities of a well-defined neuronal circuit, the GFS, of *DSC1* knockout flies were examined. My main findings are: 1) the *DSC1* channel is a voltage-gated cation channel that is permeable to Na^+ , Ca^{2+} , and Ba^{2+} ; 2) compared with wild-type flies, the *DSC1* knockout flies are more sensitive to heat shock and less tolerant to starvation; 3) the *DSC1* knockout flies are more susceptible to pyrethroids than wild-type flies; and 4) modifications in the activities of the GFS in *DSC1* knockout flies correlated with the behavioral alterations.

Based on my findings and the information previously obtained from the study of the *DSC1* ortholog, *BSC1*, Below, I proposed a working model on the role of the *DSC1* channel in insect neurophysiology. The *DSC1* channel functions along with sodium channels to dampen neuronal excitability by modulating the initiation and propagation of the action potential mediated by the sodium channel. The *DSC1* channel could be activated during the rising phase of an action potential in which could enhance the depolarization and/or prolong the duration of the action potential. This modulation by the *DSC1* channel may be too subtle to be detected

at room temperature. In response to heat shock which alters the conductance of sodium and potassium channels (Huxley, 1959), or when sodium channels are activated by pyrethroid insecticides, the modulating role of the DSC1 channel becomes evident.

A practical implication of the findings reported in Chapter 3 and 4 is that the DSC1 channel may be used as a novel target for the development of new insecticides. Exposure of insects to chemicals that block the DSC1 channel could make insects hypersensitive to pyrethroids and possibly more vulnerable to environmental stresses in nature. Moreover, the DSC1 family of ion channels is unique in invertebrate animals. Thus, DSC1 channel-targeted chemicals may have the advantage of being highly selective and safe to mammals. However, the interaction between pyrethroids and the DSC1 channel is not fully understood and needs further investigation. Additional studies focusing on identification of *DSC1* orthologs in beneficial insects and investigations of the interactions between these orthologs and pyrethroids could further our understanding of the selectivity of DSC1 channel-targeted insecticides to insect pests.

5.2 Future studies

The discoveries I made in my dissertation study are the first step toward comprehensive understanding of the role of the DSC1 channel in modulating

neuronal excitability. Below I highlight the major research areas for future studies.

Molecular analyses indicate that *DSC1* transcripts are alternatively spliced. However, the tissue and/or developmental distributions of these *DSC1* variants are not clear. It is possible that alternative splicing of *DSC1* transcripts is regulated in a tissue- and/or developmental stage-dependent manner. If so, study of the underlying regulatory mechanisms would be important. Furthermore, some of the alternative exons contain in-frame stop codons that would result in truncated *DSC1* proteins. Why the truncation occurs and whether the truncated protein forms functional channels are worth of further research.

More extensive *in vitro* electrophysiological recording in dissociated neurons or *in vivo* recording of specific neuronal circuits should be used, for example, to measure the resting membrane potential, action potential, and neurotransmitter release. Such studies could be combined with a more detailed examination of the distribution of *DSC1* channels in axons and synapses or the distribution of specific *DSC1* variants in distinct neurons. Together, these experiments could provide us with more clues to understand how the *DSC1* channel regulates neuronal excitability. Genetically, our *DSC1* mutant alleles could be crossed with other ion channel mutants to study the interactions between ion channels. It will also be interesting to knockout the *DSC1* gene in a specific group of neurons, such as odor receptor neurons, to characterize the roles played by the *DSC1* channel in

these particular neurons.

Voltage-gated sodium channel has been showed to regulate the development of the nervous system (Brackenbury et al., 2008; Brackenbury et al., 2010). Although the *DSC1* knockout flies exhibit normal appearance and behavior under standard laboratory conditions it is not known whether the DSC1 channel contributes to neuronal development. The giant fiber system and neuromuscular junction are good models in adults and larvae for studying the development of the nervous system, such as the axon guidance and the generation of synapses. Therefore, detailed morphological study of the giant fiber system and the neuromuscular junction of *DSC1* knockout flies may be another direction to take in the future. Of course, the morphological study could always be coupled with genetic and electrophysiological approaches to obtain a more comprehensive understanding.

Sodium channels and calcium channels consist of several subunits. For example, the Para channel requires the accessory subunit TipE for maximal function (Feng et al., 1995). Although expression of DSC1 alone in *Xenopus* oocytes results in detectable currents, it is not clear whether the DSC1 channel requires another subunit for maximal function. Because DSC1 is highly homologous to the Para channel, it might need TipE or a TipE-like protein for optimal function. In *Drosophila*, there are four *TipE* homologous genes (*TEH1-4*). Possible interactions between DSC1 channels and these proteins could be

investigated using multiple methods, such as protein-protein interaction assays, two-electrode voltage clamp recordings in *Xenopus* oocytes, gene mutation analyses, and co-localization assays.

BIBLIOGRAPHY

- Agnew WS, Moore AC, Levinson SR, Raftery MA (1980) Identification of a large molecular weight peptide associated with a tetrodotoxin binding protein from the electroplax of *Electrophorus electricus*. *Biochem Biophys Res Commun* 92:860-866.
- Allen M, Godenschwege, TA, Tanouye, MA, Phelan, P. (2006) Making an escape: development and function of the *Drosophila* giant fibre system. *Semin Cell Dev Biol* 17:31-41.
- Aman TK, Grieco-Calub TM, Chen C, Rusconi R, Slat EA, Isom LL, Raman IM (2009) Regulation of persistent Na current by interactions between beta subunits of voltage-gated Na channels. *J Neurosci* 29:2027-2042.
- Amat C, Lapied B, French AS, Hue B (1998) Na⁺-dependent neuritic spikes initiate Ca²⁺-dependent somatic plateau action potentials in insect dorsal paired median neurons. *J Neurophysiol* 80:2718-2726.
- Beneski DA, Catterall WA (1980) Covalent labeling of protein components of the sodium channel with a photoactivable derivative of scorpion toxin. *Proc Natl Acad Sci U S A* 77:639-643.
- Bloomquist JR (1993) Neuroreceptor mechanisms in pyrethroid mode of action and resistance. *Rev Pestic Toxicol* 2:185-230.
- Börjesson SI, Elinder F (2008) Structure, function, and modification of the voltage sensor in voltage-gated ion channels. *Cell Biochem Biophys* 52:149-174.
- Brackenbury WJ, Djamgoz MB, Isom LL (2008) An emerging role for voltage-gated Na⁺ channels in cellular migration: regulation of central nervous system development and potentiation of invasive cancers. *Neuroscientist* 14:571-583.
- Brackenbury WJ, Calhoun JD, Chen C, Miyazaki H, Nukina N, Oyama F, Ranscht B, L. IL (2010) Functional reciprocity between Na⁺ channel Nav1.6 and beta1 subunits in the coordinated regulation of excitability and neurite outgrowth. *Proc Natl Acad Sci U S A* 107:2283-2288.

- Burr SA, Ray DE (2004) Structure-activity and interaction effects of 14 different pyrethroids on voltage-gated chloride ion channels. *Toxicol Sci* 77:341-346.
- Casida JE (1980) Pyrethrum flowers and pyrethroid insecticides. *Environ Health Perspect* 34:189-202.
- Castella C, Amichot M, Bergé JB, Pauron D (2001) DSC1 channels are expressed in both the central and the peripheral nervous system of adult *Drosophila melanogaster*. *Invert Neurosci* 4:85-94.
- Catterall W (1986) Voltage-dependent gating of sodium channels: correlating structure and function. *Trends in Neurosciences* 9:7-10.
- Catterall WA (1992) Cellular and molecular biology of voltage-gated sodium channels. *Physiol Rev* 72:S15-48.
- Catterall WA (2000) From ionic currents to molecular mechanisms: the structure and function of voltage-gated sodium channels. *Neuron* 26:13-25.
- Catterall WA, Perez-Reyes E, Snutch TP, Striessnig J (2005) International Union of Pharmacology. XLVIII. Nomenclature and structure-function relationships of voltage-gated calcium channels. *Pharmacol Rev* 57:411-425.
- Catterall WA, Cestèle S, Yarov-Yarovoy V, Yu FH, Konoki K, Scheuer T (2007) Voltage-gated ion channels and gating modifier toxins. *Toxicon* 49:124-141.
- Clements AN, May TE (1977) The actions of pyrethroids upon the peripheral nervous system and associated organs in the locust. *Pestic Sci* 8:661-680.
- Defaix A, Lapied B (2005) Role of a novel maintained low-voltage-activated inward current permeable to sodium and calcium in pacemaking of insect neurosecretory neurons. *Invert Neurosci* 5:135-146.
- Derst C, Walther C, Veh RW, Wicher D, Heinemann SH (2006) Four novel sequences in *Drosophila melanogaster* homologous to the auxiliary Para sodium channel subunit TipE. *Biochem Biophys Res Commun* 339:939-948.

- Dong K (2007) Insect sodium channels and insecticide resistance. *Invert Neurosci* 7:17-30.
- Du Y, Nomura Y, Liu Z, Huang ZY, Dong K (2009a) Functional expression of an arachnid sodium channel reveals residues responsible for tetrodotoxin resistance in invertebrate sodium channels. *J Biol Chem* 284:33869-33875.
- Du Y, Lee JE, Nomura Y, Zhang T, Zhorov BS, Dong K (2009b) Identification of a cluster of residues in transmembrane segment 6 of domain III of the cockroach sodium channel essential for the action of pyrethroid insecticides. *Biochem J* 419:377-385.
- Elkins T, Ganetzky B (1990) Conduction in the giant nerve fiber pathway in temperature-sensitive paralytic mutants of *Drosophila*. *J Neurogenet* 6:207-219.
- Elliott M (1980) Established pyrethroid insecticides. *Pestic Sci* 11:119-128.
- Elliott M, Janes NF (1978) Synthetic pyrethroids - a new class of insecticide. *Chem Soc Rev* 7.
- Elliott M, Farnham AW, Janes NF, Needham PH, Pulman DA, Stevenson JH (1973) A photostable pyrethroid. *Nature* 246:169-170.
- Engel JE, Xie XJ, Sokolowski MB, Wu CF (2000) A cGMP-dependent protein kinase gene, *foraging*, modifies habituation-like response decrement of the giant fiber escape circuit in *Drosophila*. *Learn Mem* 7:341-352.
- Fayyazuddin A, Zaheer MA, Hiesinger PR, Bellen HJ (2006) The nicotinic acetylcholine receptor *Dalpha7* is required for an escape behavior in *Drosophila*. *PLoS Biol* 4:420-431.
- Feng G, Deák P, Chopra M, Hall LM (1995) Cloning and functional analysis of *TipE*, a novel membrane protein that enhances *Drosophila* para sodium channel function. *Cell* 82:1001-1011.
- Germeraad S, O'Dowd D, Aldrich RW (1992) Functional assay of a putative *Drosophila* sodium channel gene in homozygous deficiency neurons. *J Neurogenet* 8:1-16.

- Godenschwege T, Forde R, Davis CP, Paul A, Beckwith K, Duttaroy A (2009) Mitochondrial superoxide radicals differentially affect muscle activity and neural function. *Genetics* 183:175-184.
- Goldin AL (1992) Maintenance of *Xenopus laevis* and oocyte injection. *Methods Enzymol* 207.
- Goldin AL (2001) Resurgence of sodium channel research. *Annu Rev Physiol* 63:871-894.
- Goldin AL (2003) Mechanisms of sodium channel inactivation. *Curr Opin Neurobiol* 13:284-290.
- Gong WJ, Golic KG (2003) Ends-out, or replacement, gene targeting in *Drosophila*. *Proc Natl Acad Sci U S A* 100:2556-2561.
- Gorczyca M, Hall JC (1984) Identification of a cholinergic synapse in the giant fiber pathway of *Drosophila* using conditional mutations of acetylcholine synthesis. *J Neurogenet* 1:289-313.
- Gray AJ, Soderlund DM (1985) Mammalian toxicology of pyrethroids. New York: Wiley.
- Guy HR, Seetharamulu P (1986) Molecular model of the action potential sodium channel. *Proc Natl Acad Sci U S A* 83:508-512.
- Hall CA (1978) The efficiency of cypermethrin (NRDC 149) for the treatment and eradication of the sheep louse *Damalinia ovis*. *Aust Vet J* 54:471-472.
- Heinemann SH, Terlau H, Stühmer W, Imoto K, Numa S (1992) Calcium channel characteristics conferred on the sodium channel by single mutations. *Nature* 356:441-443.
- Hille B (1992) *Ionic Channels of Excitable Membranes*. Sunderland, MA: Sinauer Associates, Inc..
- Hodgkin AL, Huxley AF (1952) The components of membrane conductance in the giant axon of *Loligo*. *J Physiol* 116.
- Hong CS, Ganetzky B (1994) Spatial and temporal expression patterns of two sodium channel genes in *Drosophila*. *J Neurosci* 14:5160-5169.

- Hoopengardner B, Bhalla T, Staber C, Reenan RA (2003) Nervous system targets of RNA editing identified by comparative genomics. *Science* 301:832-836.
- Huxley AF (1959) Ion movements during nerve activity. *Ann N Y Acad Sci* 81:221-246.
- Isom LL, Ragsdale DS, De Jongh KS, Westenbroek RE, Reber BF, Scheuer T, Catterall WA (1995) Structure and function of the beta 2 subunit of brain sodium channels, a transmembrane glycoprotein with a CAM motif. *Cell* 83:433-442.
- Isom LL, De Jongh KS, Patton DE, Reber BF, Offord J, Charbonneau H, Walsh K, Goldin AL, Catterall WA (1992) Primary structure and functional expression of the beta 1 subunit of the rat brain sodium channel. *Science* 256:839-842.
- Jeyaratnam J (1990) Acute pesticide poisoning: a major global health problem. *World Health Stat Q* 43:139-144.
- Kerr NC, Holmes FE, Wynick D (2008) Novel mRNA isoforms of the sodium channels Na_v1.2, Na_v1.3 and Na_v1.7 encode predicted two-domain, truncated proteins. *Neuroscience* 155:797-808.
- Koenig JH, Ikeda K (2005) Relationship of the reserve vesicle population to synaptic depression in the tergotrochanteral and dorsal longitudinal muscles of *Drosophila*. *J Neurophysiol* 94:2111-2119.
- Konradsen F (2007) Acute pesticide poisoning—a global public health problem. *Dan Med Bull* 54:58-59.
- Kontis KJ, Rounaghi A, Goldin AL (1997) Sodium channel activation gating is affected by substitutions of voltage sensor positive charges in all four domains. *J Gen Physiol* 110:391-401.
- Kosaka T, Ikeda K (1983) Possible temperature-dependent blockage of synaptic vesicle recycling induced by a single gene mutation in *Drosophila*. *J Neurobiol* 14:207-225.
- Kulkarni NH, Yamamoto AH, Robinson KO, Mackay TF, Anholt RR (2002) The DSC1 channel, encoded by the smi60E locus, contributes to odor-guided

- behavior in *Drosophila melanogaster*. *Genetics* 161:1507-1516.
- Lin WH, Wright DE, Muraro NI, Baines RA (2009) Alternative splicing in the voltage-gated sodium channel DmNav regulates activation, inactivation, and persistent current. *J Neurophysiol* 102:1994-2006.
- Littleton JT, Ganetzky B (2000) Ion channels and synaptic organization: analysis of the *Drosophila* genome. *Neuron* 26:35-43.
- Liu Z, Chung I, Dong K (2001) Alternative splicing of the BSC1 gene generates tissue-specific isoforms in the German cockroach. *Insect Biochem Mol Biol* 31:703-713.
- Liu Z, Song W, Dong K (2004) Persistent tetrodotoxin-sensitive sodium current resulting from U-to-C RNA editing of an insect sodium channel. *Proc Natl Acad Sci USA* 101:11862-11867.
- Loughney K, Kreber R, Ganetzky B (1989) Molecular analysis of the para locus, a sodium channel gene in *Drosophila*. *Cell* 58:1143-1154.
- Lowenstein O (1942) A method of physiological assay of pyrethrum extracts. *Nature* 150:760-762.
- Lund AE, Narahashi T (1983) Kinetics of sodium channel modification as the basis for the variation in the nerve membrane effects of pyrethroids and DDT analogs. *Pestic Biochem Physiol* 20:203-216.
- Männikkö R, Elinder F, Larsson HP (2002) Voltage-sensing mechanism is conserved among ion channels gated by opposite voltages. *Nature* 419:837-841.
- McLaughlin GA (1973) *History of pyrethrum*. New York: Academic.
- Morgan K, Stevens EB, Shah B, Cox PJ, Dixon AK, Lee K, Pinnock RD, Hughes J, Richardson PJ, Mizuguchi K, Jackson AP (2000) beta 3: an additional auxiliary subunit of the voltage-sensitive sodium channel that modulates channel gating with distinct kinetics. *Proc Natl Acad Sci U S A* 97:2308-2313.
- Motomura H, Narahashi T (2000) Temperature dependence of pyrethroid modification of single sodium channels in rat hippocampal neurons. *J*

Membr Biol 177:23-39.

Narahashi T (1962a) Nature of the negative after-potential increased by the insecticide allethrin in cockroach giant axons. J Cell Comp Physiol 59:67-76.

Narahashi T (1962b) Effect of the insecticide allethrin on membrane potentials of cockroach giant axons. J Cell Comp Physiol 59:61-65.

Narahashi T (1988) Molecular and cellular approaches to neurotoxicology: past, present and future. In: Neurotox '88: molecular basis of drug and pesticide action.: New York: Elsevier.

Narahashi T (1992) Nerve membrane Na⁺ channels as targetes of insecticides. Trends Pharmacol Sci 13:236-241.

Narahashi T (1996) Neuronal ion channels as the target sites of insecticides. Pharmacol Toxicol 79:1-14.

Narahashi T (2000) Neuroreceptors and ion channels as the basis for drug action: past, present, and future. J Pharmacol Exp Ther 294:1-26.

Narahashi T, Zhao X, Ikeda T, Nagata K, Yeh JZ (2007) Differential actions of insecticides on target sites: basis for selective toxicity. Hum Exp Toxicol 26:361-366.

Noda M, Suzuki H, Numa S, Stühmer W (1989) A single point mutation confers tetrodotoxin and saxitoxin insensitivity on the sodium channel II. FEBS Lett 259:213-216.

Noda M, Ikeda T, Suzuki H, Takeshima H, Takahashi T, Kuno M, Numa S (1986) Expression of functional sodium channels from cloned cDNA. Nature 322:826-828.

Noda M, Shimizu S, Tanabe T, Takai T, Kayano T, Ikeda T, Takahashi H, Nakayama H, Kanaoka Y, Minamino N (1984) Primary structure of *Electrophorus electricus* sodium channel deduced from cDNA sequence. Nature 312:121-127.

O'Dowd DK, Gee JR, Smith MA (1995) Sodium current density correlates with expression of specific alternatively spliced sodium channel mRNAs in

- single neurons. *J Neurosci* 15:4005-4012.
- Olson R, Liu Z, Nomura Y, Zhang T, Song W, Dong K (2008) Molecular and functional characterization of Para sodium channels in *Drosophila melanogaster*. *Insect Biochem Mol Biol* 38:604-610.
- Park Y, Taylor MF, Feyereisen R (1999) Voltage-gated sodium channel genes *hscp* and *hDSC1* of *Heliothis virescens* F. genomic organization. *Insect Mol Biol* 8:161-170.
- Piper MD, Skorupa D, Partridge L (2005) Diet, metabolism and lifespan in *Drosophila*. *Exp Gerontol* 40:857-862.
- Plummer NW, McBurney MW, Meisler MH (1997) Alternative splicing of the sodium channel *SCN8A* predicts a truncated two-domain protein in fetal brain and non-neuronal cells. *J Biol Chem* 272:24008-24015.
- Ramaswami M, Tanouye MA (1989) Two sodium-channel genes in *Drosophila*: implications for channel diversity. *Proc Natl Acad Sci U S A* 86:2079-2082.
- Ratcliffe CF, Westenbroek RE, Curtis R, Catterall WA (2001) Sodium channel $\beta 1$ and $\beta 3$ subunits associate with neurofascin through their extracellular immunoglobulin-like domain. *J Cell Biol* 154:427-434.
- Ray DE, Fry JR (2006) A reassessment of the neurotoxicity of pyrethroid insecticides. *Pharmacol Ther* 111:174-193.
- Rion S, Kawecki TJ (2007) Evolutionary biology of starvation resistance: what we have learned from *Drosophila*. *J Evol Biol* 20:1655-1664.
- Rohl CA, Boeckman FA, Baker C, Scheuer T, Catterall WA, Klevit RE (1999) Solution structure of the sodium channel inactivation gate. *Biochemistry* 38:855-861.
- Salkoff L, Butler A, Wei A, Scavarda N, Giffen K, Ifune C, Goodman R, Mandel G (1987) Genomic organization and deduced amino acid sequence of a putative sodium channel gene in *Drosophila*. *Science* 237:744-749.
- Satin J, Kyle JW, Chen M, Bell P, Cribbs LL, Fozzard HA, Rogart RB (1992) A mutant of TTX-resistant cardiac sodium channels with TTX-sensitive properties. *Science* 256:1202-1205.

- Shafer TJ, Meyer DA (2004) Effects of pyrethroids on voltage-sensitive calcium channels: a critical evaluation of strengths, weaknesses, data needs, and relationship to assessment of cumulative neurotoxicity. *Toxicol Appl Pharmacol* 196:303-318.
- Shahidullah M, Reddy S, Fei H, Levitan IB (2009) In Vivo Role of a Potassium Channel-Binding Protein in Regulating Neuronal Excitability and Behavior. *J Neurosci* 29:13328-13337.
- Siddiqi O, Benzer S (1976) Neurophysiological defects in temperature-sensitive paralytic mutants of *Drosophila melanogaster*. *Proc Natl Acad Sci U S A* 73:3253-3257.
- Silver K, Soderlund DM (2005) Action of pyrethroid-type insecticides at neuronal target sites. *Pestic Biochem Physiol* 81:136–143.
- Sivilotti L, Okuse K, Akopian AN, Moss S, Wood JN (1997) A single serine residue confers tetrodotoxin insensitivity on the rat sensory-neuron-specific sodium channel SNS. *FEBS Lett* 409:49-52.
- Soderlund D, Bloomquist, JR (1990) Molecular mechanisms of insecticide resistance. In: *Pesticide resistance in arthropods*.: Chapman and Hall, New York,.
- Soderlund DM, Bloomquist JR (1989) Neurotoxic actions of pyrethroid insecticides. *Annu Rev Entomol* 34:77-96.
- Song JH, Narahashi T (1996) Modulation of sodium channels of rat cerebellar Purkinje neurons by the pyrethroid tetramethrin. *J Pharmacol Exp Ther* 277:445-453.
- Song W, Liu Z, Tan J, Nomura Y, Dong K (2004) RNA editing generates tissue-specific sodium channels with distinct gating properties. *J Biol Chem* 279:32554-32561.
- Stafstrom CE (2007) Persistent sodium current and its role in epilepsy. *Epilepsy Curr* 7:15-22.
- Stühmer W, Conti F, Suzuki H, Wang XD, Noda M, Yahagi N, Kubo H, Numa S (1989) Structural parts involved in activation and inactivation of the sodium channel. *Nature* 339:597-603.

- Suzuki DT, Grigliatti T, Williamson R (1971) Temperature-Sensitive Mutations in *Drosophila melanogaster*, VII. A Mutation (parats) Causing Reversible Adult Paralysis. In, pp 890-893.
- Tan J, Liu Z, Nomura Y, Goldin AL, Dong K (2002) Alternative splicing of an insect sodium channel gene generates pharmacologically distinct sodium channels. *J Neurosci* 22:5300-5309.
- Tanouye MA, Wyman RJ (1980) Motor outputs of giant nerve fiber in *Drosophila*. *J Neurophysiol* 44:405-421.
- Tatebayashi H, Narahashi T (1994) Differential mechanism of action of the pyrethroid tetramethrin on tetrodotoxin-sensitive and tetrodotoxin-resistant sodium channels. *J Pharmacol Exp Ther* 270:595-603.
- Terlau H, Heinemann SH, Stühmer W, Pusch M, Conti F, Imoto K, Numa S (1991) Mapping the site of block by tetrodotoxin and saxitoxin of sodium channel II. *FEBS Lett* 293:93-96.
- Thackeray JR, Ganetzky B (1994) Developmentally regulated alternative splicing generates a complex array of *Drosophila* para sodium channel isoforms. *J Neurosci* 14:2569-2578.
- Thackeray JR, Ganetzky B (1995) Conserved alternative splicing patterns and splicing signals in the *Drosophila* sodium channel gene para. *Genetics* 141:203-214.
- Trimarchi JR, Schneiderman AM (1993) Giant fiber activation of an intrinsic muscle in the mesothoracic leg of *Drosophila melanogaster*. *J Exp Biol* 177:149-167.
- Trimarchi JR, Schneiderman AM (1995a) Flight initiations in *Drosophila melanogaster* are mediated by several distinct motor patterns. *J Comp Physiol A* 176:355-364.
- Trimarchi JR, Schneiderman AM (1995b) Different neural pathways coordinate *Drosophila* flight initiations evoked by visual and olfactory stimuli. *J Exp Biol* 198:1099-1104.
- Trimarchi JR, Schneiderman AM (1995c) Initiation of flight in the unrestrained fly, *Drosophila melanogaster*. *J Zool* 235:211-223.

- Verschoyle RD, Aldridge WN (1980) Structure-activity relationships of some pyrethroids in rats. *Arch Toxicol* 45:325-329.
- Vijverberg HPM, van der Bercken J (1990) Neurotoxicological effects and the mode of action of pyrethroid insecticides. *CRC Crit Rev Toxicol* 21:106-126.
- Vijverberg HPM, van der Zalm JM, van der Bercken J (1982) Similar mode of action of pyrethroids and DDT on sodium channel gating in myelinated nerves. *Nature* 295:601-603.
- Walker DW, Muffat J, Rundel C, Benzer S (2006) Overexpression of a *Drosophila* homolog of apolipoprotein D leads to increased stress resistance and extended lifespan. *Curr Biol* 16:674-679.
- Warmke JW, Reenan RA, Wang P, Qian S, Arena JP, Wang J, Wunderler D, Liu K, Kaczorowski GJ, Van der Ploeg LH, Ganetzky B, Cohen CJ (1997) Functional expression of *Drosophila* para sodium channels. Modulation by the membrane protein TipE and toxin pharmacology. *J Gen Physiol* 110:119-133.
- Welsh JH, Gordon HT (1947) The mode of action of certain insecticides on the arthropod nerve axon. *J Cell Physiol* 30:147-171.
- West JW, Patton DE, Scheuer T, Wang Y, Goldin AL, Catterall WA (1992) A cluster of hydrophobic amino acid residues required for fast Na⁽⁺⁾-channel inactivation. *Proc Natl Acad Sci U S A* 89:10910-10914.
- Wicher D, Walther C, Wicher C (2001) Non-synaptic ion channels in insects-basic properties of currents and their modulation in neurons and skeletal muscles. *Prog Neurobiol* 64:431-525.
- Wood JN, Boorman JP, Okuse K, Baker MD (2004) Voltage-gated sodium channels and pain pathways. *J Neurobiol* 61:55-71.
- Yu FH, Catterall WA (2003) Overview of the voltage-gated sodium channel family. *Genome Biol* 4:207-213.
- Yu FH, Yarov-Yarovoy V, Gutman GA, Catterall WA (2005) Overview of molecular relationships in the voltage-gated ion channel superfamily. *Pharmacol Rev* 57:387-395.

- Yu FH, Westenbroek RE, Silos-Santiago I, McCormick KA, Lawson D, Ge P, Ferriera H, Lilly J, DiStefano PS, Catterall WA, Scheuer T, Curtis R (2003) Sodium channel beta4, a new disulfide-linked auxiliary subunit with similarity to beta2. *J Neurosci* 23:7577-7585.
- Zhao X, Ikeda T, Yeh JZ, Narahashi T (2003) Voltage-dependent block of sodium channels in mammalian neurons by the oxadiazine insecticide indoxacarb and its metabolite DCJW. *Neurotoxicology* 24:83-96.
- Zhao Y, Yarov-Yarovoy V, Scheuer T, Catterall WA (2004) A gating hinge in Na⁺ channels; a molecular switch for electrical signaling. *Neuron* 41:859-865.
- Zhou W, Chung I, Liu Z, Goldin AL, Dong K (2004) A voltage-gated calcium-selective channel encoded by a sodium channel-like gene. *Neuron* 42:101-112.

MICHIGAN STATE UNIVERSITY LIBRARIES



3 1293 03220 8872